THE STEADY MOTION OF A FLAT SHIP INCLUDING AN INVESTIGATION OF LOCAL FLOW NEAR THE BOW

BY

R.P. OERTEL B.Sc. (Hons.)(Adel.)

Thesis submitted for the degree of Doctor of Philosophy in the University of Adelaide

Department of Applied Mathematics

July 1975

SUMMARY

This thesis concerns the flow produced by a ship-like body moving steadily across the surface of a fluid. The relevant equations are linearized using the assumption that the body is "flat", i.e. that its length and breadth are much greater than its draft. This leads to an integral equation to determine the pressure distribution under the hull. Various simplifying limiting cases of this equation are discussed.

It is first shown that if the wetted area of the body is prescribed then the hull shape is necessarily partly determined by the solution. Conversely, if the hull shape is prescribed, the extent to which it is wetted must be determined by the solution. This means that, for a given hull shape and location, the range of integration of the integral equation is one of the unknowns, a fact which has received insufficient consideration in previous theoretical work in this subject.

In the particular case of bodies of infinite span in two-dimensional flow, this indeterminacy reduces to indeterminacy (for a given hull shape and vertical location) about the wetted length. The problem can be solved in an inverse manner by fixing the wetted length and allowing the vertical location of the hull to be determined by the solution. An efficient numerical procedure is outlined for solving this problem at arbitrary Froude number, and the results presented for flat and parabolic surfaces. In the

former case, comparison with previous solutions is given, as well as new forms of presentation of the results, which have relevance to the practical problem of planing boats. In the case of curved hulls, some consideration is given to the problem of finding the detachment point for non-sharp trailing edges.

For bodies of finite span, the limit as the Froude number tends to infinity is treated first, and it is demonstrated in particular that the assumption of a triangular wetted waterplane implies that the body has an approximately V-shaped hull. The case of three-dimensional flow at finite Froude number is also dealt with briefly.

Finally some consideration is given to the details of two-dimensional flow at the attachment point present at the bow. The exact non-linear free surface condition is used to derive a non-linear integral equation, which is solved in the high Froude number limit.

Signed Statement

The contents of this thesis have not been submitted to any university for the purpose of obtaining any other degree or diploma. Also, to the best of my knowledge and belief, the thesis contains no material previously published or written by another person, except where due reference is made in the text.

R.P. Oertel

ACKNOWLEDGEMENTS

I wish to express my thanks to my Supervisor, Professor E.O. Tuck, for his encouragement and numerous suggestions, as well as for valuable discussions on many aspects of the work. I am also indebted to Mrs. Dawn Darwent and Mrs. Janet Tieste for the typing of the manuscript. The author acknowledges the provision by the Australian Government of a Commonwealth Postgraduate Research Award during the three years full-time research spent on this thesis.

R.P. Oertel

CONTENTS

GENERAL INTRODUCTION

There can be few people who are not aware of the fact that the motion of a body across the surface of water produces a V-shaped pattern of waves. Swimming water-birds provide an attractive example of this phenomenon. The first mathematical study which explained the detailed character of these waves, was that by Kelvin [10], who used a model in which the action of the moving body was replaced by that of a concentrated pressure point moving steadily across the surface.

A significant part of the resistance to forward motion of a ship is due to the energy used up in maintaining this system of gravity waves which accompanies it. It is therefore of practical interest to investigate how this resistance depends on the detailed shape of the hull. The first investigation into this problem was that of Michell [14], who, by assuming the ship was "thin", was able to obtain an expression for the wave resistance in terms of the hull shape. In Michell's paper, and those mentioned below, viscosity, compressibility and non-steady effects are ignored, since attention is being directed at the ship solely as a producer of a steady pattern of gravity waves. The further assumption of thinness is necessary so that the boundary conditions may be linearized. There have been many subsequent papers on thin-ship theory, among the most thorough being those of Peters and Stoker [19] and Newman [17].

One may linearize the boundary conditions by making assumptions other than that the ship is thin. Another approach

is to assume that the ship is "slender", i.e. that it may be approximated by a line rather than a plane as in thin-ship theory. This slender ship approach was the subject of theses by Vossers [34] and Tuck [29] and was expanded further in a paper by Newman and Tuck [18].

Whereas it is probably true that most ships are essentially "slender" rather than "thin", it is nevertheless the case that many water craft are also "flat". This is particularly true of high speed planing boats. This thesis will deal with the motion of such bodies, although rather than directly investigating the connection between hull shape and wave resistance, we shall instead be more concerned with showing that the hull shape is in fact part of the solution to the hydrodynamical problem, when the wetted area is prescribed.

Chapter one introduces the general mathematical problem and an integral equation is derived for the pressure distribution on the hull. This integral equation contains an arbitrary function, and it is shown that this function manifests the indeterminacy in the hull shape when the wetted area, which provides the limits of the integral equation, is prescribed. Various simplifying limiting cases of this integral equation are discussed.

In Chapter two we give a new treatment of two-dimensional flow, i.e. flow about bodies of infinite span, a topic which has been considered by many previous authors. In this case the arbitrary function present in the three-dimensional integral equation reduces to a constant, which, for a given wetted length, provides as part of the solution the vertical

location of the hull. An efficient numerical scheme used to solve the two-dimensional integral equation is outlined. Wedge-shaped hulls are dealt with in detail and the results presented in a new form relevant to the motion of actual planing boats. For parabolic (i.e. curved) hull shapes, we investigate the problem of finding where the flow detaches when the body has a non-cut-off trailing edge.

Chapter three deals with bodies of finite span and a general numerical scheme for solution of the three-dimensional integral equation is given. Results are first presented for the limit as the Froude number tends to infinity. It is shown that the assumption of a rectangular wetted area gives, as part of the solution, that the hull is almost flat, whereas if the wetted area is triangular, the hull is approximately V-shaped. The general form of the free surface at infinite Froude number is also deduced. It is then shown that the numerical solution of the problem at finite Froude number essentially reduces to the numerical evaluation of the infinite integral of a slowly decaying oscillatory function.

In Chapter four some consideration is given to the details of two-dimensional flow at the attachment and separation points present at the bow and stern. The exact non-linear free surface condition is used to derive a non-linear integral equation, assuming attachment occurs without the formation of a jet. For the case where a jet does form, the problem is formulated and solved at infinite Froude number. Some inferences are then drawn about the nature of the solution at finite Froude number.

CHAPTER 1

THE FLAT SHIP PROBLEM

1.1 Introduction

This chapter will introduce the linearized flat ship problem and illustrate some ways in which simplified versions of it may be derived.

Flat ship theory is generally regarded to have originated with Hogner [9]. The two-dimensional case has been studied extensively, one of the earlier papers being that of Sretenskii [25], who represented the unknown pressure distribution by an infinite series, the first term giving a square root singularity at the leading edge - a situation well-known in aerodynamic lifting-surface theory (see e.g. [2]). Maruo [11] also used this approach and provided experimental results [12] which were in good agreement with the theory for small angles of attack, and away from the leading edge, where the theory breaks down because of the presence of the singularity. Careful local analysis (c.f. Wagner [35]) indicates that this singularity models a spray sheet.

Squire [24] used an approach similar to that of Sretenskii and Maruo in studying the motion of a simple wedge through water. However, he was one of the few authors to indicate that in this, and related problems, the height of the trailing edge, and the wetted length are unknowns and therefore must be determined as part of the solution to the problem. This point is of considerable importance in the

solution technique adopted in this thesis. Cumberbatch [4] considered the two-dimensional problem at high Froude number and produced a series for the pressure distribution in terms of inverse powers of the Froude number F as far as the F^{-4} term. Wehausen and Laitone [38] provide a more detailed review of the work mentioned above.

Recently Doctors [6] used finite pressure elements in the solution of the two-dimensional planing problem for both flat and curved plates. He also considered the problem of finding an optimum planing shape based on the minimization of the lift-squared-to-drag ratio.

Most studies of linearized three-dimensional planing have been made using further simplifying assumptions. Maruo [13] studied the high and low aspect ratio limits, and observed that the smaller the aspect ratio, the greater the importance of gravity. Low aspect ratio planing was treated in more detail by Tuck [31]. A high speed approximation was used by Wang and Rispin [37], who obtained numerical results for the pressure distributions on rectangular plates.

Peters and Stoker [19], in a lengthy paper treating both thin and flat ships, developed a careful formulation of the linearized problem and presented some results on conditions for uniqueness.

A detailed experimental study of prismatic planing surfaces was carried out by Savitsky [22]. Some comparison will be made with his results in a later chapter.

1.2 Formulation of the three-dimensional problem

Consider first the waves created by a pressure distribution moving at constant velocity U. The motion may be considered to be time-independent if we adopt coordinates (x,y,z) moving with the pressure distribution. We assume that the effect of the pressure distribution may be represented by a disturbance potential ϕ, in which case the fluid velocity $\underset{\sim}{q}$ is given by

$$\begin{aligned}\underset{\sim}{q} &= \underset{\sim}{\nabla}(-Ux+\phi) \\ &= (-U+\phi_x)\underset{\sim}{i} + \phi_y\underset{\sim}{j} + \phi_z\underset{\sim}{k}. \qquad (1.2.1)\end{aligned}$$

The kinematic boundary condition on the free surface $z = \zeta(x,y)$ is

$$\underset{\sim}{q}.\underset{\sim}{\nabla}(z-\zeta) = 0 \quad \text{on } z = \zeta(x,y)$$

$$\text{i.e.} \qquad \phi_z = (-U+\phi_x)\zeta_x + \phi_y\zeta_y. \qquad (1.2.2)$$

If the imposed pressure distribution is given by P(x,y), the dynamic boundary condition is

$$\frac{P(x,y)}{\rho} + g\zeta(x,y) + \frac{1}{2}|\underset{\sim}{q}|^2 = \text{constant} \quad \text{on } z = \zeta(x,y). \qquad (1.2.3)$$

We shall assume that as $x^2+y^2\to\infty$, $P\to 0$, $\zeta\to 0$ and $|\underset{\sim}{q}|\to U$, and hence the constant in (1.2.3) equals $\frac{1}{2}U^2$. So we have

$$\frac{P}{\rho} + g\zeta + \tfrac{1}{2}((-U+\phi_x)^2 + \phi_y^2 + \phi_z^2) = \tfrac{1}{2}U^2 \quad \text{on } z = \zeta(x,y). \qquad (1.2.4)$$

We now assume that P(x,y) is "small" in some formal sense which permits us to adopt the usual procedures of linearized theory. That is, we ignore any products of

derivatives of the disturbance quantities ϕ and ζ, and take the boundary conditions to apply on the equilibrium plane $z = 0$. We shall state the hydrodynamic problem in full, incorporating the linearized boundary conditions:

(i) Laplace's equation

$$\nabla^2\phi = 0 \qquad (1.2.5)$$

holds throughout the fluid below the free surface.

(ii) The two conditions,

(a) linearized kinematic boundary condition (from (1.2.2))

$$\phi_z = -U\zeta_x \quad \text{on } z = 0, \qquad (1.2.6)$$

and (b) linearized dynamic boundary condition (from (1.2.4))

$$\frac{P}{\rho} + g\zeta - U\phi_x = 0 \quad \text{on } z = 0, \qquad (1.2.7)$$

are combined to give

$$\kappa\phi_z + \phi_{xx} = \frac{P_x}{\rho U} \quad \text{where } \kappa = \frac{g}{U^2}. \qquad (1.2.8)$$

(iii) The radiation condition

$$\lim_{x\to+\infty}(x^2+y^2)^{\frac{1}{2}}(\phi_x^2+\phi_y^2+\phi_z^2) = 0 \qquad (1.2.9)$$

ensures that no waves exist far ahead of the disturbance. The quantity on the left can however, be expected to remain bounded as $x\to-\infty$, representing waves behind the pressure distribution.

(iv) The "bottom" condition

$$\lim_{z\to-\infty} \phi_z = 0 \quad \text{(exponentially)} \tag{1.2.10}$$

ensures that the disturbance dies away rapidly as we go down into the fluid.

(v) It is also assumed that P is absolutely integrable.

The solution to the problem (i)-(v) may be found in, e.g. Wehausen and Laitone [38].

$$\phi = -\frac{Im}{\pi^2\rho U}\int_{-\infty}^{\infty}\int_{-\infty}^{\infty} d\xi d\eta P(\xi,\eta)\int_0^{\pi/2} d\theta \sec\theta \cdot$$

$$\int_{(bp)}^{\infty} dk \frac{k e^{kz}}{k-\kappa\sec^2\theta} e^{-ik(x-\xi)\cos\theta}\cos(k(y-\eta)\sin\theta) \tag{1.2.11}$$

where (bp) indicates that the path of k-integration goes below the pole at $k = \kappa\sec^2\theta$. Thus, given a pressure distribution P(x,y), we may find ϕ from (1.2.11), and hence the form of the free surface $\zeta(x,y)$ produced by P from (1.2.7).

Now suppose we have a ship, the projection of whose wetted area on the (x,y) plane is W. It is clear that, through its motion, the ship will produce some pressure distribution P(x,y) over W; we assume that atmospheric pressure over the whole free surface is constant and without loss of generality take it to be zero. Hence if we knew this P, we could use (1.2.11) to obtain the disturbance potential produced by a ship moving with constant velocity U as

$$\phi = -\frac{Im}{\pi^2\rho U}\iint_W d\xi d\eta P(\xi,\eta)\int_0^{\pi/2} d\theta \sec\theta \cdot$$

$$\int_{(bp)}^{\infty} dk \frac{k e^{kz}}{k-\kappa\sec^2\theta}\, e^{-ik(x-\xi)\cos\theta}\cos(k(y-\eta)\sin\theta). \tag{1.2.12}$$

It must be noted that (1.2.12) was derived through a procedure which assumed P(x,y) was small, and it is here that we must make our basic supposition clear. This supposition is that we are considering ships of <u>small draft</u>; this is the <u>flatness</u> assumption which leads to the title of this thesis. A flat ship will produce a small disturbance P(x,y), which gives the formal justification for the linearization used in the first part of this section.

Since we are now concerned with a solid body, we must enforce the kinematic boundary condition (1.2.6) over W, where the longitudinal slope ζ_x of the free surface is <u>prescribed</u> as being identical to that of the given hull shape of the ship.

So, applying this boundary condition, we have

$$-U\zeta_x = \lim_{z\uparrow 0} \phi_z$$

$$= -\frac{Im}{\pi^2\rho U}\iint_W d\xi d\eta P(\xi,\eta)\int_0^{\pi/2} d\theta \sec\theta \cdot$$

$$\int_{(bp)}^{\infty} dk \frac{k^2}{k-\kappa\sec^2\theta} e^{-ik(x-\xi)\cos\theta}\cos(k(y-\eta)\sin\theta). \tag{1.2.13}$$

This equation may be treated as an integral equation for the pressure over W if the left hand side (for $(x,y)\in W$) and

W are given. However, there is a degree of non-uniqueness about the problem as may be illustrated by performing an indefinite x-integration of both sides of (1.2.13). This gives

$$U(\zeta(x,y)+C(y)) = \frac{Re}{\pi^2\rho U}\iint_W d\xi d\eta P(\xi,\eta)\int_0^{\pi/2} d\theta \sec^2\theta \cdot$$

$$\int_0^{\infty} dk \frac{k}{k-\kappa\sec^2\theta} e^{-ik(x-\xi)\cos\theta}\cos(k(y-\eta)\sin\theta).$$

(bp)

(1.2.14)

This new equation permits a unique solution when the left hand side is given. The arbitrary function C(y) is ultimately determined from the (Kutta) condition, that the pressure must equal atmospheric pressure (normalized to zero) at the trailing edge. The specific interpretation of C(y) will be discussed in section 1.4.

We now reduce the equation to non-dimensional form, assuming a typical length ℓ is available. Let us define new variables and functions in the following way:

$$\zeta' = \frac{\zeta}{\ell}, \quad \xi' = \frac{\xi}{\ell}, \quad \eta' = \frac{\eta}{\ell},$$

$$x' = \frac{x}{\ell}, \quad y' = \frac{y}{\ell}, \quad k' = k\ell,$$

$$P'(\xi',\eta') = \frac{P(\xi,\eta)}{\frac{1}{2}\rho U^2}, \quad C'(y') = \frac{C(y)}{\ell},$$

W' = W scaled with respect to ℓ. (1.2.15)

Substituting into (1.2.14) and immediately dropping the dashes, we obtain

$$\zeta(x,y)+C(y) = \frac{Re}{2\pi^2}\iint_W d\xi d\eta P(\xi,\eta)\int_0^{\pi/2} d\theta \sec^2\theta \cdot$$

$$\int_{0\,(bp)}^{\infty} dk \frac{k}{k-\gamma\sec^2\theta} e^{-ik(x-\xi)\cos\theta}\cos(k(y-\eta)\sin\theta) \qquad (1.2.16)$$

where $\gamma = \kappa\ell = \frac{g\ell}{U^2}$.

Remembering that the path of k-integration goes below the pole at $k = \gamma\sec^2\theta$, (1.2.16) may be written in terms of a Cauchy principal value integral and a residue, giving on simplification

$$\zeta(x,y)+C(y) = \frac{1}{2\pi^2}\iint_W d\xi d\eta P(\xi,\eta)\{\int_0^{\pi/2} d\theta \sec^2\theta \cdot$$

$$\fint_0^{\infty} dk \frac{k}{k-\gamma\sec^2\theta}\cos(k(x-\xi)\cos\theta)\cos(k(y-\eta)\sin\theta)$$

$$+ \gamma\pi\int_0^{\pi/2} d\theta \sec^4\theta \sin(\gamma(x-\xi)\sec\theta)\cdot$$

$$\cos(\gamma(y-\eta)\sec^2\theta\sin\theta)\}. \qquad (1.2.17)$$

All further references to the general integral equation will be to (1.2.16) or (1.2.17) and therefore implicitly to equations written in terms of the non-dimensional quantities defined in (1.2.15).

1.3 The two-dimensional problem

We now consider a simpler case to that considered in section 1.2, viz. that which applies when the "ship" has infinite width. This being so, there will be no y variation in any quantities under consideration. Thus in (1.2.16); $\zeta(x,y)\to\zeta(x)$, $C(y)\to C$, $P(\xi,\eta)\to P(\xi)$, and the (ξ,η)-integration can be taken from -1 to 1 in the ξ-direction and from $-\infty$ to ∞ in the η-direction (i.e. we are assuming the body to be of length 2ℓ in the longitudinal direction when represented in the dimensional variables).

With these changes, we have

$$\zeta(x) + C = \frac{Re}{2\pi^2}\int_{-1}^{1} d\xi \int_{-\infty}^{\infty} d\eta P(\xi) \int_{0}^{\pi/2} d\theta \sec^2\theta \cdot \int_{0}^{\infty}_{(bp)} dk \frac{k}{k-\gamma\sec^2\theta} e^{-ik(x-\xi)\cos\theta} \cos(k\eta\sin\theta). \tag{1.3.1}$$

Using

$$\int_{-\infty}^{\infty} d\eta \cos(k\eta\sin\theta) = \pi\delta(k\sin\theta)$$

and performing the θ-integration, we obtain

$$\zeta(x) + C = \frac{Re}{2\pi}\int_{-1}^{1} d\xi P(\xi) \int_{0}^{\infty}_{(bp)} \frac{dk e^{-ik(x-\xi)}}{k-\gamma}. \tag{1.3.2}$$

This is the integral equation for a two-dimensional flat ship, or planing surface of infinite aspect ratio. Sretenskii [25] performed some further manipulations before attempting to find a solution, whereas Maruo [11] and the other authors mentioned in section 1.1 deal with equations

which are essentially equivalent to (1.3.2). Solutions of this equation will be obtained in a later section.

1.4 Significance of C and C(y)

The arbitrary function C(y) present in the three-dimensional problem reduces to the constant C in the two-dimensional problem. We shall discuss the significance of this constant first, and then the more general C(y).

Consider a semi-infinite flat plate at an angle of attack, with its trailing edge dipped a distance d into water flowing at velocity U (see Fig. 1.4.1). We could, in fact, perform this experiment, and would expect to find that the wetted length ℓ depended on d. Or, more accurately, we would anticipate a functional relationship of the form

$$F_\ell = f(F_d), \tag{1.4.1}$$

where

$$F_\ell = \frac{U}{(g\ell)^{\frac{1}{2}}} \tag{1.4.2}$$

is the Froude number based on wetted length, and

$$F_d = \frac{U}{(gd)^{\frac{1}{2}}} \tag{1.4.3}$$

is the Froude number based on submergence.

However, in the theory outlined above, we fix not only F_ℓ (through γ) but also $\frac{d}{\ell}$ (through the prescribed ζ) and hence F_d. Our input may therefore not be physically realizable; i.e. it may violate (1.4.1), with $F_\ell \neq f(F_d)$. So the theoretical solution must contain a degree of freedom which permits F_ℓ or F_d to change, and this is manifest in "C". Although we input a $\frac{d}{\ell}$ for a given F_ℓ (we could consider this $\frac{d}{\ell}$ as a "guess"), we get as part of the solution "$\zeta(x)$ + C" which furnishes the <u>correct</u> $\frac{d}{\ell}$. The hull slope is still ζ_x, but our input height of the trailing edge $\zeta(-1)$

is shifted to $\zeta(-1) + C$. We are in effect inverting (1.4.1) to give $F_d = f^{-1}(F_\ell)$; i.e. the theory determines the depth of immersion, given the wetted length.

So we can never get the answer to exactly the situation we specify: the solution shifts our ship up or down by an amount C to ensure the correct vertical position (and, of course, pressure distribution) for our input F_ℓ.

The corresponding experiment in the three-dimensional case would be to take a flat plate of finite span and immerse it at various submergences d (see Fig. 1.4.2). Whereas in the two-dimensional case the wetted length ℓ was determined by d, now the wetted area W, or more specifically the contour Γ of the leading edge is determined by d.

But in the theory leading to the integral equation (1.2.17) we prescribe W and so also Γ. For example, we may take our ship to be a flat plate and our wetted area W to be a rectangle. From physical intuition or simple observation it is clear that this cannot be consistent with an experiment on a flat plate as described above, since the wetted area of a flat plate at a small angle of attack is unlikely to be rectangular.

If we write the integral equation in a symbolic notation and work by analogy from two dimensions, we have

$$\zeta_{soln}(x,y) = \zeta(x,y) + C(y) = \iint_W P(\xi,\eta)K\,d\xi\,d\eta \qquad (1.4.4)$$

where $\zeta_{soln}(x,y)$ = final hull shape (determined by solution)

$\zeta(x,y)$ = input hull shape (incorrect)

$C(y)$ = unknown (determined by solution)

W = given wetted area

$P(\xi,\eta)$ = unknown pressure distribution over W, satisfying $P_{\text{trailing edge}} = 0$

K = kernel of integral equation.

That is, we must assume that if F_ℓ and W are prescribed, then as in two dimensions we cannot exactly prescribe the hull geometry. We are even more strongly restricted than in two dimensions where we had to leave open only the option of vertical bodily movement. Now we must leave open the option of separate and non-equal vertical displacement of each buttock y = constant. In other words, an arbitrary amount of span-wise camber must be determined by the solution, if W is prescribed.

Thus if we try to use a flat plate, we will instead end up with a non-flat body, whose buttocks are still straight lines at constant angle of attack, but whose sections are not flat-bottomed.

As in the two-dimensional case the solution obtained is an inverse one; i.e. we specify the wetted area W and obtain the body. The direct or experimental problem is to specify the true $\zeta(x,y)$, (c.f. $\zeta(x,y) + C(y)$ above) and then determine W; i.e. determine the leading edge contour Γ as part of the problem: one would anticipate great difficulty in solving this direct mathematical problem, involving solution of an integral equation such as (1.2.17) over a region W which is itself unknown! Such integral equations do not seem to have been studied yet, and they present challenging mathematical problems. We shall show later how some progress may be made on the direct problem by adopting

a trial-and-error approach using solutions to the inverse problem.

1.5 Low Froude number limit

If we take the limit $F = F_{\ell} \to 0$ ($\gamma \to \infty$) in (1.2.16) we obtain

$$\zeta(x,y) + C(y) = -\frac{F^2}{2\pi^2} \iint_W d\xi d\eta P(\xi,\eta) \int_0^{\pi/2} d\theta \cdot \int_0^{\infty} dk k \cos(k(x-\xi)\cos\theta)\cos(k(y-\eta)\sin\theta) + O(F^4). \tag{1.5.1}$$

Making the change of variable

$$k_1 = k\cos\theta, \quad k_2 = k\sin\theta$$

we get

$$\zeta(x,y) + C(y) = -\frac{F^2}{2\pi^2} \iint_W d\xi d\eta P(\xi,\eta) \cdot \int_0^{\infty} dk_1 \int_0^{\infty} dk_2 \cos(k_1(x-\xi))\cos(k_2(y-\eta)).$$

The k_1 and k_2 integrals may be performed, giving

$$\zeta(x,y) + C(y) = -\frac{F^2}{2\pi^2} \iint_W d\xi d\eta P(\xi,\eta) \cdot \pi\delta(x-\xi)\pi\delta(y-\eta). \tag{1.5.2}$$

Hence we may now solve the integral equation trivially:

$$\zeta(x,y) + C(y) = \begin{cases} -\tfrac{1}{2}F^2 P(x,y) & (x,y) \in W \\ 0 & (x,y) \notin W. \end{cases} \tag{1.5.3}$$

The situation is clearer if we return to the dimensioned variables, namely

$$\zeta(x,y) + C(y) = \begin{cases} -\dfrac{P(x,y)}{\rho g} & (x,y)\in W \\ 0 & (x,y)\notin W, \end{cases}$$

or

$$P(x,y) = \begin{cases} -\rho g(\zeta(x,y)+C(y)) & (x,y)\in W \\ 0 & (x,y)\notin W. \end{cases} \quad (1.5.4)$$

The arbitrary function C(y) is determined by the condition that P = 0 along the trailing edge of the body. For example, if the trailing edge was a straight line at x = 0, we would obtain

$$P(x,y) = \begin{cases} -\rho g(\zeta(x,y)-\zeta(x,0)) & (x,y)\in W \\ 0 & (x,y)\notin W. \end{cases} \quad (1.5.5)$$

We could simply write the solution in the symbolic notation of (1.4.4) as

$$P(x,y) = \begin{cases} -\rho g\zeta_{\mathbf{soln}}(x,y) & (x,y)\in W \\ 0 & (x,y)\notin W. \end{cases} \quad (1.5.6)$$

where $\zeta_{\mathbf{soln}}$ is the actual hull shape given by the solution. Written in this way, we see that we have found that in the limit as the Froude number tends to zero, the pressure becomes purely hydrostatic.

There is, however, some ambiguity if the ship has a vertical face at its trailing edge, e.g. a transom stern of depth h. In this case the physical pressure is <u>multivalued</u> as a function of x and y, varying between zero and ρgh for any fixed (x,y) which lies on the stern. Similarly the hull function ζ(x,y) is multivalued on the stern and so inclusion of ζ(x,0) in (1.5.5) cannot serve to accurately define a

solution pressure. Though this dilemma has been presented in terms of the low Froude number limit, it is of course relevant to flow at any Froude number.

Most authors either ignore the above difficulty or resolve it in an ad hoc manner. For example, Squire [24], when he deals with the motion of a two-dimensional wedge along a water surface, assumes that, for all speeds above zero, the water breaks smoothly away from the bottom edge, and the rear face is unwetted. He does, however, consider the validity of this assumption in practice, and uses a rough analysis based on trailing wave height to conclude that it is true if $U(gh)^{-\frac{1}{2}} > 1.5$ where U is the velocity of the wedge and h the depth of immersion.

In "non-flat" theory the above problems would not arise since P would be a function of x,y and z and so be unambiguously defined at all points on a transom stern. Within the framework of such a theory it would be of interest to investigate whether there exists a definite transition from flow which wets the rear face of a transom stern (as is the case at zero speed), to a flow which leaves the hull smoothly as assumed by Squire. Should such a transition point be found (presumably as a function of hull shape and Froude number), it could be used as a definition of passage from a non-planing to a planing regime.

Some authors have investigated the specific problem of the flow at an attachment or separation point, i.e. at an air/water/solid interface. However, with regard to ships, most authors have been interested in studying attachment at the bow, specifically with regard to prediction of the onset

of a bow wave and the resultant wave-breaking resistance (see e.g. Dagan and Tulin [5]). In an attempt to resolve both this problem and that mentioned in the previous paragraph, some work was carried out on the application of the complete non-linear equations to the flow at an attachment or separation point. A brief report on this work is given in Chapter 4.

1.6 The high Froude number limit

The limit $F\to\infty$ does not afford as simple a result as the limit $F\to 0$ considered in section 1.5, and in particular, we are still left with an integral equation to find P. Letting $F\to\infty$ ($\gamma\to 0$) in (1.2.17) we obtain

$$\zeta(x,y) + C(y) = \frac{1}{2\pi^2}\iint_W d\xi d\eta P(\xi,\eta)(I+J) + O(F^{-2}) \qquad (1.6.1)$$

where

$$I = \int_0^{\pi/2} d\theta \sec^2\theta \int_0^\infty dk \cos(k(x-\xi)\cos\theta)\cos(k(y-\eta)\sin\theta)$$

and

$$J = \lim_{\gamma\to 0} \gamma\pi \int_0^{\pi/2} d\theta \sec^4\theta \sin(\gamma(x-\xi)\sec\theta)\cdot \cos(\gamma(y-\eta)\sec^2\theta\sin\theta).$$

We may perform the k-integration in I giving

$$I = \frac{\pi}{2}\int_0^{\pi/2} d\theta \sec^2\theta\{\delta((x-\xi)\cos\theta+(y-\eta)\sin\theta) + \delta((x-\xi)\cos\theta-(y-\eta)\sin\theta)\}$$

$$= \frac{\pi}{2}\frac{[(x-\xi)^2 + (y-\eta)^2]^{\frac{1}{2}}}{(y-\eta)^2}. \qquad (1.6.2)$$

Making the change of variable $\lambda = \gamma\sec^2\theta$ we obtain

$$J = \lim_{\gamma\to 0} \frac{\pi}{\gamma^{\frac{1}{2}}}\int_\gamma^\infty d\lambda \tfrac{1}{2}(\lambda-\gamma)^{-\frac{1}{2}}\lambda \sin((\lambda\gamma)^{\frac{1}{2}}(x-\xi))\cdot \cos((y-\eta)(\lambda(\lambda-\gamma))^{\frac{1}{2}})$$

$$= \tfrac{1}{2}\pi(x-\xi)\int_0^\infty d\lambda\lambda\cos((y-\eta)\lambda)$$

$$= -\frac{\pi(x-\xi)}{2(y-\eta)^2}. \quad * \qquad (1.6.3)$$

Combining (1.6.1), (1.6.2) and (1.6.3) we get as the result of our limiting process

$$\zeta(x,y) + C(y) = \frac{1}{4\pi} \iint_W d\xi d\eta P(\xi,\eta) \frac{[(x-\xi)^2+(y-\eta)^2]^{\frac{1}{2}}-(x-\xi)}{(y-\eta)^2} . \qquad (1.6.4)$$

As we should expect, following the work of Wagner [35], we obtain (except for a factor of ½), an x-integrated form of the downwash integral equation for a thin wing (see e.g. Thwaites [28]). That is, the pressure on the bottom of a ship planing at infinite Froude number is half the loading on a thin wing of equivalent longitudinal slope.

* Note added by supervisor: The candidate has provided a more-rigorous derivation of this result.

E. O. Tuck
13/1/76

CHAPTER 2

TWO-DIMENSIONAL PLANING

2.1 Introduction

When studying a general three-dimensional problem in fluid mechanics, an approach often taken is to reduce the problem to two dimensions, in the hope that the resulting equations will be easier to solve and will on solution give some insight into methods for attacking the full three-dimensional case. This will now be done for the three-dimensional planing problem under consideration.

As can be seen from equations (1.2.16) and (1.3.2), reduction of the three-dimensional equations to two dimensions has dramatically decreased the complexity of the kernel of the integral equation. In fact, as will be shown in section 2.2, the two-dimensional kernel can be expressed directly in terms of well-known functions, whereas calculation of the three-dimensional kernel involves numerical integration of the infinite integral of a highly oscillatory function - always a difficult operation.

However, one should not look on the two-dimensional approximation in the above light only; it is of use in its own right. When considering flow about bodies whose beam to length ratio is large, it is clear from physical intuition that the flow over most of the hull will be predominantly longitudinal. Variation from this will be significant only near and at the spanwise edges. Hence we would expect to be able to solve the flow problem for such

a high aspect ratio body by dividing it into longitudinal strips of fixed length, and applying two-dimensional theory to these strips. Shen [23] adopts essentially this approach in developing a theory of high aspect ratio planing surfaces.

While we basically treat the two-dimensional problem as a simplified lead-in to the much more complex three-dimensional problem, we shall, in later sections, mention how our results could be applicable to the motion of high aspect ratio planing craft.

2.2 Numerical scheme

The equation we wish to solve is (1.3.2), which we repeat, replacing k by λ:

$$\zeta(x) + C = \frac{Re}{2\pi} \int_{-1}^{1} d\xi P(\xi) \int_{o}^{\infty} \frac{d\lambda}{\lambda-\gamma} e^{-i\lambda(x-\xi)} \qquad (2.2.1)$$
$$(bp)$$

Let us split the interval $[-1,1]$ into n subintervals $[x_j, x_{j+1}]$, $j = 1,..,n$. Suppose that the pressure coefficient $P(x)$ is approximated by a constant P_j over the j-th subinterval for $j = 1,...,n$. If ζ_k gives some average value of the hull function $\zeta(x)$ over the k-th subinterval, we may write (2.2.1) in approximate form as

$$\zeta_k + C = \sum_{j=1}^{n} P_j A_{kj} \qquad k = 1,...,n \qquad (2.2.2)$$

where
$$A_{kj} = \frac{Re}{2\pi} \int_{x_j}^{x_{j+1}} d\xi \int_{o}^{\infty} \frac{d\lambda}{\lambda-\gamma} e^{-i\lambda(x_k-\xi)}. \qquad (2.2.3)$$
$$(bp)$$

After performing the ξ-integration, some algebraic manipulation and reduction to a Cauchy principal value integral and residue term, we obtain

$$A_{kj} = \frac{1}{2\pi\gamma} \Bigg[\int_{o}^{\infty} \frac{d\lambda}{\lambda} \sin(\lambda(x_k-\xi)) - \int_{o}^{\infty} \frac{d\lambda}{\lambda-\gamma} \sin(\lambda(x_k-\xi)) + \pi\cos(\gamma(x_k-\xi)) \Bigg]_{x_j}^{x_{j+1}}. \qquad (2.2.4)$$

The first integral is simply $\frac{\pi}{2}\mathrm{sgn}(x_k-\xi)$. The second integral

is $\mathrm{sgn}(x_k-\xi)\{f(\gamma|x_k-\xi|)\}e^{-\pi\cos(\gamma(x_k-\xi))}$ where $f(z)$ is defined in Abramowitz and Stegun [1], p.232, and is given by

$$f(z) = Ci(z)\sin(z) - si(z)\cos(z) \qquad (2.2.5)$$

where Ci and si are the Cosine and Sine integral respectively, defined as

$$Ci(z) = -\int_z^\infty \frac{dt}{t}\cos(t),$$

and

$$si(z) = -\int_z^\infty \frac{dt}{t}\sin(t).$$

Useful numerical approximations for the f-function are given in Abramowitz and Stegun, p.233.

We shall now give the final form of the equations which will be used to solve the two-dimensional flat ship problem. They are

$$\zeta_k + C = \sum_{j=1}^{n} P_j A_{kj} \qquad k = 1,\ldots,n, \qquad (2.2.6)$$

$$A_{kj} = \frac{1}{2\pi\gamma}\{g(\gamma(x_k-x_{j+1}))-g(\gamma(x_k-x_j))\}$$

where

$$g(x) = \begin{cases} \frac{\pi}{2} + f(x) & x\geq 0 \\ -\frac{\pi}{2} - f(-x) + 2\pi\cos(x) & x<0, \end{cases} \qquad (2.2.7)$$

and

$$P_1 = 0. \qquad (2.2.8)$$

This last condition (2.2.8) is the Kutta condition at the trailing edge, namely that the unknown pressure should equal atmospheric pressure at this edge. This is a very important condition, for without it (2.2.6) would be a system of n

linear equations in the $n+1$ unknowns $C, P_1, P_2, \ldots, P_n$ and so not have a unique solution.

Equation (2.2.6) can be written in matrix form as

$$\begin{bmatrix} A_{11} & A_{12} & \cdots & A_{1n} \\ A_{21} & A_{22} & \cdots & A_{2n} \\ \vdots & \vdots & & \vdots \\ A_{n1} & A_{n2} & \cdots & A_{nn} \end{bmatrix} \begin{bmatrix} P_1 \\ P_2 \\ \vdots \\ P_n \end{bmatrix} = \begin{bmatrix} \zeta_1 \\ \zeta_2 \\ \vdots \\ \zeta_n \end{bmatrix} + \begin{bmatrix} C \\ C \\ \vdots \\ C \end{bmatrix}. \qquad (2.2.9)$$

Since $P_1=0$, the values A_{i1}, $i = 1,\ldots,n$ are of no significance and need not (and therefore should not) be calculated. We can in fact replace P_1 by C and A_{i1}, $i = 1,\ldots,n$ by -1's to obtain

$$\begin{bmatrix} -1 & A_{12} & \cdots & A_{1n} \\ -1 & A_{22} & \cdots & A_{2n} \\ \vdots & \vdots & & \vdots \\ -1 & A_{n2} & \cdots & A_{nn} \end{bmatrix} \begin{bmatrix} C \\ P_2 \\ \vdots \\ P_n \end{bmatrix} = \begin{bmatrix} \zeta_1 \\ \zeta_2 \\ \vdots \\ \zeta_n \end{bmatrix} \qquad (2.2.10)$$

which is <u>entirely equivalent</u> to $\{(2.2.9) + (P_1 = 0)\}$ and is now in the standard form for a set of n linear equations in the n unknowns $C, P_2, \ldots, P_n$.

This solution procedure differs from that previously adopted (e.g. by Taylor [27], Tuck and Newman [32], Tuck [30]) for such equations, where (2.2.9) is solved as two separate equations, with right hand sides of $\underset{\sim}{\zeta}$ and $\underset{\sim}{1}$, giving solutions $\underset{\sim}{P}^1$ and $\underset{\sim}{P}^2$. The final solution for

$\underset{\sim}{P}$ is $\underset{\sim}{P}^1+C\underset{\sim}{P}^2$, with C found from the condition that $P_1 = P_1^1 + CP_1^2 = 0$. However, with the present solution procedure, some unnecessary calculations are eliminated and the desired solution for $\underset{\sim}{P}$ and C found in one inversion.

One specific question which must be considered is the choice of the partitioning $[x_j,x_{j+1}]$ of the interval $[-1,1]$. Equal subintervals are convenient computationally, but our choice should be examined in the light of the assumptions involved in deriving (2.2.10). The basic assumption is that pressure is constant over each subinterval. We know from other numerical and experimental results that the pressure tends to be rapidly changing near the ends of the body and more slowly changing near the middle. Therefore, in order to satisfy our assumption as closely as possible, we should adopt subintervals which are clustered near the ends. Such a set of subintervals can be simply defined by taking the endpoint of the j-th subinterval to be $x_{j+1} = -\cos(j\pi/n)$.

A computer program was written in FORTRAN to solve the problem. The inputs to the program are the number of subintervals n, $\gamma = F^{-2}$ and the hull shape ζ_k, $k = 1,\ldots,n$, where ζ_k was taken as the value of the hull function $\zeta(x)$ at the points $x_k = -\cos((k-\frac{1}{2})\pi/n)$, $k = 1,\ldots,n$. One output is the constant C, which gives the amount by which the given hull shape must be moved vertically to give the position of the solution hull shape. The other outputs are the pressure coefficients, lift coefficient, moment coefficient and centre of pressure coefficient on the solution hull, where these quantities have the following

meanings:

$$\text{pressure coefficient} = \text{dimensional pressure}/\tfrac{1}{2}\rho U^2$$
$$= P(x)$$

$$\text{lift coefficient} = \int_{-1}^{1} P(x)dx$$
$$= \text{dimensional lift per unit span} / \tfrac{1}{2}\rho U^2 \ell$$

$$\text{moment coefficient} = \int_{-1}^{1} xP(x)dx$$
$$= \text{dimensional (bow up) moment about centre of wetted length per unit span} / \tfrac{1}{2}\rho U^2 \ell^2$$

centre of pressure

$$\text{coefficient} = \frac{\text{moment coefficient}}{\text{lift coefficient}}$$
$$= \text{location of centre of pressure ahead of centre of wetted length / half wetted length.}$$

The results obtained using this program for particular choices of (n,γ,ζ) are given in the following sections.

2.3 The flat plate

In this section we consider the situation when $\zeta(x)=\alpha x$; i.e. when the body is a flat plate at angle of attack α. We assume that the water leaves the trailing edge smoothly. As mentioned before, Squire [24] considers the validity of this assumption, and gives an analysis based on trailing wave height to deduce that the flow will leave smoothly so long as the Froude number based on trailing edge height is greater than 1.5.

Note that throughout this section the pressure, lift and moment coefficients are the respective quantities defined in section 2.2, divided by α.

It was found that the rapidity of convergence with respect to n of the numerical scheme described in section 2.2 increased with Froude number. For $F=1.0$ ($\gamma=1.0$) the integrated quantities (lift and moment coefficients) were already within 5% of their converged values for $n=10$.

Results presented are for $n=50$ for which the integrated quantities are within 0.2% of converged values for all $\gamma<25$ ($F>0.2$). Computing time on a CDC6400 for this value of n was approximately 2 seconds for each value of γ.

The pressure coefficient for various values of γ is given in Fig. 2.3.1. Fig. 2.3.2 gives a plot of pressure coefficient/lift coefficient so that the area under each curve is equal, and changes in shape of the pressure distribution with γ are more easily seen. The hydrostatic pressure/lift distribution corresponding to $U=0$ ($\gamma\to\infty$) is also shown.

Since our method has converged, it represents in principle an exact solution of the relevant equation. It is therefore of interest to compare our results with those

of other authors, particularly those who use series or asymptotic methods. Maruo [11] and Squire [24] both use a series to approximate the pressure distribution: the former uses six terms and considers values of γ up to 0.5, whereas the latter retains only four terms. It was found that Maruo's results for $\gamma=0.5$ corresponded very closely to our own, but Squire's differed by up to 25% (see Fig. 2.3.3), showing the accuracy lost in retaining fewer terms. Cumberbatch [4] adopts a high Froude number approach and uses a series in terms of $\gamma=F^{-2}$. He considers results for γ up to 0.1. We found that his results for the pressure distribution at $\gamma=0.1$ give values within 7% of ours, but consistently higher. Doctors' [6] use of finite pressure elements gives converged results identical to our own.

As we have stressed, our basic approach is an inverse one, and in this spirit we give graphs of the raw integrated output of our program based on a fixed wetted length. These are graphs of the lift, moment and centre of pressure coefficients and scaled trailing edge height as functions of Froude number, presented in Figs. 2.3.4 - 2.3.6. Note that the last-mentioned quantity is $h/\ell\alpha=C+\zeta(-1)$, where h is the dimensional height of the trailing edge, C is the constant found as part of the solution and $\zeta(-1)$ is the input height of the trailing edge assuming $\alpha=1$ and the wetted length equals 2. These graphs are interesting in themselves, but we can obtain results which are more meaningful physically if we perform some further manipulations with our output data. Although we actually input to the program the quantity $\gamma=g\ell/U^2$, the wetted length 2ℓ is, as pointed out in section 1.3,

essentially an unknown and should instead be found as part of the solution.

To fix ideas, we consider three specific situations involving flow on a flat plate - two "experimental" and one "practical". In Fig. 2.3.7 are represented two possible idealized experimental set-ups. In the first a rigidly-held wedge-shaped body is subject to uniform flow, with the height of the trailing edge fixed. In this case we can take α and h as given quantities. In the second experiment we have a flat bottomed body of fixed weight and angle of attack which is constrained so that it can only move vertically without rotation. Here α and L are given. Since, in the second experiment, we could, when a certain h is attained, clamp the wedge and vary U, it is clear that the first experiment is in a sense a variation of the second. Because of this we will consider the second experiment first.

This situation is in fact the one treated by Squire, who assumes L, ρ, g and α are known and constructs a non-dimensional speed parameter, $V=U(\rho\alpha/gL)^{\frac{1}{4}}$. However, we may simply observe that, at rest, $L=\frac{1}{2}\rho g\alpha(2\ell_0)^2$ where $2\ell_0$ is the wetted length at rest. Since L and α are fixed we may adopt ℓ_0 as a reference length (c.f. ℓ in raw output) and define the Froude number based on this length as $F_0=U/(g\ell_0)^{\frac{1}{2}}$. It follows that

$$U/(g\ell_0)^{\frac{1}{2}} = U/(\tfrac{1}{2}g(\frac{2L}{\rho g\alpha})^{\frac{1}{2}})^{\frac{1}{2}} = U(\frac{2\rho\alpha}{gL})^{\frac{1}{4}} = 2^{\frac{1}{4}}V.$$

From the computer output we get pairs of values of $L/\frac{1}{2}\rho U^2\alpha\ell$ and $g\ell/U^2$. We may, from these pairs, deduce a

functional relationship

$$\frac{g\ell}{U^2} = f(2^{\frac{1}{2}}/(\frac{g\ell}{U^2}\cdot\frac{L}{\frac{1}{2}\rho U^2\alpha\ell})^{\frac{1}{4}}) = f(F_0).$$

Introducing ℓ_0 again, to scale ℓ, we get

$$\frac{\ell}{\ell_0} = \frac{U^2}{g\ell_0}f(F_0) = F_0^2\ f(F_0).$$

Another output is $h/\ell\alpha=C+\zeta(-1)$. If h_0 is the trailing edge height at rest, then $h_0=-2\ell_0\alpha$ and

$$\frac{h}{h_0} = \frac{h}{\ell\alpha}\cdot\frac{\ell_0\alpha}{h_0}\cdot\frac{\ell}{\ell_0} = -\ (C+\zeta(-1))\cdot\tfrac{1}{2}\cdot F_0^2 f(F_0).$$

So in the foregoing manner we can, from our output, find $\frac{\ell}{\ell_0}$ and $\frac{h}{h_0}$ as functions of F_0. This is essentially a trial-and-error approach, since, for our input γ, we do not know what the value of F_0 will be, and so cannot, in a direct calculation, find $\frac{\ell}{\ell_0}$ and $\frac{h}{h_0}$ for a chosen F_0.

What we can do, however, is to run the program for many values of γ and obtain a series of values of F_0 from which we can obtain a plot of $\frac{\ell}{\ell_0}$ and $\frac{h}{h_0}$ against F_0.

This has been done and we present the results in Fig. 2.3.8, with some comparison points from Squire's results.
Fig. 2.3.9 gives a graph of F_0 against F and this may be used in conjunction with Fig. 2.3.1 to get an idea of the pressure distribution for any particular F_0.

We can now see what happens when a flat plate planes at fixed lift and angle of attack. For speeds just above zero, the pressure drop at the stern (see Fig. 2.3.2) is

not fully compensated by the pressure rise at the bow and so the body initially lowers in the water. This is shown in Fig. 2.3.8 as an initial increase in both wetted length and immersion. However, as speed rises, the pressure increases and so the plate lifts in the water. The accompanying decrease in wetted length moderates this lifting effect and as speed gets large both the trailing edge height and wetted length tend to zero.

This tendency of the wetted length to zero has interesting implications when considering investigations such as that of Green [7], where it is assumed that $F=U/(g\ell)^{\frac{1}{2}}\to\infty$ with ℓ fixed. As we have shown, such a limit is of doubtful physical validity, although it should still give results for the pressure distribution which are accurate at high speed. However, the well-known result which follows from Green's analysis that the free surface falls away logarithmically to a negative infinity is a peculiarity of the formulation of the problem. Alternatively, we can observe that although the ratio "trailing edge height/wetted length" does tend to a positive infinity, both the trailing edge height and the wetted length separately tend to zero (c.f. Figs. 2.3.6, 2.3.8).

We now return to the first experimental case of a rigidly-fixed wedge. Our experimental procedure must involve starting with the wedge below the surface of the water and gradually raising it, letting the flow settle down for each fixed h. We might expect, however, that if we raise the wedge above the level of the undisturbed free surface, i.e. make h positive, the flow will remain

attached only for U greater than some minimum speed.

Since the dimensional height h and the angle of attack α are fixed, it is convenient to define a Froude number based on this height as $F_h=U(\alpha/g|h|)^{\frac{1}{2}}$. The change in pressure distribution with F_h can be found using Figs. 2.3.9 and 2.3.1. We have as an output of our program $h/\ell\alpha=C+\zeta(-1)$, where this quantity is associated with a known $\gamma=g\ell/U^2$. From these pairs of values we may deduce a functional relationship

$$1/(\frac{h}{\ell\alpha}) = f(1/(\frac{g\ell}{U^2}.\frac{|h|}{\ell\alpha})^{\frac{1}{2}}),$$

i.e.
$$\frac{\ell\alpha}{h} = f(F_h).$$

That is, essentially we have wetted length as a function of speed, with α and h serving as scaling factors. A graph of this relationship is given in Fig. 2.3.10. Since the scaling involves division by h, both independent and dependent variables tend to plus infinity as h passes through zero. We can, however, deduce from Fig. 2.3.6 that where this occurs $\ell\simeq0.014U^2$ metres and so the graphs for $h<0$ and $h>0$ will both approach a parabola.

If we took a fixed U and gradually raised the wedge (increased h, starting with a negative value), we would "follow" the first curve out to infinity ($h=0$) and then "return" along the second. However, as anticipated, we see that we cannot raise the wedge indefinitely: there is in fact a minimum for $U(\alpha/g|h|)^{\frac{1}{2}}$ when $h>0$. That is, for a flow to exist with the wedge above the free surface, we must have $U(\alpha/g|h|)^{\frac{1}{2}}>3.75$. Also, we see that the remainder

of the curve, shown dashed, is not attainable if we adopt the experimental procedure outlined above: as we increase h at fixed U, or decrease U at fixed h, we always follow the curve down to the turning point and "lose" the flow.

It is, however, attainable if we use the second experimental apparatus. We have indicated on Fig. 2.3.10 the approximate position corresponding to maximum height which occurs in Fig. 2.3.8 at $F_0 \simeq 2.4$. Clearly if we were to let the moving wedge reach this position, clamp it (fix h) and then vary U, we would be following the lower curve. In fact we need not wait until the maximum height occurs. As shown in Fig. 2.3.10 the turning point occurs at $F_0 \simeq 2.0$ and so we could clamp the wedge for any higher F_0 and be on the lower curve.

Considering again the fixed wedge, we see that when $h<0$, wetted length increases with speed. This is also true if we are on the upper part of the $h>0$ curve. However, if we have manoeuvred ourselves onto the lower part and fixed h, we see that wetted length <u>decreases</u> with speed.

It is of interest to consider the relevance of the present study to real high-speed planing boats. In practice we know that if such a planing boat has a wetted area of moderate aspect ratio in the resting condition, as it approaches operating speed the wetted length decreases markedly while the wetted span remains constant. Hence the operational wetted area is of high aspect ratio - we might say the boat is "flying on a line". As mentioned in the

Introduction to this Chapter, the study of two-dimensional flow is applicable to high aspect ratio bodies and for this reason we will conduct a brief investigation into practical aspects of our results as they would apply to a flat-bottomed planing boat.

While we can still assume that L is constant, we now wish to treat α, h and ℓ all as unknowns and determine them as functions of U. In order to fix a length scale, we shall presume now that the position of the centre of gravity is a fixed distance X ahead of the trailing edge, and equate this to the position of the centre of pressure. One of our raw computer outputs is the "centre of pressure coefficient" defined in section 2.2 which we shall call COFP. The dimensional distance of the centre of pressure ahead of the trailing edge is then $X=(COFP+1)\ell$. We adopt a Froude number based on X given by

$$F_X = F/(COFP+1)^{\frac{1}{2}} = U/(gX)^{\frac{1}{2}}.$$

Figs. 2.3.9 and 2.3.1 may be used to find the change in pressure distribution with F_X. The wetted length, scaled with respect to X, is

$$WLX = \frac{2\ell}{(COFP+1)\ell} = \frac{2}{COFP+1}.$$

The lift coefficient is $L = L/\frac{1}{2}\rho U^2 \alpha \ell$; hence

$$\begin{aligned}\alpha &= \frac{L}{\frac{1}{2}\rho U^2 \ell L} \\ &= \frac{L}{\frac{1}{2}\rho U^2 \ell L}\cdot\frac{U^2 gX}{U^2 gX}\cdot\frac{COFP+1}{COFP+1} \\ &= \frac{L}{\frac{1}{2}\rho g X^2}\cdot\frac{1}{F_X^2}\cdot\frac{2}{WLX}\cdot\frac{1}{L}\end{aligned}$$

i.e. $$(\frac{\frac{1}{2}\rho g X^2}{L})\alpha = \frac{2}{F_X^2 \cdot WLX \cdot L} .$$

Another raw output is $\frac{h}{\ell\alpha}$; hence we can find

$$(\frac{\frac{1}{2}\rho g X}{L})h = \frac{h}{\ell\alpha} \cdot \frac{\frac{1}{2}\rho g X^2}{L}\alpha \cdot \frac{1}{COFP+1}$$

for a particular F_X.

That is, we can find $\frac{2\ell}{X}$, $(\frac{\frac{1}{2}\rho g X^2}{L})\alpha$ and $(\frac{\frac{1}{2}\rho g X}{L})h$ as functions of F_X. These are graphed in Figs. 2.3.11, 2.3.12 and 2.3.13. A further quantity of interest is the ratio of dynamic lift to total lift. If we define static lift as that due to the water displaced below the equilibrium free surface level, we have

$$\text{static lift (SL)} = \tfrac{1}{2}\rho g h^2/\alpha$$

$$= L((\frac{\frac{1}{2}\rho g X}{L})^2 h^2/((\frac{\frac{1}{2}\rho g X^2}{L})\alpha))$$

$$= L((\text{scaled } h)^2/(\text{scaled } \alpha)).$$

Hence $$\frac{\text{dynamic lift}}{\text{total lift}} = \frac{L-SL}{L}$$

$$= 1 - (\text{scaled } h)^2/(\text{scaled } \alpha).$$

This quantity is graphed in Fig. 2.3.14. We stop the graph when $h=0$ since our definition of static lift is of doubtful significance when $h>0$. From the figure we see that at first (low speed) the dynamic lift as defined is negative (a sinkage force), i.e. the dynamic effects decrease the lift when considered separately from the static forces. However, as F_X nears one, the dynamic

lift increases dramatically and rapidly dominates the flow.

We will now, using Figs. 2.3.11 - 2.3.14 follow the course of a flat-bottomed boat as U goes from zero to large values. As U increases from zero, the trailing edge of the boat lowers considerably, the angle of attack increases and the wetted length decreases. As the speed rises, the trailing edge height passes through a (negative) minimum just before the angle of attack reaches a maximum. The height then rapidly increases again, the angle of attack falls and the wetted length settles down to a constant value of 4/9 of the wetted length at rest. The angle of attack continues to decrease while the height reaches a (positive) maximum just above the equilibrium free surface level and then very gradually falls to zero as U gets very large.

Note that the rapid rise in trailing edge height, fall in the angle of attack and levelling off in wetted length all occur near $F_X=1$. These effects are also mirrored in Fig. 2.3.14, where we see, as mentioned before, that near this value of F_X the dynamic lift rapidly becomes the reigning force in the flow: it is interesting to note that the dynamic and static lifts are equal at $F_X\simeq 1.08$. It would seem reasonable to associate all these occurrences with the onset of "planing". Thus if we are in a craft which is "nearly" planing, one way to initiate planing is to strive to increase F_X. This result is corroborated by the experience of yachtsmen, who know that if planing seems imminent, it helps if all the crew rush to the back of the boat: this serves to decrease X and thereby increase F_X.

We now give two cases in which values are assigned to L and X: we approximate these for a large speedboat and a small yacht and calculate quantities of interest.

First take L=400×9.8 newtons/metre span (i.e. mass = 400 kg/metre span) and $X = \frac{8}{3}$ metres. The wetted length at rest is 8 metres, since at rest the centre of pressure is $\frac{1}{3}$ of the distance to the bow. Then we may produce from our graphs the following table of events of interest.

Event	F_X U	m/sec (knots)	wetted length	α (deg)	h(m)
Squire's limit	0.63	3.22 (6.25)	6.67	1.83	-0.186
maximum sinkage	0.75	3.83 (7.44)	5.87	2.75	-0.231
minimum h	0.85	4.35 (8.45)	4.80	4.13	-0.267
dynamic lift = 0	0.92	4.70 (9.13)	4.21	4.64	-0.252
maximum α	0.95	4.86 (9.44)	4.00	4.70	-0.240
dynamic = static lift (planing begins?)	1.08	5.52 (10.72)	3.65	3.95	-0.162
h=0	2.20	11.25 (21.85)	3.47	0.57	0
maximum h	3.35	17.13 (33.28)	3.52	0.17	+0.006

Secondly, we take L=75×9.8 newtons/metre span and X=1.2 metres. The corresponding table is:

Event	F_X	U m/sec (knots)	wetted length	α (deg)	h(m)
Squire's limit	0.61	2.09 (4.06)	3.10	1.55	-0.075
maximum sinkage	0.75	2.57 (4.99)	3.00	2.58	-0.096
minimum h	0.85	2.92 (5.67)	2.16	3.84	-0.111
dynamic lift = 0	0.92	3.16 (6.14)	1.90	4.30	-0.105
maximum α	0.95	3.26 (6.33)	1.80	4.35	-0.100
dynamic = static lift (planing begins?)	1.08	3.70 (7.19)	1.64	4.18	-0.068
h=0	2.20	7.54 (14.65)	1.56	0.52	0
maximum h	3.35	11.49 (22.32)	1.58	0.17	+0.003

Suppose this yacht is travelling with F_X=0.9 (U=3.9 m/sec; 6 knots): we are then in the transition region prior to planing. If the crew moves back so that X decreases from 1.2 metres to 0.6 metres the following changes occur (at fixed speed). F_X increases from 0.9 to 1.27 (well into the planing region), the wetted length decreases from 1.92 metres to 0.78 metres, the angle of attack increases from 4.2° to 10.5° and the trailing edge height increases from -0.11 metres to -0.08 metres. Note in particular that the wetted length decreases to less than half, thereby decreasing the friction drag in about the

same ratio. This should result in a substantial increase in U, giving a further increase in F_X and putting the boat more certainly in the planing regime.

2.4 The parabola

In this section we will be concerned with the hull shape $\zeta = \alpha(x+a)^2$, $x \in [-1,1]$, for various values of a. When considering the flat plate, not only was it assumed that the fluid left the trailing edge smoothly, but also tacitly that the fluid remained attached to the hull until it left this trailing edge. However, when considering curved hull shapes, the situation is no longer so clear. For example, if we had the hull shape with $a = 0$ which has its lowest point amidships $(x=0)$, then it seems likely that, at least at high speed, the fluid will not remain attached beyond the low point and may in fact detach even before this. The difficult question is to decide where detachment actually occurs on a smooth hull such as a parabola.

Doctors [6] gives graphs of the pressure distribution for $a=1$ in which the trailing edge is the lowest point, and finds that for low values of γ regions of negative pressure occur near the trailing edge. Our program confirms Doctors' results and we give graphs of pressure coefficient/lift coefficient in Fig. 2.4.1. Note that the flow is assumed to remain attached until the lowest point of the parabola is reached. This may not be valid physically and therefore the occurrence of negative pressure must be treatment with some scepticism.

In an attempt to clarify the situation we introduce a condition often cited in separation problems involving cavities (see e.g. Milne-Thomson [15], p.318): we assume a priori that smooth separation occurs with constant curvature, i.e. the curvature of the free surface immediately after

separation is equal to the curvature of the body at the separation point. In order to obtain a formula for the curvature we start with our basic two-dimensional integral equation (equation 2.2.1)), and write the kernel in a new form:

$$\zeta(x) + C = \frac{Re}{2\pi}\int_{-1}^{1} d\xi P(\xi)\int_{0}^{\infty}\frac{d\lambda}{\lambda-\gamma}e^{-i\lambda(x-\xi)}$$

(bp)

$$= \frac{1}{2\pi}\int_{-1}^{1} d\xi P(\xi)\{\int_{0}^{\infty}\frac{d\lambda}{\lambda-\gamma}\cos(\lambda(x-\xi))+\pi\sin(\gamma(x-\xi))\}$$

$$= \frac{1}{2\pi}\int_{-1}^{1} d\xi P(\xi)\{g(\gamma|x-\xi|)-\pi\sin(\gamma|x-\xi|)$$

$$+\pi\sin(\gamma(x-\xi))\} \qquad (2.4.1)$$

where the g-function is defined in Abramowitz and Stegun [1] p.232, and has as one of its integral representations

$$g(z) = \int_{0}^{\infty}\frac{t}{t^2+1}e^{-zt}dt.$$

Using this form for g it can easily be shown that

$$g''(z) = \frac{1}{z^2} - g(z).$$

We now differentiate both sides of (2.4.1) to get, for $x<-1$

$$\zeta''(x) = \frac{1}{2\pi}\int_{-1}^{1} d\xi P(\xi)\{\frac{1}{(\xi-x)^2} - \gamma^2 g(\gamma(\xi-x))+\gamma^2\pi\sin(\gamma(\xi-x))\}$$

$$= \frac{1}{2\pi}\int_{-1}^{1}\frac{P(\xi)d\xi}{(\xi-x)^2} - \gamma^2(\zeta(x)+C). \qquad (2.4.2)$$

Hence, in order to obtain the exact value of the curvature we need to know the solution pressure P and the constant C. Such a solution is available in closed form only for the case $\gamma = 0$, when the first derivative of (2.4.1) gives a finite Hilbert transform which may be inverted directly. If we adopt the general hull shape given by $\zeta=\alpha(x+a)^2$, $x\in[-1,1]$ with its lowest point at $x = -a$, then for $\gamma = 0$ the solution pressure is

$$P(x) = 4\alpha(x+a-1)\left(\frac{1+x}{1-x}\right)^{\frac{1}{2}} \qquad x\in[-1,1]. \qquad (2.4.3)$$

The second term in (2.4.2) vanishes for $\gamma = 0$, so substituting for P we get

$$\zeta''(x) = 2\alpha + \frac{\alpha}{\sqrt{2}}(a-2)(-x-1)^{-\frac{1}{2}}. \qquad (2.4.4)$$

The curvature at separation is given by taking the limit as x approaches -1 from below. Since the curvature at all points on the hull is 2α, separation will occur with constant curvature if and only if $a = 2$. Observe also that for all values of $a \neq 2$ separation occurs with <u>infinite</u> curvature, the sign of the infinity depending on the value of a.

We now follow the behaviour of P and the curvature as a passes through the value 2. We first write (2.4.3) in another form:

$$P(x) = \frac{4\alpha}{(1-x)^{\frac{1}{2}}}\{(a-2)(1+x)^{\frac{1}{2}}+(1+x)^{3/2}\}. \qquad (2.4.5)$$

Using both (2.4.5) and (2.4.3) we see that when $0<a<2$, P has a square-root zero at $x = -1$ and takes <u>negative</u> values for $-1<x<1-a$. Also from (2.4.4) the flow separates

with negative infinite curvature: the fluid surface at separation is concave downwards, i.e. it is trying to "get away" or detach from the body, and this solution is unlikely to be achievable in practice. However, when a=2, P has a three-halves-power zero at x = -1 and is positive for x>-1 and the curvature is continuous at separation. When a>2, P again has a square-root zero at x = -1 and is positive for all x. But the flow now separates with positive infinite curvature: the fluid surface at separation is concave upwards, i.e. it is trying to "get into" or remain attached to, the body. This case is acceptable in practice if the trailing edge is sharply cut off, as in a transom stern; for example, the flat plate solutions all have positive infinite curvature at their trailing edges.

Suppose we had used our program to solve this problem, taking various portions of the parabola as the wetted length - this is the same as taking various values of the parameter a. As we "moved" our wetted length (of constant magnitude 2) from left to right along the parabola $\zeta=\alpha x^2$ (this is the same as taking increasing values of a), we would find the solution had an unacceptable region of negative pressure, at first over the whole wetted length, then decreasing in size and eventually disappearing. If we stopped at exactly the point where this region disappears we would have, on the basis of our present criterion, a physically acceptable solution for smooth detachment from a non-cut-off stern. If we move further forward, the solution is acceptable only for transom sterns.

In fact there is an easier way to "find" the solution for smooth detachment. First observe that for a given

value of a, the trailing edge is a-1 units to the right of the axis of symmetry. If we take any solution which has a region of negative pressure less than 2 units long, then the pressure is zero at a point 2-a units ahead of the trailing edge (x=1-a from equation (2.4.3)). But this point is a-1+2-a = 1 unit ahead of the axis of symmetry - which is exactly where the trailing edge is when a=2. So (at least when $\gamma=0$) the zero-pressure point is always a "marker" for the correct position of the trailing edge, the region of negative pressure indicating that, physically, the flow has already detached.

Working by analogy from the $\gamma=0$ solution we assert now that for all finite γ the behaviour of the pressure near the trailing edge x = -1 will be given by

$$P(x) \sim C_1(1+x)^{\frac{1}{2}} + C_2(1+x)^{3/2} \qquad (2.4.6)$$

for some constants C_1, C_2. Substituting this into (2.4.2) gives

$$\zeta''(x) \sim C_1\frac{\pi/2}{(-x-1)^{\frac{1}{2}}} + O(1) - \gamma^2(\zeta(x)+C) \qquad (2.4.7)$$

for x near -1. For $\lim_{x\uparrow -1} \zeta''(x)$ to be finite we must require $C_1 = 0$. Note that this coincides with the elimination of the one-half-power term in (2.4.6). Hence, from our previous experience with $\gamma=0$, we deduce that to get the correct solution for a given γ, we should consider a sequence of solutions obtained by moving the wetted length along the parabola, and take that solution for which the region of negative pressure ($C_1<0$) has just disappeared ($C_1=0$). Alternatively, we could attempt to predict the correct

position of the trailing edge by looking for the point where the pressure is zero, in a solution with a region of negative pressure. However, for $\gamma \neq 0$, we must expect that this will not give exactly the right position for the trailing edge as it did in the case $\gamma=0$.

Such a "search" was carried out for various values of γ, based on a two-units long wetted length of the shape $\zeta=\alpha(x+a)^2$, $x\in[-1,1]$, for various a. It was found that the accuracy of prediction using the "point of zero-pressure" technique was poor except for very low γ and so in general the trailing edge position was found using a direct search. In Fig. 2.4.2 we give a graph against F of the position of the trailing edge with respect to the axis of symmetry of $\zeta=\alpha x^2$, assuming a wetted length of 2 and detachment with constant curvature from a non-cut-off stern. It is interesting to note that the trailing edge, which would be one unit behind the axis of symmetry at rest ($F=0$), reaches a maximum of around 2.6 units ahead at about $F = 2.2$ before decreasing to one unit ahead as $F\to\infty$. Fig. 2.4.3 gives graphs of pressure coefficient/lift coefficient for the solution hull for various values of F. Figs. 2.4.4, 2.4.5 and 2.4.6 give graphs against F of lift coefficient, moment coefficient, centre of pressure coefficient and the scaled height of the lowest point of the hull. Note that since the search procedure involves a considerable amount of computer time (about 70 seconds for each F), only six values of F were considered, viz. $F(\gamma)$ = 0.71(2), 1.0(1), 1.4(0.5), 2.2(0.2), 3.2(0.1), 4.5 (0.05). Therefore, any turning points in the graphs presented must be taken as approximate.

A further glance at (2.4.6) and our requirement for $C_1=0$ suggests yet another method to find the correct trailing edge computationally. If we assume P varies like (2.4.6) near the trailing edge then we have

$$P'(x) \sim \tfrac{1}{2}C_1(1+x)^{-\frac{1}{2}} + \frac{3}{2}C_2(1+x)^{\frac{1}{2}}$$

and $C_1=0$ corresponds to $P'(-1) = 0$. That is, if we could enforce computationally the condition $P'(-1) = 0$, then the solution having separation with constant curvature would be available in one calculation. No attempt was made in this study to investigate how this condition might be applied.

Much work remains to be done on the subject of curved hulls. Specifically, it was assumed throughout this section that the curvature of the hull was constant for all γ. However, it seems likely that in practice the shape of the hull will be a function of speed. For example, if the lift is held constant, but the boat is free to trim, it is to be expected that the axis of symmetry of the parabola will not remain vertical under all operating conditions, thus changing the effective value of the curvature parameter α of the hull.

CHAPTER 3

THREE-DIMENSIONAL PLANING

3.1 Introduction

In this chapter we shall be concerned with the case where the length and span of the flat body under consideration are of the same order. This being so, it is necessary to treat the flow as truly three-dimensional. We are not aware of previous work in which this problem has been treated in its full generality, although various limiting cases have been considered, as outlined in section 1.1.

Maruo [13], while presenting results for the high and low aspect ratio approximations, makes a rather pessimistic comment on the general problem; viz. "the kernel of the integral equation is complicated enough to frustrate any attempt at solving it". While it is true that the problem is formidable, it is in the first place quite amenable to brute-force approximation, although this would involve excessive computing time. However, we feel that it should be possible to do better than this, speeding convergence of the integration through the use of special analytical or computational procedures.

Much space will be allotted in this chapter to consideration of the infinite Froude number limit. In this limit, three-dimensional flat ship theory is essentially equivalent to aerodynamic lifting surface theory. The equation actually used in aerodynamics is our (1.6.4),

differentiated once with respect to the longitudinal co-ordinate x. Because this form is used, the arbitrary function C(y) is not present and therefore the question of its interpretation does not arise. This difference is basically a reflection of the lack of any "free surface" in aerodynamics. There is a large body of literature on aerodynamic lifting surface theory; for example, a well-known early paper is that by Multhopp [16] who used a collocation method to solve the integral equation. In a more recent paper, Wagner [36] developed an improved scheme in which control points were allowed at the leading edge of the wing, in contrast to previous methods, including Multhopp's, where this was not permitted. Hess [8] has applied a generalization of Multhopp's method in his study of boomerangs and helicopter rotors.

The kernel of the flat ship integral equation in the limit $F\to\infty$ is quite simple, and results obtained help to show some general characteristics of the three-dimensional planing problem. However, some mention should be made of the implications involved in treating bodies of finite aspect ratio as $F\to\infty$. In practice we know that as a planing craft increases speed, the aspect ratio of its wetted area also increases. Hence, if the aspect ratio at high speed is to be of order one, the aspect ratio at low speed must be small, and it is only to planing craft satisfying this requirement that the results to be presented at infinite Froude number are applicable.

3.2 Numerical scheme for a general kernel

We now derive a numerical scheme for solution of the three-dimensional integral equation, using a general kernel $K(x-\xi,y-\eta)$. Specific forms for K will be treated later. The general equation (1.2.16) is

$$\zeta(x,y) + C(y) = \iint_W d\xi d\eta P(\xi,\eta)K(x-\xi,y-\eta). \qquad (3.2.1)$$

We assume the wetted area W is symmetric about the centre-plane $y=0$, and that the pressure is therefore even in y, i.e. $P(x,-y)=P(x,y)$. This assumption is useful in simplifying later computations.

Let W' be the half-waterplane $y\geq 0$. Suppose W' is divided into N pieces W'_k, $k=1,..,N$, on each of which P is constant and equal to P_k. P will also be equal to P_k on W''_k, the image of W'_k in the centre-plane. Then (3.2.1) may be approximated by

$$\zeta_j + C_j = \sum_{k=1}^{N} A_{jk}P_k \qquad j=1,..,N \qquad (3.2.2)$$

where

$$A_{jk} = \int\int_{W'_k+W''_k} d\xi d\eta \; K(x_j-\xi,y_j-\eta) \qquad (3.2.3)$$

and $\zeta_j = \zeta(x_j,y_j)$, $C_j = C(y_j)$; (x_j,y_j) being some point within W'_j.

The choice of mesh was made in such a way that the pieces W'_k lay in longitudinal strips and the value of y_j was taken to be the same for all pieces in a given strip. Since C is a function of y only, it follows that the

value of C_j is the same for each piece on a given strip. Again considering a given strip, the value of P corresponding to the piece on the trailing edge was set to zero, in accordance with the Kutta condition. The following generalization can then be made of the solution technique introduced in section 2.2. Supose W' is cut into n strips each of m pieces, where $m \times n = N$. Then the N unknowns involved are $C_1, P_2, .., P_m, C_2, P_{m+2}, ..., C_n$, $P_{(n-1)m+2}, .., P_{nm}$. We thus make a similar substitution as we did in the two-dimensional equations, when P_1 was replaced by C. Computationally, we need not calculate the coefficients $A_{j(i-1)m+1}$, $j=1,..,N$; $i=1,..,n$; but may set them to zero. To account for the C_j's we then place one "-1" in each row; in the j-th row it is put in the $([(j-1)/m]m+1)$-th position, where "[ ]" is the integer-part function.

An example will help to illustrate the above procedure. Suppose $m=3$, $n=2$: then, in matrix form, equation (3.2.2) is

$$\begin{bmatrix} A_{11} & A_{12} & A_{13} & A_{14} & A_{15} & A_{16} \\ A_{21} & A_{22} & A_{23} & A_{24} & A_{25} & A_{26} \\ A_{31} & A_{32} & A_{33} & A_{34} & A_{35} & A_{36} \\ A_{41} & A_{42} & A_{43} & A_{44} & A_{45} & A_{46} \\ A_{51} & A_{52} & A_{53} & A_{54} & A_{55} & A_{56} \\ A_{61} & A_{62} & A_{63} & A_{64} & A_{65} & A_{66} \end{bmatrix} \begin{bmatrix} P_1 \\ P_2 \\ P_3 \\ P_4 \\ P_5 \\ P_6 \end{bmatrix} = \begin{bmatrix} \zeta_1 \\ \zeta_2 \\ \zeta_3 \\ \zeta_4 \\ \zeta_5 \\ \zeta_6 \end{bmatrix} + \begin{bmatrix} C_1 \\ C_1 \\ C_1 \\ C_2 \\ C_2 \\ C_2 \end{bmatrix} ;$$

but $P_1 = P_4 = 0$. Hence, following the method given above, the new system is

$$\begin{bmatrix} -1 & A_{12} & A_{13} & 0 & A_{15} & A_{16} \\ -1 & A_{22} & A_{23} & 0 & A_{25} & A_{26} \\ -1 & A_{32} & A_{33} & 0 & A_{35} & A_{36} \\ 0 & A_{42} & A_{43} & -1 & A_{45} & A_{46} \\ 0 & A_{52} & A_{53} & -1 & A_{55} & A_{56} \\ 0 & A_{62} & A_{63} & -1 & A_{65} & A_{66} \end{bmatrix} \begin{bmatrix} C_1 \\ P_2 \\ P_3 \\ C_2 \\ P_5 \\ P_6 \end{bmatrix} = \begin{bmatrix} \zeta_1 \\ \zeta_2 \\ \zeta_3 \\ \zeta_4 \\ \zeta_5 \\ \zeta_6 \end{bmatrix} .$$

We now have a standard set of linear equations in N=6 unknowns.

A further consideration is the choice of mesh, where we need to decide the spacing of the intervals in two directions. The particular choice found best for the waterplanes treated will be given in the relevant sections.

3.3 The coefficients A_{jk} for infinite Froude number

As shown in section 1.6, the kernel of the three-dimensional integral equation, for $F\to\infty$, reduces to

$$K(x-\xi,y-\eta) = \frac{1}{4\pi}\ \frac{[(x-\xi)^2+(y-\eta)^2]^{\frac{1}{2}}-(x-\xi)}{(y-\eta)^2}\ . \quad (3.3.1)$$

We shall suppose that the wetted area W has a straight trailing edge of width 2 at $x=0$ and is of constant or decreasing width for increasing $x>0$. Let $x=\ell(y), 0\leqslant y\leqslant 1$, define the leading edge of the half-waterplane W', the maximum wetted length being $\ell(0)$.

With this specification, equation (3.2.1) becomes

$$\zeta(x,y) + C(y) = \frac{1}{4\pi}\left\{\int_0^1\int_0^{\ell(\eta)} + \int_{-1}^0\int_0^{\ell(-\eta)}\right\} d\xi\, d\eta P(\xi,\eta)\cdot$$

$$\frac{[(x-\xi)^2+(y-\eta)^2]^{\frac{1}{2}}-(x-\xi)}{(y-\eta)^2}\ . \quad (3.3.2)$$

We now make the substitution $\lambda=\xi/\ell(\eta)$, and also use $P(x,-y) = P(x,y)$, giving

$$\zeta(x,y)+C(y) = \frac{1}{4\pi}\int_0^1\int_0^1 d\lambda\, d\eta P(\lambda\ell(\eta),\eta)\cdot$$

$$\{\ell(\eta)\cdot[\frac{[(x-\lambda\ell(\eta))^2+(y-\eta)^2]^{\frac{1}{2}}-(x-\lambda\ell(\eta))}{(y-\eta)^2}$$

$$+ \frac{[(x-\lambda\ell(\eta))^2+(y+\eta)^2]^{\frac{1}{2}}-(x-\lambda\ell(\eta))}{(y+\eta)^2}\ ]\}\cdot \quad (3.3.3)$$

We have thereby transformed our integral equation into one over the unit square, with a kernel given by the expression in curly brackets, which we denote $K_\ell(\lambda,\eta;\ell(\eta);x,y)$. This transformation is equivalent to taking a distorted mesh

over W', as we illustrate in Fig. 3.3.1, using an equal mesh over the unit square for clarity.

In the solution technique adopted, the unit square was split up into a mesh with cosine intervals longitudinally (λ) and either equal or cosine intervals in the spanwise (η) direction. If the mesh over the unit square has nodes given by λ_i, i=0,..,m; η_j, j=0,..,n, then the k-th grid square is bounded by λ_{a-1}, λ_a, η_{b-1}, η_b where $a = k-[(k-1)/m]m$, $b = n-[(k-1)/m]$; and A_{jk} is given by

$$A_{jk} = \frac{1}{4\pi} \int_{\lambda_{a-1}}^{\lambda_a} \int_{\eta_{b-1}}^{\eta_b} d\lambda d\eta K_\ell(\lambda,\eta;\ell(\eta);x_j,y_j). \quad (3.3.4)$$

For a rectangular wetted area, $\ell(\eta) = \beta$ for some constant β and both integrals for A_{jk} may be evaluated analytically. For a wetted area with a leading edge of constant slope (i.e. a cropped or an uncropped delta), $\ell(\eta) = \alpha\eta+\beta$ for some constants α,β and only the η-integration may be done analytically, leaving the λ-integration to be done numerically. For other $\ell(\eta)$ both integrations must in general be evaluated numerically, unless further approximations are made. In fact, since the range of η-integration, $[\eta_{b-1},\eta_b]$, can be made small by taking large n, $\ell(\eta)$ may be replaced by a constant or linear function over this range. This is equivalent to approximating $\ell(\eta)$ in a piecewise fashion by a straight line for each longitudinal strip. If this is done, one or both of the integrals may be evaluated analytically.

Note that (3.3.4) contains an inverse-square singularity when $y_j \in [\eta_{b-1},\eta_b]$. Where this occurs we adopt a Hadamard

principal value, the strict meaning of which is considered with some care in an Appendix to Multhopp's paper contributed by W. Mangler, [16] p.34. However, in practice, when an analytical primitive exists, this type of principal value may be treated in the same way as a Cauchy principal value: that is, we simply evaluate the integral in the normal fashion, using the primitive. For example

$$\int_{y-a}^{y+b} \frac{d\eta}{(y-\eta)^2} = \left[(y-\eta)^{-1} \right]_{y-a}^{y+b} \qquad (a,b>0)$$

$$= - \frac{a+b}{ab} \qquad (3.3.5)$$

Note that the result is negative, although we are integrating a positive function: such counter-intuitive results are common when dealing with such integrals. Our results will always depend on the analytic evaluation of the (Hadamard) η-integration and so the difficulties involved in the numerical evaluation of such integrals will not arise.

3.4 Rectangular wetted area

For a rectangular wetted area, the leading edge is defined by $\ell(y) = \beta$, $0 \leq y \leq 1$, for some constant β, giving a body of aspect ratio $2/\beta$. As mentioned in section 3.3, the A_{jk} may be evaluated analytically in this case and so there are no computational difficulties associated with this portion of the program. The indefinite integral required in the evaluation of (3.3.4) is

$$\iint \frac{(u^2+v^2)^{\frac{1}{2}} - u}{v^2}\, du\,dv$$

$$= -\frac{u(u^2+v^2)}{2v} + \tfrac{1}{2} v \log \left| \frac{u+(u^2+v^2)^{\frac{1}{2}}}{v} \right|$$

$$+ u \log \left| \frac{v+(u^2+v^2)^{\frac{1}{2}}}{u} \right| + \frac{u^2}{2v} .$$

The input $\zeta(x,y)$ was taken to be that corresponding to a flat plate at an angle of attack α, i.e. $\zeta(x,y) = \alpha x$, $x \in W$. It was found that a mesh with cosine spacing in both directions provided the most rapid convergence. Results were obtained for rectangles of aspect ratios 0.5, 1, 2, 3, 4, 5 and 6. In Fig. 3.4.1 the lift slope is compared with results given by Thwaites [28]. The centre-line pressure coefficient for aspect ratio equals one (Fig. 3.4.2) was found to be in close agreement with the infinite Froude number result given by Wang and Rispin [37], who approximated the pressure coefficient using a double series.

A new result is that of the solution hull shape, given in Fig. 3.4.3. This shows that for a rectangular wetted area, the hull must be slightly "tunnelled". This is what we might expect, since, if we have a truly flat hull, the

wetted area would have a slightly curved leading edge: the "tunnelling" serves to counteract this effect, giving a straight leading edge. Note also the tendency for the scaled height (height/α· wetted length) of the solution body to increase as the aspect ratio increases. This is as anticipated, since we know that as $F \to \infty$ in two-dimensional theory, the scaled height tends to plus infinity.

3.5 Wetted areas with triangular fore-pieces

For a wetted area which is an uncropped or a cropped delta, we have $\ell(y) = \alpha y+\beta$, $0\leq y\leq 1$, for some constants $\alpha<0, \beta$. When $\beta=-\alpha$, the wetted area is strictly triangular, whereas when $\beta>-\alpha$ the wetted area is of the form of a rectangle with a triangular fore-piece, where the leading triangle is of aspect ratio $2/(-\alpha)$ (see Fig. 3.5.1). In equation (3.3.4) for A_{jk}, we may now perform only the η-integration analytically, using the following indefinite integral:

$$\int d\eta(\alpha\eta+\beta)\{\frac{[(x-\lambda(\alpha\eta+\beta))^2+(y\pm\eta)^2]^{\frac{1}{2}}-(x-\lambda(\alpha\eta+\beta))}{(y\pm\eta)^2}\}$$

$$= (\alpha\nu-(-\alpha y\pm\beta))(A\nu^2+B\nu+C)^{\frac{1}{2}}/\nu$$

$$+ (\tfrac{1}{2}\alpha B+A(-\alpha y\pm\beta))A^{-\frac{1}{2}}\log|2A^{\frac{1}{2}}(A\nu^2+B\nu+C)^{\frac{1}{2}}+2A\nu+B|$$

$$- (\alpha C+\tfrac{1}{2}B(-\alpha y\pm\beta))C^{-\frac{1}{2}}\log|(2C^{\frac{1}{2}}(A\nu^2+B\nu+C)^{\frac{1}{2}}+B\nu+2C)/\nu|$$

$$\pm \lambda\alpha^2\nu+(\lambda(\pm\alpha)(-\alpha y\pm\beta)-\alpha(x\pm\lambda\alpha y-\lambda\beta))\log|\nu|$$

$$+ (-\alpha y\pm\beta)(x\pm\lambda\alpha y-\lambda\beta)/\nu$$

where $\nu = y\pm\eta$,

$A = 1+(\lambda\alpha)^2$,

$B = -2\lambda(\pm\alpha)(x\pm\lambda\alpha y-\lambda\beta)$

and $C = (x\pm\lambda\alpha y-\lambda\beta)^2$. (3.5.1)

The numerical calculation of the λ-integration is straightforward, although care must be taken over the logarithmic singularity which arises from the first logarithmic term in (3.5.1).

The input $\zeta(x,y)$ was again taken to be that corresponding to a flat plate at an angle of attack α, i.e. $\zeta(x,y) = \alpha x$, $x \in W$. Both equal and cosine spanwise mesh spacings were used with cosine longitudinal spacing, and it was found that neither of these gave consistently better convergence for the shapes considered. Results quoted are for equal spanwise spacing with m=n=10 (N=100): computing time was approximately 115 seconds for each $\ell(y)$, and the results for the shape of the body were then within 1% of converged values.

Thwaites [28] gives results for the centre-line pressure coefficient on the body given by $\ell(y) = -y+7/6$, a cropped delta, as calculated by various workers from the point of view of aerodynamic lifting surface theory. In Fig. 3.5.2 we give our results for this body, compared with the two most recent results given by Thwaites.

A new result obtained through our approach is that of the shape and location of the hull, given a triangular wetted area. In his paper on prismatic planing surfaces, Savitsky [22] states that for V-shaped hulls, the half-leading edge of the wetted area is "slightly convex, but since the curvature is small, it is neglected". (p.75), i.e. for a V-shaped hull we get a wetted area which has a triangular fore-piece. Savitsky then considers the problem of finding a relationship between the deadrise, angle of attack and wetted area of deadrise planing surfaces. We quote from Savitsky's paper, p.77.

> "Wagner computed the wave-rise for a two-dimensional wedge penetrating a fluid surface vertically, and found the actual wetted width of the wedge was $\pi/2$ times the wetted width defined by the calm water intersection with the

> bottom. The motion of a deadrise planing surface can be represented as a two-dimensional problem by considering the water flow between two vertical planes normal to the plane of symmetry of the planing surface. To an observer located between these planes, the passage of the prismatic Vee planing surface will appear identical to the vertical immersion of a wedge. This being the case, the $\pi/2$ wave-rise factor computed by Wagner is applicable,..."

giving

$$\frac{\tan(\text{deadrise angle})}{\tan(\text{angle of attack})} = \frac{\pi}{\text{aspect ratio of triangular fore-piece}}. \qquad (3.5.2)$$

Savitsky follows on to say that experimental evidence confirms the result (3.5.2).

If our results for hull shape are to be consistent with this formula, we should find that our solution hull shapes are, at least approximately, V-shaped, the angle of the "V" being dependent only on the aspect ratio of the triangular fore-piece and independent of the size of any rectangular "tail". This was found to be true for rectangular tails up to four times the length of the fore-piece, these being the longest tails considered. We present results for the hull shape corresponding to various triangular fore-pieces in Fig. 3.5.3. The deadrise angle predicted by (3.5.2) is shown for the V-shaped hull which has the same minimum height at the trailing edge as that computed. Note that since the computed variation from flatness in the hull is a function of span only, all spanwise cross-sections of the hull are identical. From Fig. 3.5.3 we observe that agreement with Savitsky's formula is better, the smaller the aspect ratio. This is to be expected since the argument involved in its derivation is essentially a low aspect ratio one.

3.6 The free surface at infinite Froude number

In this section we investigate the form of the free surface produced by a flat ship of arbitrary wetted area travelling at infinite Froude number. To do this we use equation (1.6.2). In this equation let us define S by

$$S(x,y) = 4\pi(\zeta(x,y)+C(y))$$

$$= \iint_W d\xi d\eta P(\xi,\eta)\frac{[(x-\xi)^2+(y-\eta)^2]^{\frac{1}{2}}-(x-\xi)}{(y-\eta)^2} \qquad (3.6.1)$$

and consider the form of S in the far field, i.e. at points (x,y) far removed from W.

Suppose first that $|x| \gg |y| \gg |\xi|, |\eta|$; then expansion of the kernel of (3.6.1) yields, for $x<0$

$$S \sim \iint_W d\xi d\eta P(\xi,\eta)\{-\frac{2x}{y^2} + \frac{4\eta x}{y^3} + \text{higher order terms}\}$$

$$= -\frac{2x}{y^2}\iint_W d\xi d\eta P(\xi,\eta) + \frac{4x}{y^3}\iint_W d\xi d\eta\eta P(\xi,\eta) + \ldots$$

The first integral is equal to L, the lift, whereas the second is zero since $\eta P(\xi,\eta)$ is odd in η and W is symmetric about the ξ-axis. Hence

$$S \sim -\frac{2x}{y^2}L. \qquad (3.6.2)$$

On the other hand, for $x>0$

$$S \sim \iint_W d\xi d\eta P(\xi,\eta)\{\frac{1}{2x} - \frac{\eta}{xy^2} + \text{h.o.t.}\}$$

i.e. $S \sim \frac{L}{2x} \to 0$ for large x. (3.6.3)

Suppose secondly $|x| \sim |y| \gg |\xi|, |\eta|$; then (3.6.1) is approximated to first order by

$$S \sim \frac{(x^2+y^2)^{\frac{1}{2}}-x}{y^2} L \to 0 \text{ for large } |x|, |y|. \qquad (3.6.4)$$

In the third case, $|y| \gg |x|$

$$S \sim \iint_W d\xi d\eta P(\xi,\eta)\{\frac{1}{|y|} + \frac{-\eta+x-\xi}{y^2} + \text{h.o.t.}\}$$

$$\sim \frac{L}{|y|} \to 0 \text{ for large } |y|. \qquad (3.6.5)$$

When considering the shape of the free surface directly behind and ahead of the body we can no longer expand $(y-\eta)^{-2}$ in power series as has been done implicitly in the preceding analysis. So, finally, for $|x| \gg |y| \sim |\eta|, |\xi|$, we have, for $x<0$

$$S \sim \iint_W d\xi d\eta \frac{P(\xi,\eta)}{(y-\eta)^2} \{-2x + \text{h.o.t.}\}$$

$$\sim -2x \iint_W d\xi d\eta \frac{P(\xi,\eta)}{(y-\eta)^2}, \qquad (3.6.6)$$

while for $x>0$

$$S \sim \iint_W d\xi d\eta \frac{P(\xi,\eta)}{(y-\eta)^2} \{\frac{(y-\eta)^2}{2x} + \text{h.o.t.}\}$$

$$\sim \frac{L}{2x} \to 0 \text{ for large } x. \qquad (3.6.7)$$

Care is needed in the interpretation of (3.6.6): note that since we are considering the free surface in the track of the body, the integral multiplying "-2x" has an inverse-square singularity which is to be treated as a Hadamard

principal value. As shown in (3.3.5), such an integral can be expected to be negative for positive P, and so (3.6.6) shows that the free surface falls away linearly to minus infinity in the track of the body.

Let us now follow a locus of constant height S=H in the free surface starting (see equation (3.6.7)) from x=L/(2H) directly ahead of the body. Equation (3.6.3) shows that the locus is initially perpendicular to the direction of motion, while from (3.6.4) we deduce that for $y \sim x$, the locus assumes the form

$$y^2 = \left(\frac{L}{H}\right)^2 - \frac{2L}{H}x, \qquad (3.6.8)$$

that is, it is parabolic. As we enter the region $y \gg x$, (3.6.5) indicates that $y = \frac{L}{H}$ which is consistent with (3.6.8). For $x<0$ we again deduce from (3.6.4) that the form (3.6.8) is appropriate, and for $-x>>y$ (3.6.2) shows that $y^2 \sim -\frac{2L}{H}x$, again consistent with (3.6.8).

Hence each locus of constant height in the free surface at infinite Froude number is essentially a parabola, open in the downstream direction, with the body at the focus. The free surface elevation tends to zero like x^{-1} ahead of the body and like $|y|^{-1}$ abeam of the body. However, it falls continuously and ultimately linearly to minus infinity in the immediate track of the body, and this may be looked upon as representing a trailing wave of infinite wavelength - the free surface drops continuously down into a bottomless trough. In contrast, from equation (3.6.2) we deduce that the free surface rises linearly to plus infinity downstream,

when we consider the height taken along any line parallel to the direction of motion, but off the track of the body.

3.7 The coefficients A_{jk} for finite Froude number

In this section we show how the problem of calculating the A_{jk} for finite Froude number revolves around the numerical calculation of an infinite integral of a slowly decaying oscillatory function. From equations (1.2.16) and (3.2.3) the coefficients A_{jk} are given by

$$A_{jk} = \frac{R\varrho}{2\pi^2} \iint_{W_k'+W_k''} d\xi d\eta \int_0^{\pi/2} d\theta \sec^2\theta \cdot \int_{0\,(bp)}^{\infty} \frac{d\lambda\lambda}{\lambda-\gamma\sec^2\theta} e^{-i\lambda(x_j-\xi)\cos\theta} \cos(\lambda(y_j-\eta)\sin\theta). \tag{3.7.1}$$

We rewrite this as

$$A_{jk} = \frac{1}{2\gamma\pi^2} \iint_{W_k'+W_k''} d\xi d\eta \frac{\partial^2}{\partial\xi\partial\eta} B(x_j-\xi, y_j-\eta) \tag{3.7.2}$$

where $B(x,y) = \mathcal{R}e\, i\gamma \int_0^{\pi/2} d\theta \sec^3\theta \operatorname{cosec}\theta \cdot \int_{0\,(bp)}^{\infty} \frac{d\lambda}{\lambda(\lambda-\gamma\sec^2\theta)} e^{-i\lambda x\cos\theta} \sin(\lambda y\sin\theta).$

By doing this, it is possible to dispense with the η- and ξ-integrations for a rectangular mesh, since (3.7.2) can then be evaluated exactly by finding eight values of the B-function, one corresponding to each of the four corners of the two rectangles W_k' and W_k''. The numerical calculation of "B" is also less formidable than would have been the case if we had retained the initial kernel. Observe that $B(x,-y) = -B(x,y)$ and so we only need consider $y \geq 0$.

Making the substitution $\lambda = \gamma\sec^2\theta k$ we get

$$B(x,y) = Re\,i \int_0^{\pi/2} d\theta \sec\theta \operatorname{cosec}\theta \cdot$$

$$\int_{0\,(bp)}^{\infty} \frac{dk}{k(k-1)}\, e^{-ik\gamma x\sec\theta} \sin(k\gamma y\sec^2\theta\sin\theta)$$

$$= \int_0^{\pi/2} d\theta \sec\theta \operatorname{cosec}\theta F(\theta) \qquad (3.7.3)$$

where $$F(\theta) = Re\,i \left\{ \int_{0\,(bp)}^{\infty} \frac{dk}{k-1}\, e^{-ika} \sin(kb) \right.$$

$$\left. - \int_{0\,(bp)}^{\infty} \frac{dk}{k}\, e^{-ika} \sin(kb) \right\}$$

with $a = \gamma x\sec\theta$, $b = \gamma y\sec^2\theta\sin\theta$.

Evaluation of these integrals gives

$$F(\theta) = G(a-b) - G(a+b)$$

where $G(x) = \frac{1}{2}g(|x|) + \frac{1}{2}\log|x| + \pi\sin(x)H(-x)$.

The g-function is an auxiliary function for the Sine and Cosine integrals and is treated in detail in Abramowitz and Stegun [1] p.232, 233. Note in particular that g is a positive and strictly decreasing function of $|x|$. H is the Heaviside unit step function.

Consider now the numerical evaluation of (3.7.3), first with reference to the "g" and "log" terms of G. We first investigate the behaviour of $F(\theta)$ near the upper limit $\frac{\pi}{2}$. As $\theta \uparrow \frac{\pi}{2}$, $|a-b|$ and $|a+b|$ get large, but we know

(Abramowitz and Stegun [1] p.233) that $g(z) \sim z^{-2}$ for large z and so we need only be concerned with the logarithmic term. For $\theta \uparrow \frac{\pi}{2}$ we have

$$F(\theta)\sec\theta\operatorname{cosec}\theta \sim \tfrac{1}{2}\sec\theta \log \left|\frac{x\cos\theta - y\sin\theta}{x\cos\theta + y\sin\theta}\right|$$

$$= \tfrac{1}{2}\sec\theta \log \left|-1 + \frac{2x\cos\theta}{x\cos\theta + y\sin\theta}\right|$$

$$\sim \tfrac{1}{2}\sec\theta \cdot -\frac{2x}{y}\cot\theta$$

$$\sim -\frac{x}{y}$$

and hence the integrand is bounded at the upper limit. Also, for x near zero $g(|x|) \sim -\gamma - \log|x|$ (γ = Euler's constant = 0.5772...) and so $\frac{1}{2}g(|x|) + \frac{1}{2}\log|x|$ is bounded for x near zero. Thus the integrand due to the "g" and "log" terms is bounded and smoothly varying and so efficient numerical evaluation of (3.7.3) may be performed using standard techniques.

The evaluation problem posed by the "$\pi\sin(x)H(-x)$" term is, however, much more difficult. If we write B_s for the contribution to B arising from this term we have

$$B_s(x,y) = \pi \int_{\arctan(x/y)}^{\pi/2} d\theta \sec\theta \operatorname{cosec}\theta \cdot \sin(\gamma x \sec\theta - \gamma y \sec^2\theta \sin\theta)$$

for $x>0$, and

$$B_s(x,y) = \pi\int_0^{\pi/2} d\theta \sec\theta \operatorname{cosec}\theta \cdot$$

$$\sin(\gamma x\sec\theta - \gamma y\sec^2\theta\sin\theta)$$

$$- \pi\int_0^{\arctan(-x/y)} d\theta \sec\theta \operatorname{cosec}\theta \cdot$$

$$\sin(\gamma x\sec\theta + \gamma y\sec^2\theta\sin\theta)$$

for $x<0$. With the substitution $t = \tan\theta$, these integrals become

$$B_s(x,y) = \pi\int_{x/y}^{\infty} \frac{dt}{t} \sin((t^2+1)^{\frac{1}{2}}\gamma(x-yt))$$

for $x>0$, and

$$B_s(x,y) = \pi\int_0^{\infty} \frac{dt}{t}\sin((t^2+1)^{\frac{1}{2}}\gamma(x-yt))$$

$$- \pi\int_0^{-x/y} \frac{dt}{t}\sin((t^2+1)^{\frac{1}{2}}\gamma(x+yt))$$

for $x<0$. From these forms, the unpleasant nature of the integrals is clear: they are <u>infinite integrals of slowly decaying oscillatory functions</u>, and supply the hard core of the problem in finite Froude number flat ship theory.

There is in fact a further computational trap in the method presented here - this is the problem of "disappearing digits". Recall that the A_{jk} are found by summing eight values of B - four with a plus sign and four with a minus sign. It was found that while the values of B were $O(1)$, the resulting A_{jk} was in general $O(10^{-2})$. This means that we "lose" two of our hard-won significant figures in

the calculation of A_{jk} from B - to get three figure accuracy in A_{jk} we need at least five figure accuracy in B.

Several standard methods were used in an attempt to evaluate the integrals B_s and although converging results were obtained, it was always at the cost of considerable computer time for <u>each</u> B value. If five figure accuracy was sought the time required to compute a complete solution was prohibitive. Some results were obtained using lower accuracy but their validity was so doubtful that we shall not present them here.

Future work on this topic must focus on more sophisticated methods of tackling the evaluation of B_s. This may either be through rotation of the path of integration into the complex plane to produce a rapidly decaying integrand, or through numerical techniques which are specifically tailored to deal with such integrals. It may also be of value to attempt to remove the problem of the disappearing digits through partial reformulation at an early stage, e.g. by evaluating A_{jk} in a different manner depending on whether the j and k mesh rectangles are adjacent or widely separated.

CHAPTER 4

TWO-DIMENSIONAL BOW FLOW

4.1 Introduction

In recent years it has been recognised that an important contribution to the resistance to forward motion of full-form ships is caused by the production of a breaking wave at the bow. For example, Baba [3] reported that in towing-tank tests with a geosim of a tanker, the wave-breaking resistance was 18% of the total resistance, whereas the energy radiated by the waves was only 6%, these measurements being done for a Froude number based on draft of 1.7.

It is to be expected that the inception and strength of the breaking wave will depend on the bow shape as well as the Froude number. In fact, it has been found that "bulbous bows", initially designed to reduce the wave resistance, also serve under some conditions to reduce wave-breaking resistance (see e.g. Taniguchi, Tamura and Baba [26]). It is therefore of interest to attempt a mathematical analysis of the non-linear flow problem involved.

A related topic is that of the flow at the stern of a ship. Particular reasons for wishing to investigate stern flow were outlined in section 1.5. However, there is a significant mathematical difference between the two problems of bow and stern flow. If it is assumed that the ships concerned are of semi-infinite length, then we need to consider the boundary conditions at only either upstream or downstream infinity. For bow flow the condition is simply that the free surface elevation tends to zero upstream and

the potential tends to that of a free stream. But for stern flow, we expect that waves will be present at downstream infinity, and it is difficult to specify a priori the form of these waves, in a manner consistent with the assumed non-linearity of the flow. For this reason we orient the following discussion to an analysis of two-dimensional bow flow. Dagan and Tulin [5] studied this problem using perturbation expansions, one for low Froude number and one for high Froude number. We attempted to solve the problem exactly using numerical techniques applied directly to the integral equation involved. However an exact (analytical) solution was obtained only for flow at infinite Froude number.

4.2 Flow without a jet

The following transformation was apparently first introduced by Rudzki [21] and is also presented by Wehausen and Laitone [38]. If ϕ and ψ are the velocity potential and stream function respectively, we write, with $z = x + iy$

$$f(z) = \phi + i\psi$$

and $$f'(z) = w = u - iv.$$

If θ is the angle between the velocity vector $\bar{w}=u+iv$ and the positive x-axis we may write

$$w = U e^{-i\Omega}$$

where $$\Omega = \theta + i\tau.$$

We consider θ as an analytic function of ϕ and ψ, i.e.

$$\theta = \theta(\phi,\psi) = Re(\Omega(f))$$

where we will take $\psi=0$ to correspond to the free surface; i.e. $\theta(\phi,0)$ gives the angle of the free surface. The exact free surface condition is

$$gy + \tfrac{1}{2}|w|^2 = \tfrac{1}{2}U^2$$

i.e. $$gy + \tfrac{1}{2}U^2 e^{2\tau} = \tfrac{1}{2}U^2.$$

Differentiating with respect to ϕ gives

$$gy_\phi + U^2 e^{2\tau}\tau_\phi = 0 \text{ on } \psi = 0. \qquad (4.2.1)$$

But we also have

$$\frac{dz}{df} = \frac{1}{U} e^{-\tau} e^{i\theta} = x_\phi + iy_\phi,$$

or
$$y_\phi = \frac{1}{U} e^{-\tau}\sin\theta, \qquad (4.2.2)$$

and so (4.2.2) and (4.2.1) give

$$\tau_\phi = -\kappa_1 e^{-3\tau}\sin\theta \qquad \kappa_1 = \frac{g}{U^3}. \qquad (4.2.3)$$

Rearranging (4.2.3) gives

$$\frac{\partial}{\partial\phi}(e^{3\tau}) = -3\kappa_1\sin\theta$$

and hence
$$e^{3\tau} = \text{constant} - 3\kappa_1\int\sin\theta d\phi.$$

If we suppose that as $\phi\to\infty$ (upstream), $\tau\to 0$ ($|w|\to U$) then

$$e^{3\tau} = 1-3\kappa_1\int_{-\infty}^{\phi}\sin\theta(\alpha,0)d\alpha$$

or
$$\tau(\phi,0) = \frac{1}{3}\log(1-3\kappa_1\int_{-\infty}^{\phi}\sin\theta(\alpha,0)d\alpha). \qquad (4.2.4)$$

We now make use of the Plemelj relations, that if χ_1 and χ_2 are the real and imaginary parts of a function analytic in the lower half plane, then, along the real axis

$$\chi_2 = \frac{1}{\pi}\int_{-\infty}^{\infty}\frac{\chi_1 d\beta}{\beta-\phi} \qquad (4.2.5)$$

and
$$\chi_1 = -\frac{1}{\pi}\int_{-\infty}^{\infty}\frac{\chi_2 d\beta}{\beta-\phi}. \qquad (4.2.6)$$

Using (4.2.5) for $\chi_1 = \theta(\phi) = \theta(\phi,0)$; $\chi_2 = \tau(\phi) = \tau(\phi,0)$

we have

$$\tau(\phi) = \frac{1}{\pi}\int_{-\infty}^{\infty} \frac{\theta(\beta)d\beta}{\beta-\phi}. \qquad (4.2.7)$$

Suppose we are considering the flow situation shown in Fig. 4.2.1, with two-dimensional flow abutting a semi-infinite body of finite draft and "bow" angle $\theta_w>0$. If we specify $\phi=0$ at attachment and $\phi = \phi_0>0$ at the corner, $\theta(\phi)$ may be written

$$\theta(\phi) = \theta(\phi)H(-\phi) - \theta_w(H(\phi)-H(\phi-\phi_0)). \qquad (4.2.8)$$

Using (4.2.8) and (4.2.4) in (4.2.7) we get our basic integral equation for $\theta(\phi)$, $\phi<0$:

$$\frac{1}{3}\log(1-3\kappa_1\int_{-\infty}^{\phi}\sin\theta(\alpha)d\alpha) =$$

$$\frac{1}{\pi}\int_{-\infty}^{0}\frac{\theta(\beta)d\beta}{\beta-\phi} - \frac{\theta_w}{\pi}\log\left|\frac{\phi_0-\phi}{\phi}\right|. \qquad (4.2.9)$$

This equation may be expressed in another way by taking the inverse Hilbert transform:

$$\theta(\phi) = -\frac{(-\phi)^{\frac{1}{2}}}{\pi}\int_{-\infty}^{0}\frac{1}{3}\log(1-3\kappa_1\int_{-\infty}^{\beta}\sin\theta(\alpha)d\alpha)\frac{d\beta}{(-\beta)^{\frac{1}{2}}(\beta-\phi)}$$

$$- \frac{2\theta_w}{\pi}\arctan(-\phi_0/\phi)^{\frac{1}{2}}. \qquad (4.2.10)$$

It is of interest to consider $\lim_{\phi\uparrow 0}\theta(\phi)$, i.e. the angle at which the fluid attaches to the solid surface. A naive limiting process in (4.2.10) gives $\theta(0) = -\theta_w$, i.e. the fluid attaches tangentially and flows down the wall. But more

care is needed in treating the first term. Straightforward local analysis of attachment with a stagnation point suggests that, near the stagnation point, $\tau(\phi) \sim A \log|\phi|$ for some constant A. It is clear that in (4.2.10) only the behaviour of $\tau(\phi)$ near zero will be important as $\phi \uparrow 0$, and so we may write

$$\theta(\phi) \sim \frac{-A(-\phi)^{\frac{1}{2}}}{\pi}\int_{-\varepsilon}^{0} \log|\beta| \frac{d\beta}{(-\beta)^{\frac{1}{2}}(\beta-\phi)} + O((-\phi)^{\frac{1}{2}}) - \theta_W \quad (\varepsilon>0)$$

$$= \frac{-A(-\phi)^{\frac{1}{2}}}{\pi}\int_{-\infty}^{0} \log|\beta| \frac{d\beta}{(-\beta)^{\frac{1}{2}}(\beta-\phi)} + O((-\phi)^{\frac{1}{2}}) - \theta_W$$

$$= \frac{-A(-\phi)^{\frac{1}{2}}}{\pi} \cdot \frac{-\pi^2}{(-\phi)^{\frac{1}{2}}} + O((-\phi)^{\frac{1}{2}}) - \theta_W$$

i.e. $\theta(0) = A\pi - \theta_W$.

Therefore, for consistency, a solution with a horizontal stagnation point such that $\theta(0)=0$ must satisfy $\tau(\phi) \sim \frac{\theta_W}{\pi} \log|\phi|$ for $\phi \uparrow 0$.

Various iterative techniques were used in an attempt to solve (4.2.10) but none was found which would converge satisfactorily. However, the formulation leading to (4.2.10) contains a rather restrictive assumption, namely that the only possible stagnation point on the body is at attachment. This is enforced by prescribing that the whole free surface is given by $\psi=0$ and also by the specification (4.2.8) for $\theta(\phi)$. We therefore implicitly rule out any solutions which may have a stagnation point elsewhere, as would be the case if a bow-climbing jet formed at attachment as shown in Fig. 4.2.2. It would no longer then be

true that the whole free surface could be given by $\psi=0$ and in addition the specification (4.2.8) for $\theta(\phi)$ would have to be changed due to the 180° change in flow direction at the internal stagnation point. An equation similar to, but considerably more complicated than, (4.2.9), may be formulated for this general situation, but we shall consider only the case $\kappa_1=0$, i.e. the gravity-free problem.

4.3 Flow with a jet

We assume at first that we have a flow as shown in Fig. 4.3.1, with the corresponding f-plane as in Fig. 4.3.2. Let us define the ζ-plane by the mapping

$$f = \frac{\psi_0}{\pi}(\zeta - \log(\zeta + \xi_0)). \qquad (4.3.1)$$

In the transformed plane (Fig. 4.3.3) the real (ξ) axis corresponds to the free surface ($\xi<0$) and the body ($\xi>0$). Applying the Plemelj formula to the variables in the transformed plane, we have

$$\tau(\xi) = \frac{1}{\pi}\int_{-\infty}^{\infty} \frac{d\beta\theta(\beta)}{\beta-\xi}. \qquad (4.3.2)$$

But since we are considering the gravity-free case, we can immediately say $\tau=0$ for $\xi<0$ and so (4.3.2) gives

$$0 = \frac{1}{\pi}\int_{-\infty}^{\infty} \frac{d\beta\theta(\beta)}{\beta-\xi} \qquad \xi<0. \qquad (4.3.3)$$

As shown in Fig. 4.3.3, we have, for $\xi>0$

$$\theta(\xi) = \begin{cases} \theta_W & 0\leq\xi<1 \\ -\theta_W & 1<\xi<\xi_1 \\ 0 & \xi>\xi_1, \end{cases} \qquad (4.3.4)$$

and hence, substituting into (4.3.3), we obtain

$$0 = \frac{1}{\pi}\int_{-\infty}^{0} \frac{d\beta\theta(\beta)}{\beta-\xi} + \frac{\theta_W}{\pi}\log\left|\frac{1-\xi}{-\xi}\right| - \frac{\theta_W}{\pi}\log\left|\frac{\xi_1-\xi}{1-\xi}\right|.$$

Inverting the semi-infinite Hilbert transform yields the result

$$\theta(\xi) = \frac{2\theta_W}{\pi}\,[\,2\arctan(-\xi)^{-\frac{1}{2}} - \arctan(\xi_1/(-\xi))^{\frac{1}{2}}]$$

$$+ (-\xi)^{-\frac{1}{2}}\{\frac{4\theta_W}{\pi} - \frac{2\theta_W}{\pi}(\xi_1)^{\frac{1}{2}} + c\}$$

where c is an arbitrary constant arising from the inversion. Since θ must be well-behaved as $\xi\uparrow 0$, the term in curly brackets must vanish: hence the solution for θ is

$$\theta(\xi) = \frac{2\theta_W}{\pi}[\,2\arctan(-\xi)^{-\frac{1}{2}} - \arctan(\xi_1/(-\xi))^{\frac{1}{2}}]\,. \quad (4.3.5)$$

Consider now the angle of the jet; this is given by

$$\theta(-\xi_0) = \frac{2\theta_W}{\pi}[2\arctan(\xi_0)^{-\frac{1}{2}} - \arctan(\xi_1/\xi_0)^{\frac{1}{2}}]$$

$$< \frac{2\theta_W}{\pi}\arctan(\xi_0)^{-\frac{1}{2}} \quad \text{since } \xi_1>1$$

$$< \theta_W.$$

Hence the angle of the jet is <u>less than</u> the angle of the bow! This indicates that the jet in fact never leaves the solid surface. The true situation is as shown in Fig. 4.3.4, and the points E and F are coincident, with $\xi_0=0$. Alternatively, if the bow is cut off horizontally, the jet is able to pass over the top of the body as shown in Fig. 4.3.5, and a flow with $\xi_0\neq 0$ is possible. However, we shall from now on assume that the situation is that depicted in Fig. 4.3.4, and take $\xi_0=0$.

We now consider the behaviour of θ as $\xi \to -\infty$, i.e. upstream. From (4.3.5) we have

$$\theta(\xi) \sim \frac{2\theta_W}{\pi}(2-\xi_1^{\frac{1}{2}})(-\xi)^{-\frac{1}{2}} + O((-\xi)^{-3/2}). \qquad (4.3.6)$$

But, from (4.2.2) and (4.3.1) we may deduce, that for small θ

$$y(\xi) \sim \frac{\psi_0}{\pi U}\int \theta(\xi)(1-\xi^{-1})d\xi,$$

and so if the free surface is to tend to a constant level upstream we must require that $\theta(\xi)$ go to zero faster than $(-\xi)^{-\frac{1}{2}}$. Hence, from (4.3.6) we get $\xi_1=4$, giving a final solution for $\theta(\xi)$ of

$$\theta(\xi) = \frac{2\theta_W}{\pi}[2\arctan(-\xi)^{-\frac{1}{2}} - \arctan\, 2(-\xi)^{-\frac{1}{2}}]. \qquad (4.3.7)$$

We now restrict our attention to $\theta_W = \frac{\pi}{2}$ (vertical bow) and using (4.3.7) calculate the x- and y-coordinates of the free surface as

$$x(\xi) = \frac{\psi_0}{\pi U}\left(-2\log\left|\frac{\sqrt{(-\xi)} - \sqrt{(4-\xi)}}{2}\right| - \sqrt{(-\xi)}\sqrt{(4-\xi)}\right)+x(0) \qquad (4.3.8)$$

and $$y(\xi) = -\frac{\psi_0}{\pi U}\log\left|\frac{\sqrt{(4-\xi)}-2}{\sqrt{(4-\xi)}+2}\right| + y(-\infty). \qquad (4.3.9)$$

In order to find the y-coordinates of the stagnation point and the corner we first calculate $\tau(\xi)$ for $\xi>0$. To do this we substitute (4.3.7) into (4.3.2) giving

$$\tau(\xi) = -\log\left|\frac{(\sqrt{\xi}+1)^2\sqrt{|4-\xi|}}{(1-\xi)(\sqrt{\xi}+2)}\right| \qquad \xi>0$$

and hence $y(\xi) = -\frac{2\psi_0}{\pi U}\{\tfrac{1}{2}\sqrt{\xi}\sqrt{(4-\xi)} + 2\arcsin(\tfrac{1}{2}\sqrt{\xi})$

$$- 2\arcsin(\tfrac{1}{2}\sqrt{(\sqrt{\xi}+2)}) - \log\left|\frac{2+\sqrt{(4-\xi)}}{\sqrt{\xi}}\right|$$

$$- \tfrac{1}{2}\sqrt{3} + \frac{\pi}{3} + \log(2+\sqrt{3})\} + y(1)$$

$$0<\xi<4 \qquad (4.3.10)$$

where $y(1)$ is the y-coordinate of the stagnation point, $\xi=1$. To obtain $y(1)$ we match the two solutions (4.3.9) and (4.3.10) as ξ approaches zero from below and above respectively. This gives

$$\lim_{\xi\uparrow 0} -\frac{\psi_0}{\pi U}\{\log(-\xi) - \log(16)\} + y(-\infty)$$

$$= \lim_{\xi\downarrow 0} -\frac{2\psi_0}{\pi U}\{\tfrac{1}{2}\log(\xi) - \log(4) - \frac{\pi}{2} - \frac{\sqrt{3}}{2}$$

$$+ \frac{\pi}{3} + \log(2+\sqrt{3})\} + y(1),$$

from which it follows that

$$y(1) = \frac{2\psi_0}{\pi U}\{-\frac{\sqrt{3}}{2} - \frac{\pi}{6} + \log(2+\sqrt{3})\} + y(-\infty)$$

$$= -0.52\,\frac{\psi_0}{U} + y(-\infty).$$

The y-coordinate of the corner ($\xi=4$) is

$$y(4) = -\frac{2\psi_0}{\pi U}\{\pi-\pi-\frac{\sqrt{3}}{2}+\frac{\pi}{3}+\log(2+\sqrt{3})\}$$

$$+ \frac{2\psi_0}{\pi U}\{-\frac{\sqrt{3}}{2}-\frac{\pi}{6}+\log(2+\sqrt{3})\} + y(-\infty)$$

$$= -\frac{\psi_0}{U} + y(-\infty).$$

As $\tau=0$ for $\xi<0$ and $\tau\to 0$ as $\xi\downarrow 0$, the width of the jet will

tend to $\frac{\psi_0}{U}$.

The flow described by the solution is sketched in Fig. 4.3.6. Note in particular the result $y(4) = -\psi_0/U + y(-\infty)$, which indicates that the fluid comprising the jet is exactly that fluid above the level of the bottom of the solid body, i.e. the body is "skimming off" an amount of fluid exactly equal to its displacement.

The solution given above is relevant to the general problem with gravity in that it can be regarded as a local solution for bow flow. In the flow region near the bow attachment point, the free surface is strongly curved and the fluid is subject to high acceleration due to inertial effects - the effect of gravity is negligible. It is of interest to ask what happens to the jet as it rises up the vertical bow and gravitational effects become significant. The answer in practice is essentially that it just falls back onto itself giving a non-steady turbulent "mess". However, in theory, there seem to be two possibilities - either the jet detaches smoothly or it rises to a stagnation point and then falls away from the body.

The first possibility may be excluded since we have shown that it does not occur in the gravity-free case, and so will not occur if gravity is present - in either case there are no forces present which will make the fluid leave the body in a still-climbing jet. Note that this conclusion is made for a vertical bow - it may well be unjustified if the bow is overhanging and gravity can pull the fluid away from the body.

The second possibility is that already illustrated

in Fig. 4.2.2. There is some evidence that this sort of flow may exist. This is in the form of an exact solution introduced by Richardson [20] and discussed in more detail by Vitousek [33]. This solution satisfies the exact non-linear free surface conditions and was found in an inverse manner which is described in detail in Wehausen and Laitone [38], p.736-738. Fig. 4.3.7 shows the corresponding flow - it is of the nature of a flow which rises up a vertical wall to a stagnation point and then falls away, attaching to another wall tangentially. Note in particular that the upward climbing "jet" leaves the wall with a stagnation point, as we predict would happen with a bow flow in which a jet has formed.

The two types of bow flow we have considered - without or with a jet - are usually looked upon as those which would occur at low and high Froude number respectively, where the Froude number F_T is based on <u>draft</u>. The question then arises of how, and at what F_T, does the transition from one to the other occur. Dagan and Tulin [5] have considered this problem and suggest that transition occurs through a steepening of the free surface and the formation of a breaking wave at $F_T \simeq 1.5$. If the assumption of these two distinct bow flow regimes is valid, i.e. attachment with or without a jet, then it should be possible to show that, for a given configuration of the bow, the two integral equations concerned have solutions only for a restricted range of F_T-this would be a very interesting result.

CONCLUSION

It has been demonstrated that in fluid mechanical problems involving the motion of bodies across the surface of water, an a priori specification of the wetted area means that the hull shape and location must be treated as unknown, and found as part of the solution to the problem. Studies where the wetted area, shape and location of the hull are all taken as known may in fact produce results which are unphysical, e.g. involving negative pressures, or misleading, e.g. suggest the body is an infinite distance above the undisturbed free surface. Ideally, further work should focus on solution techniques for the direct physical problem, where only the hull shape is given, and the wetted area and vertical location are part of the solution.

However, failing this, the inverse method given in this thesis is worthy of further exploration. In order to proceed, numerical techniques need to be found which will expedite the calculation of the kernel in the three-dimensional finite Froude number case.

A further topic of interest is that introduced in Chapter 4. It would be of considerable value to ship designers if the relationship between bow-shape and the inception and strength of the bow-wave were clarified.

BIBLIOGRAPHY

[1] ABRAMOWITZ, M. & STEGUN, I.A.
"Handbook of Mathematical Functions"
Dover (1965)

[2] ASHLEY, H. & LANDAHL, M.T.
"Aerodynamics of Wings and Bodies"
Addison-Wesley (1965)

[3] BABA, E.
"Study on Separation of Ship Resistance Components"
Mitsubishi Technical Bulletin, No. 59 (1969) p.16

[4] CUMBERBATCH, E.
"Two-dimensional Planing at High Froude Number"
J. Fluid Mechanics, Vol.4, Part 5 (1958) pp.466-478

[5] DAGAN, G. & TULIN, M.P.
"Two dimensional free-surface gravity flow past blunt bodies"
J. Fluid Mechanics, Vol.51, Part 3 (1972) pp.529-543

[6] DOCTORS, L.J.
"Representation of Planing Surfaces by Finite Pressure Elements"
Fifth Australasian Conference on Hydraulics and Fluid Mechanics (1974)

[7] GREEN, A.E.
"Note on the Gliding of a Plate on the Surface of a Stream"
Proc. Cambridge Phil. Soc. Vol.32 (1936) pp.248-252

[8] HESS, F.
"Rotating airfoils in steady flow"
Mathematisch Instituut Rijksuniversiteit Groningen, Report TW-111

[9] HOGNER, E.
"Über die theorie der von einem Schiff erzeugten Wellen und des Wellenwiderstandes"
Proceedings of the first International Congress for Applied Mechanics, Delft (1924) pp.146-160

[10] KELVIN, LORD (Sir. W. THOMSON)
"On the Waves Produced by a Single Impulse in Water of Any Depth, or in a Dispersive Medium"
Proc. Roy. Soc. London, Ser. A. Vol.42 (1887) pp.80-85

[11] MARUO, H.
"Two Dimensional Theory of the Hydroplane"
Proceedings of the 1st Japan National Congress for Applied Mechanics, (1951) pp.409-415

[12] MARUO, H.
"Hydromechanic Researches of the Hydroplane" 1,11,111 (Japanese)
J. Zôsen Kiôkai, Vol.91 (1956) pp.9-16; Vol.92 (1957) pp.57-63; Vol.105 (1959) pp.23-26.

[13] MARUO, H.
"High-and-Low-Aspect-Ratio Approximation of Planing Surfaces"
Schiffstechnik, Bd.14, Heft 72 (1967) pp.57-64

[14] MICHELL, J.H.
"The Wave-Resistance of a Ship"
London, Dublin and Edinburgh, Philosophical Magazine, Ser. 5, Vol.45 (1898) pp.106-123

[15] MILNE-THOMSON, L.M.
"Theoretical Hydrodynamics"
MacMillan (1968) fifth edition

[16] MULTHOPP, H.
"Methods for Calculating the Lift Distribution of Wings (Subsonic Lifting-Surface Theory)"
Aeronautical Research Council, London, Reports and Memoranda No. 2884, Jan.1950

[17] NEWMAN, J.N.
"A Linearized Theory for the Motion of a Thin Ship in Regular Waves"
J. Ship Research, Vol.5, June 1961, pp.34-55

[18] NEWMAN, J.N. & TUCK, E.O.
"Current Progress in the Slender Body Theory for Ship Motions"
Fifth Symposium on Naval Hydrodynamics, Bergen (1964) pp.129-166

[19] PETERS, A.S. & STOKER, J.J.
"The Motion of a Ship, as a Floating Rigid Body, in a Seaway"
Communications on Pure and Applied Mathematics, Volume X (1957) pp.399-490

[20] RICHARDSON, A.R.
"Stationary Waves in Water"
Phil. Mag. (6) Vol. 40 (1920) pp.97-110

[21] RUDZKI, M.P.
"Über eine Klasse hydronamischer Probleme mit besonderen Grenzbedingungen"
Math. Ann. Vol.40 (1898) pp.269-281

[22] SAVITSKY, D.
"Hydrodynamic Design of Planing Hulls"
Marine Technology, Vol.1, No.1 (1964) pp.71-95

[23] SHEN, Y.-T.
"Theory of High-Aspect-Ratio Planing Surfaces"
Department of Naval Architecture and Marine Engineering, University of Michigan, Report No. 102 (1970)

[24] SQUIRE, H.B.
"The Motion of a Simple Wedge along the Water Surface"
Proc. Roy. Soc. London, Ser. A, Vol.243 (1957) pp.48-64

[25] SRETENSKII, L.N.
"On the Motion of a Glider on Deep Water"
Izv. Akad. Nauk SSSR, Otdel. Mat. Estest. Nauk (1933) pp.817-835 (In English)

[26] TANIGUCHI, K., TAMURA, K. & BABA, E.
"Reduction of Wave-Breaking Resistance by "MHI-Bow""
Japan Shipbuilding and Marine Engineering, Vol. 7, No. 1 (1973) pp.7-14

[27] TAYLOR, P.J.
"The effect of beam seas on a stationary ship in shallow water"
Ph. D. Thesis, University of Adelaide (1971)

[28] THWAITES, B.
"Incompressible Aerodynamics"
Oxford (1960)

[29] TUCK, E.O.
"The steady motion of a slender ship"
Ph. D. Thesis, University of Cambridge (1963)

[30] TUCK, E.O.
"The effect of span-wise variations in amplitude on the thrust-generating performance of a flapping thin wing"
Symposium on Swimming and Flying in Nature, California Institute of Technology, Pasadena, California, July 1974

[31] TUCK, E.O.
"Low-Aspect-Ratio Flat-Ship Theory"
Department of Naval Architecture and Marine Engineering, University of Michigan, Report No. 144, June 1973 (To appear in J. Hydronautics, 1975)

[32] TUCK, E.O. & NEWMAN, J.N.
"Hydrodynamic interaction between ships"
10th Symposium on Naval Hydrodynamics, Massachusetts Institute of Technology (1974)

[33] VITOUSEK, M.J.
"Some flows in a gravity field satisfying the exact free surface condition"
Applied Mathematics and Statistics Laboratory, Stanford University, Stanford, California, Technical Report No. 25 (1954)

[34] VOSSERS, G.
"Some applications of the slender body theory to ship hydrodynamics"
Ph.D. Thesis, Technische Hogeschool, Delft (1962)

[35] WAGNER, H.
"Über Stoss- und Gleitvorgänge an der Oberflächen von Flüssigkeiten"
Zeitschrift für Angewandte Mathematik und Mechanik,

Bd.12, Heft 4 (1932) pp.193-215

[36] WAGNER, S.

"On the Singularity Method of Subsonic Lifting-Surface Theory"

J. Aircraft, Vol.6, No. 6, Nov.-Dec. 1969, pp.549-558

[37] WANG, D.P. & RISPIN, P.

"Three-dimensional Planing at High Froude Number"

J. Ship Research, Vol.15, No. 3 (1971) pp.221-230

[38] WEHAUSEN, J.V. & LAITONE, E.V.

"Surface Waves"

Handbuch der Physik, Springer-Verlag, Berlin (1960) pp.446-778

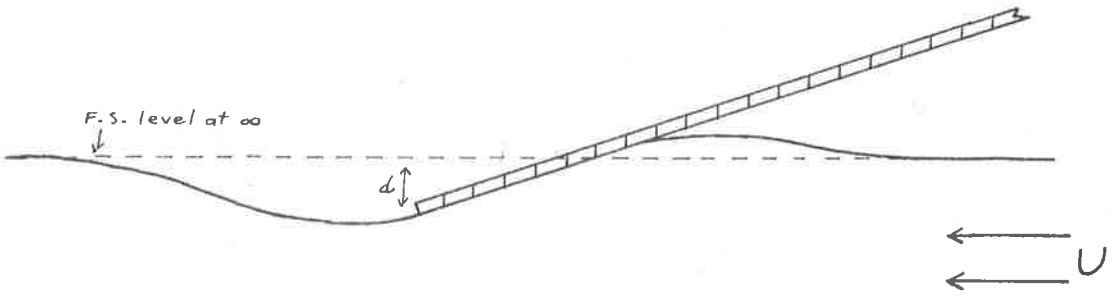

Fig. 1.4.1.

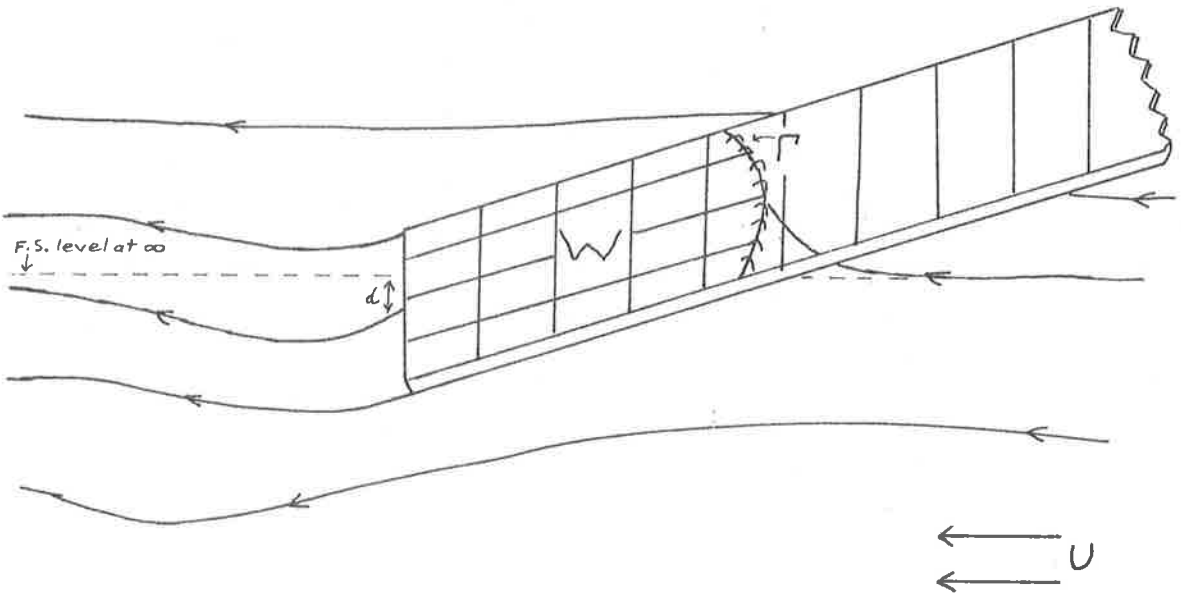

Fig. 1.4.2.

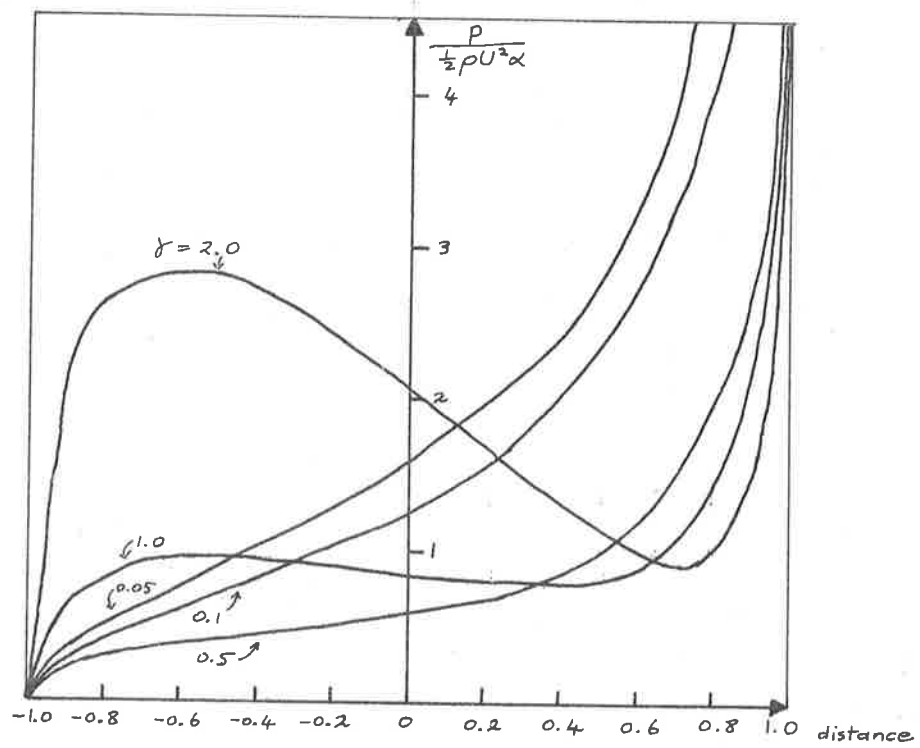

Fig. 2.3.1 - Pressure coefficient/α for a flat plate at angle of attack α.

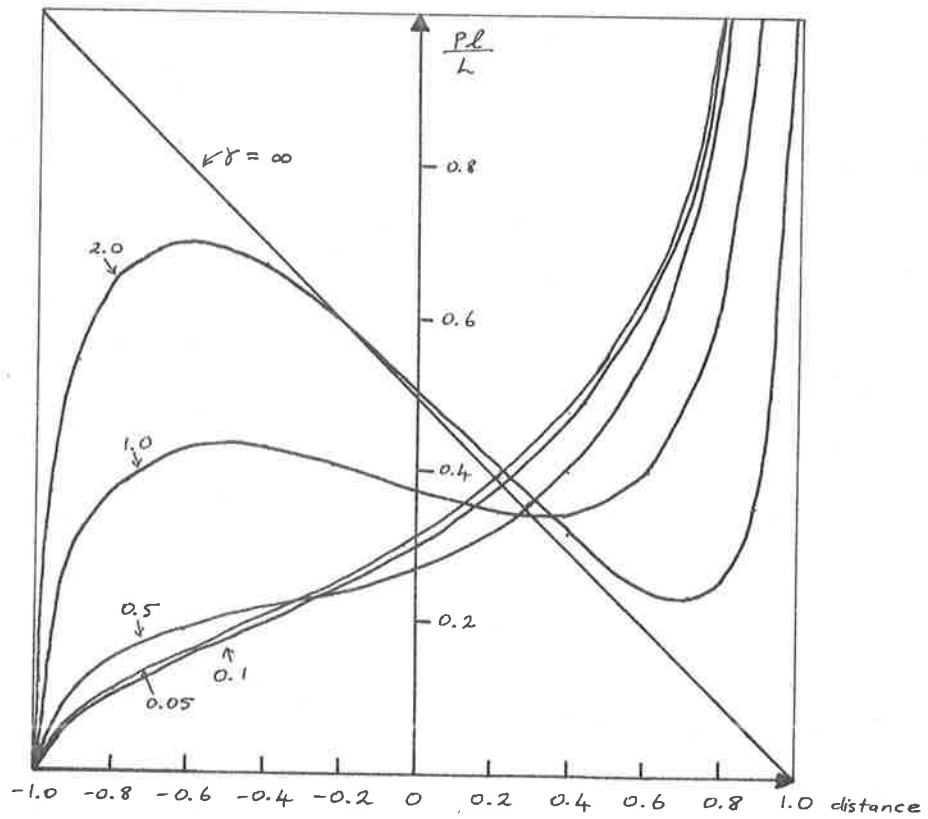

Fig. 2.3.2 - Pressure coefficient/lift coefficient for a flat plate .

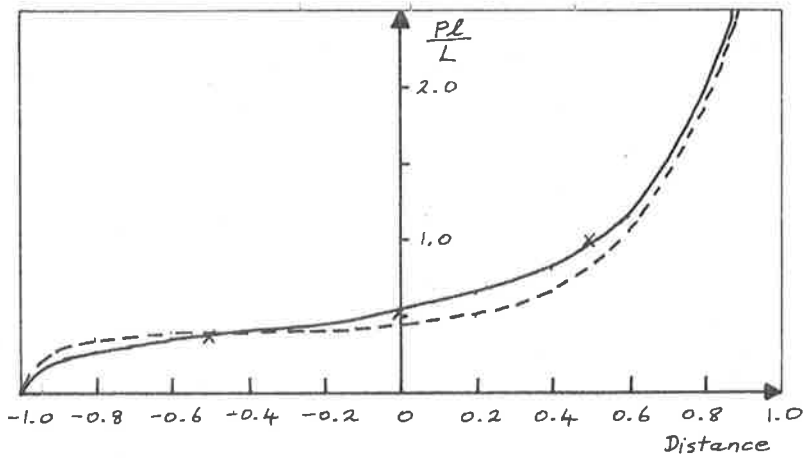

Fig. 2.3.3 - Comparison of pressure coefficient/lift coefficient for a flat plate (γ=0.5); ---, Squire's results; x, Maruo's results; ——, present results.

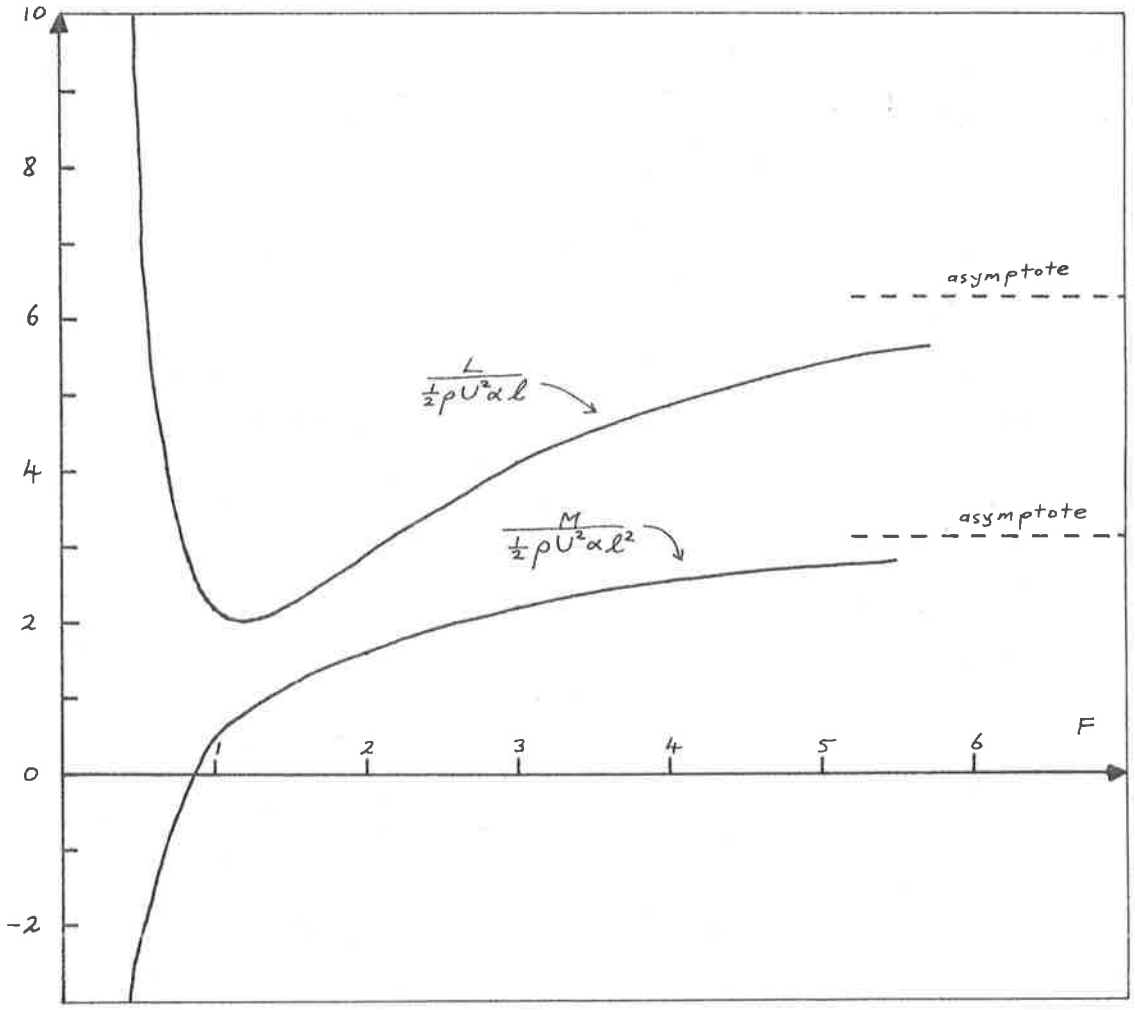

Fig. 2.3.4 - Lift and moment coefficients against Froude number based on wetted length for a flat plate.

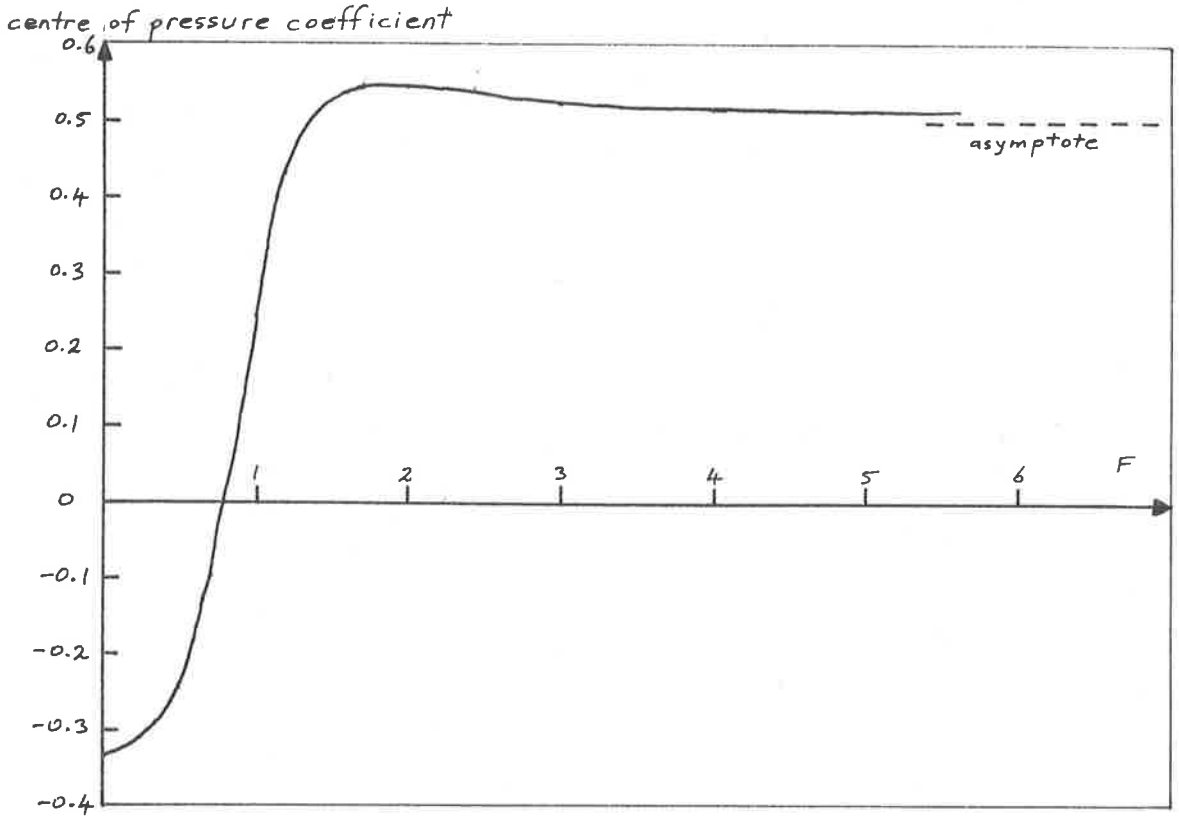

Fig. 2.3.5 - Centre of pressure coefficient against Froude number based on wetted length for a flat plate.

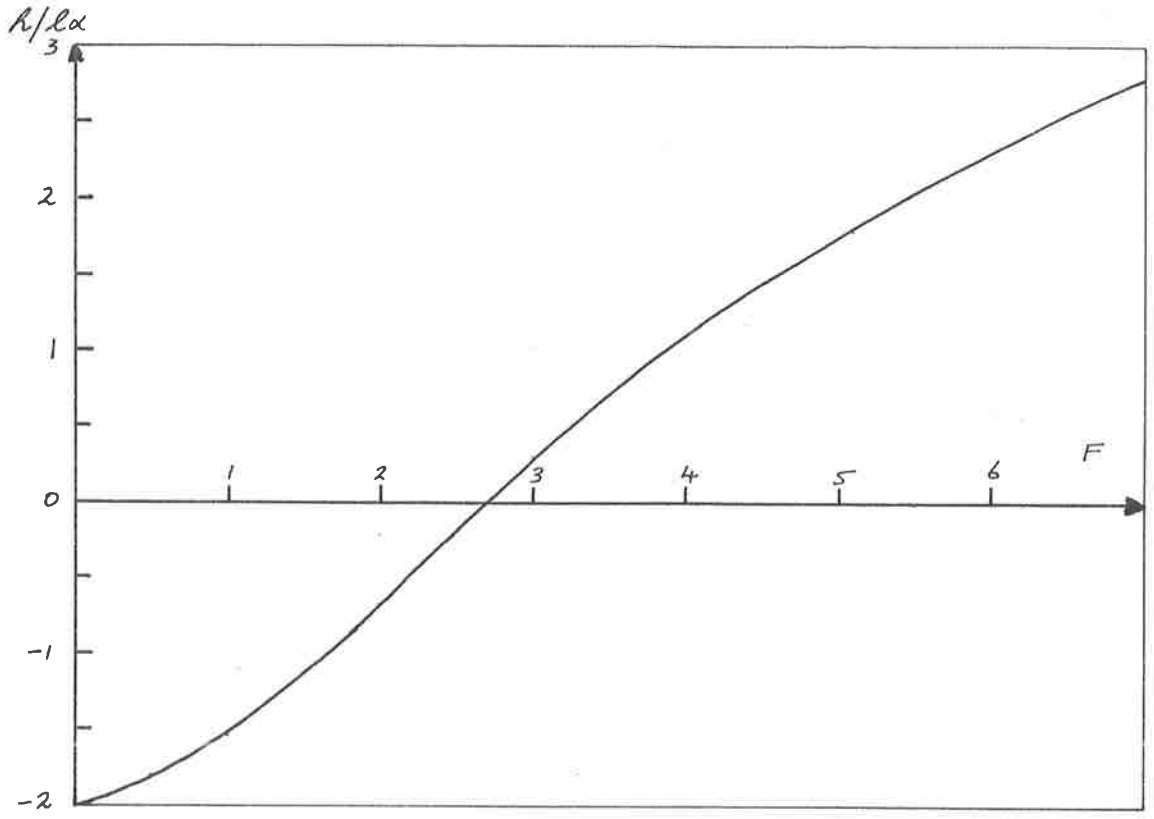

Fig. 2.3.6 - Scaled height of the trailing edge against Froude number based on wetted length for a flat plate.

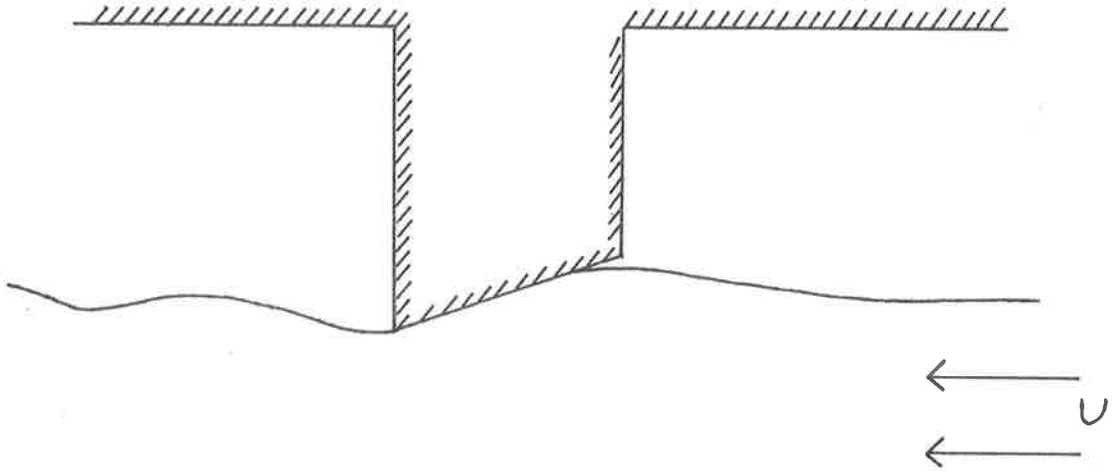

First experiment - α and h fixed.

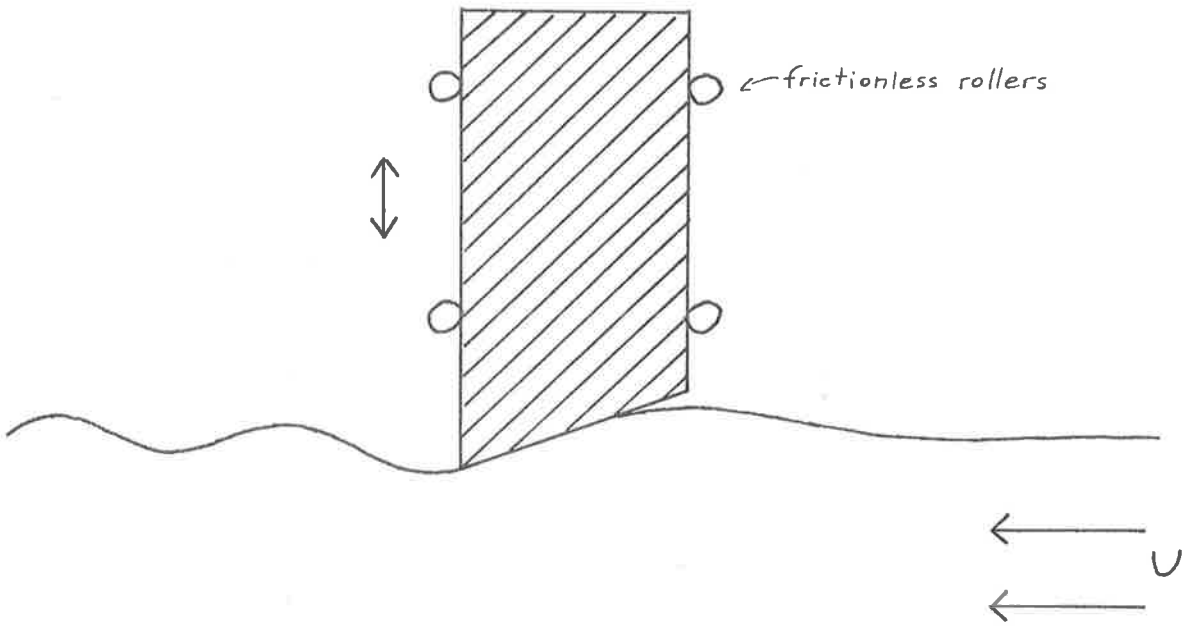

Second experiment - α and L fixed.

Fig. 2.3.7.

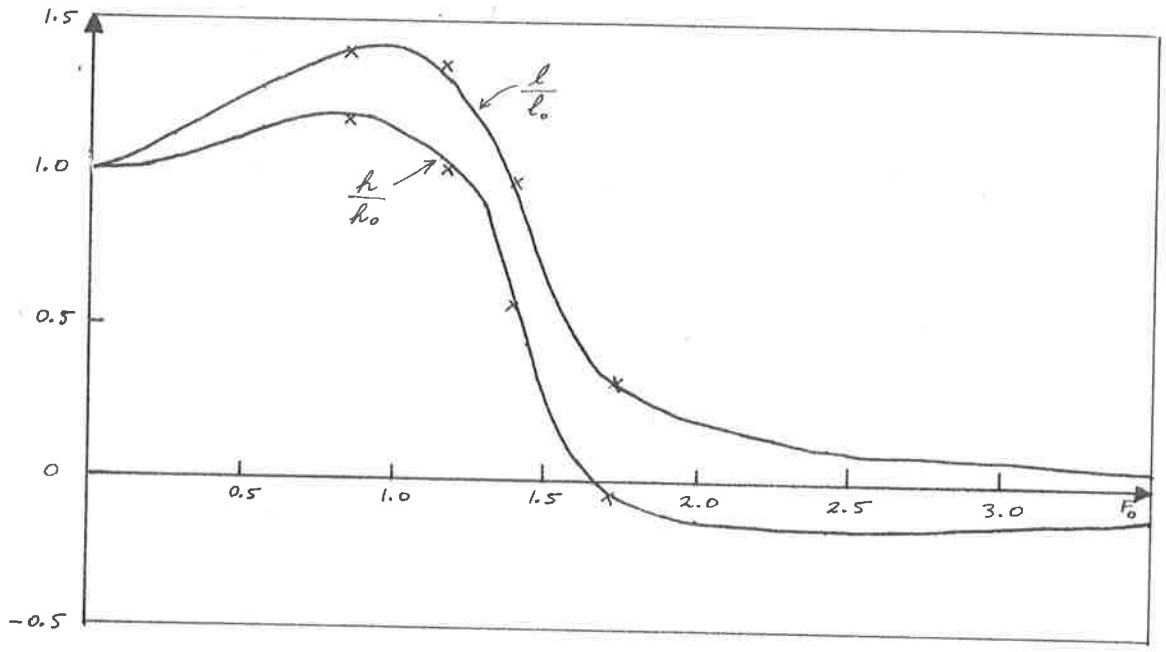

Fig. 2.3.8 - Scaled wetted length and trailing edge height against Froude number based on wetted length at rest for a flat plate; x Squire's results.

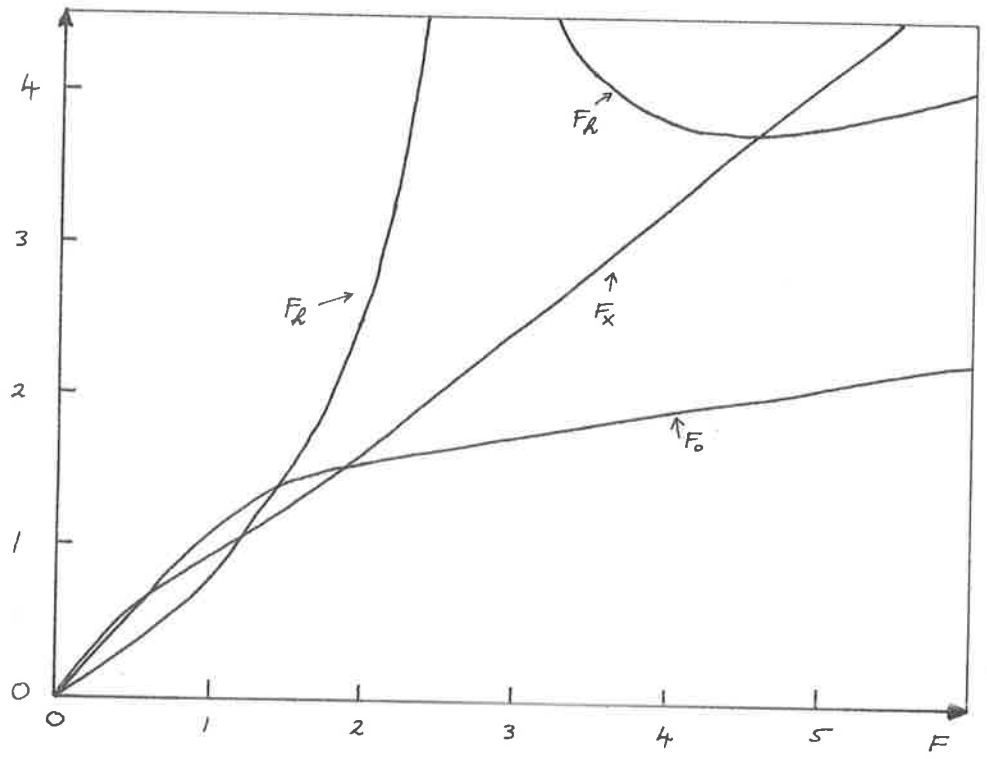

Fig. 2.3.9 - Froude numbers based on wetted length at rest, F_0; fixed height and angle of attack, F_h; and fixed centre of pressure, F_x; against Froude number based on wetted length for a flat plate.

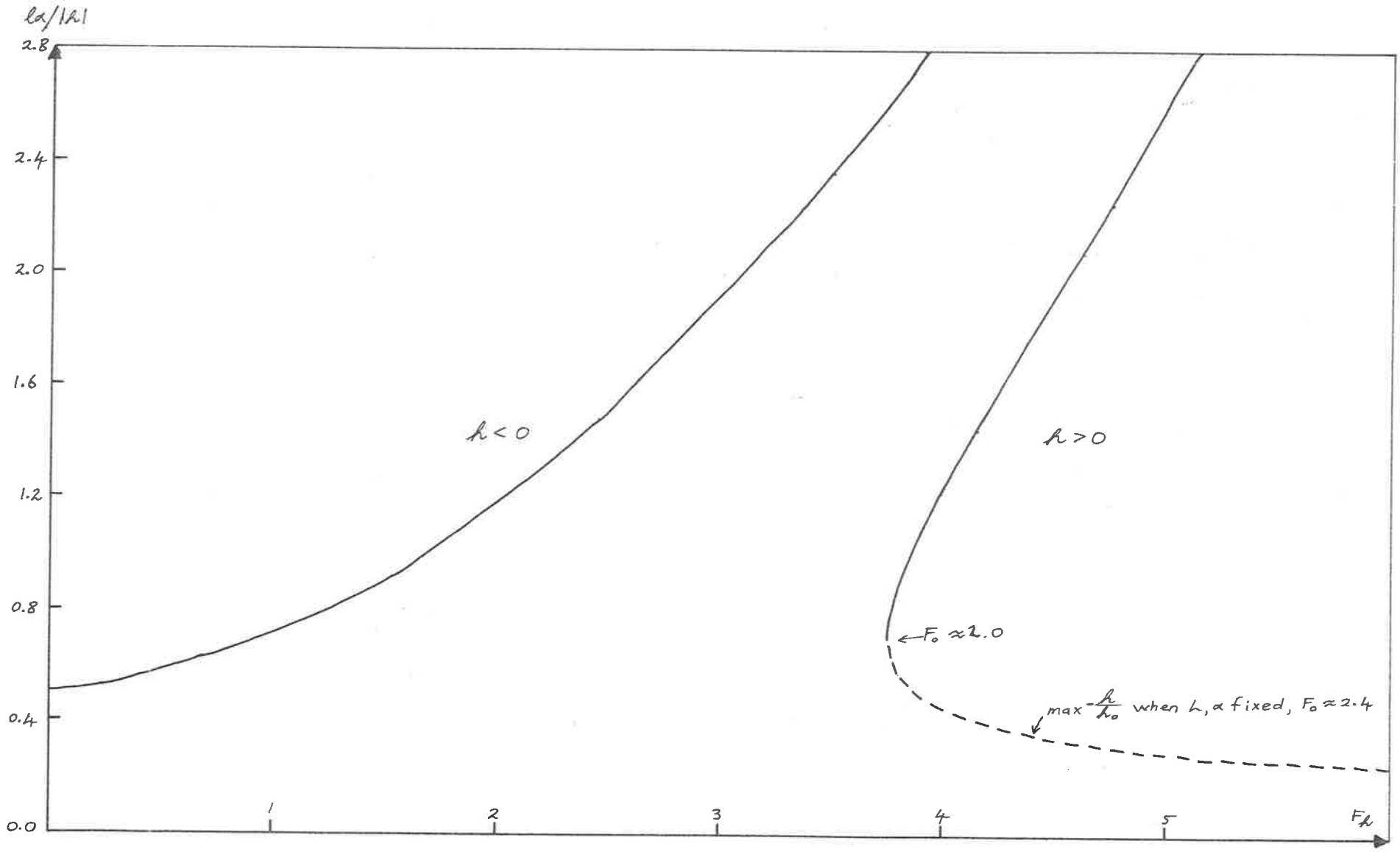

Fig. 2.3.10 - Scaled wetted length against Froude number based on fixed height and angle of attack for a flat plate.

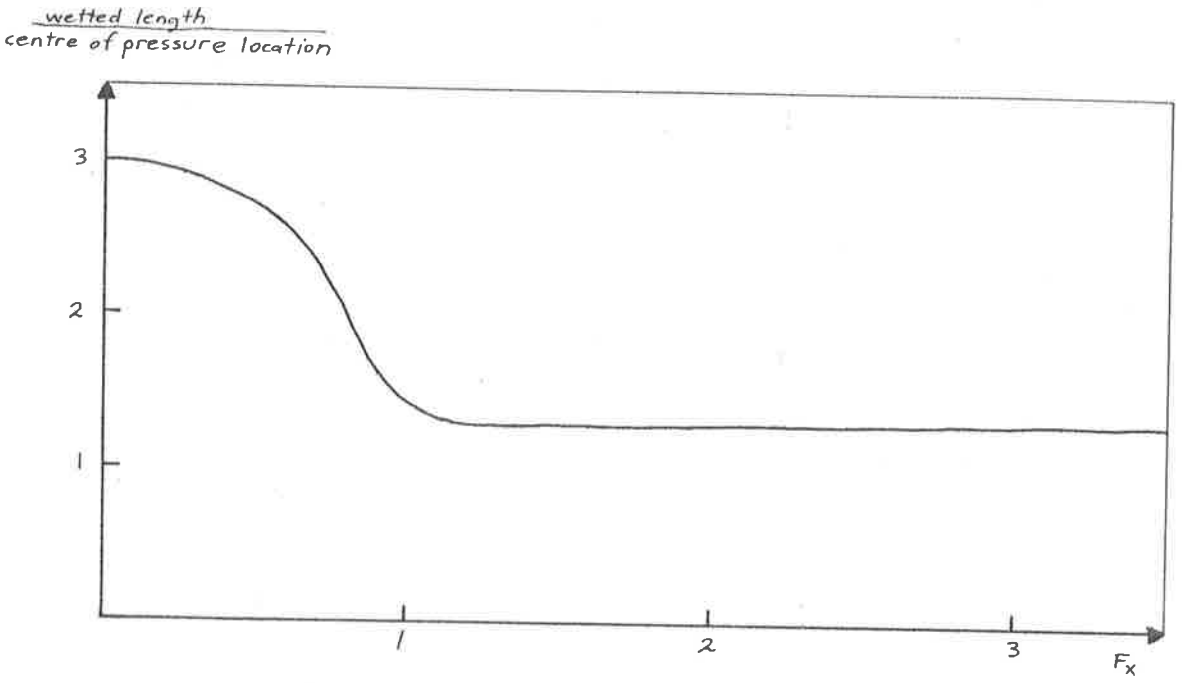

Fig. 2.3.11 - Scaled wetted length against Froude number based on fixed centre of pressure for a flat plate.

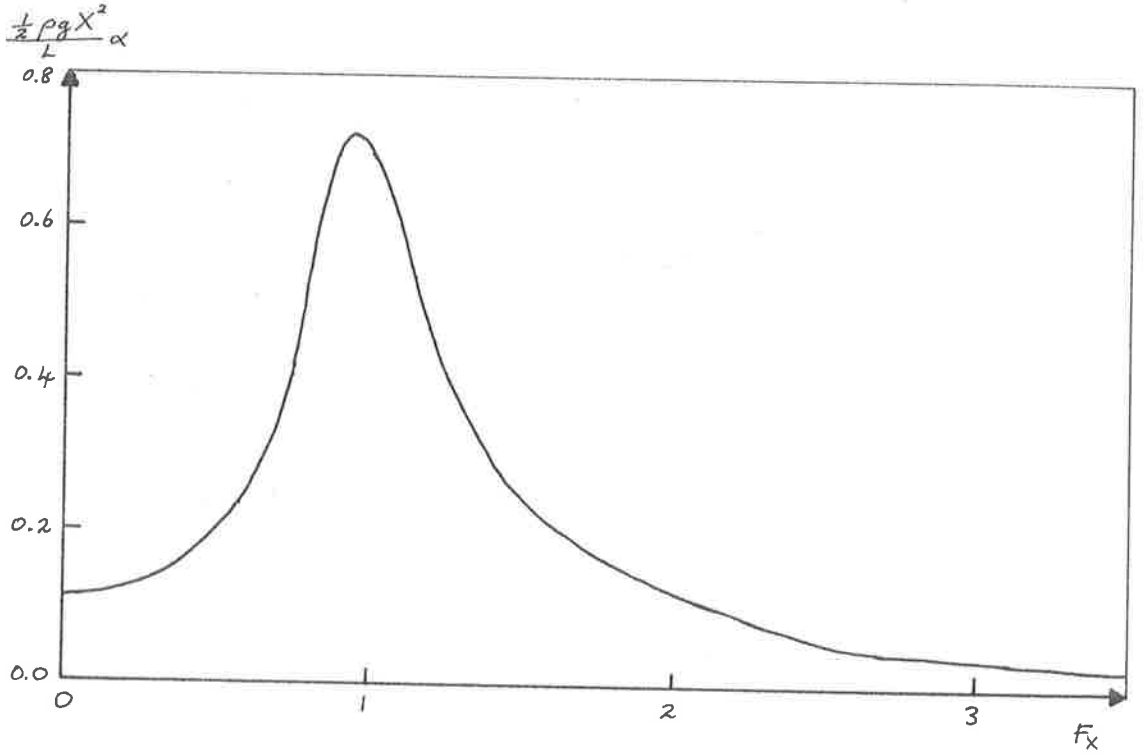

Fig. 2.3.12 - Scaled angle of attack against Froude number based on fixed centre of pressure for a flat plate.

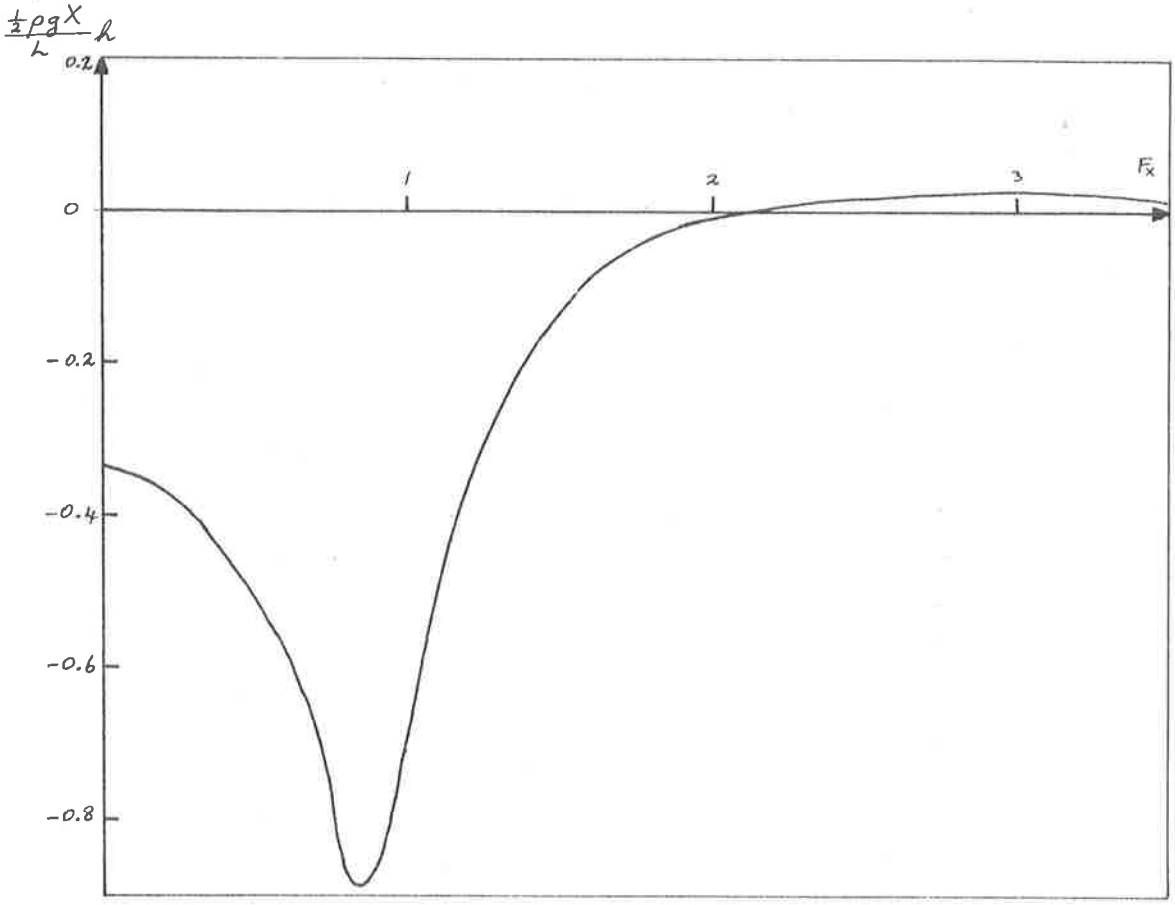

Fig. 2.3.13 - Scaled height of the trailing edge against Froude number based on fixed centre of pressure for a flat plate.

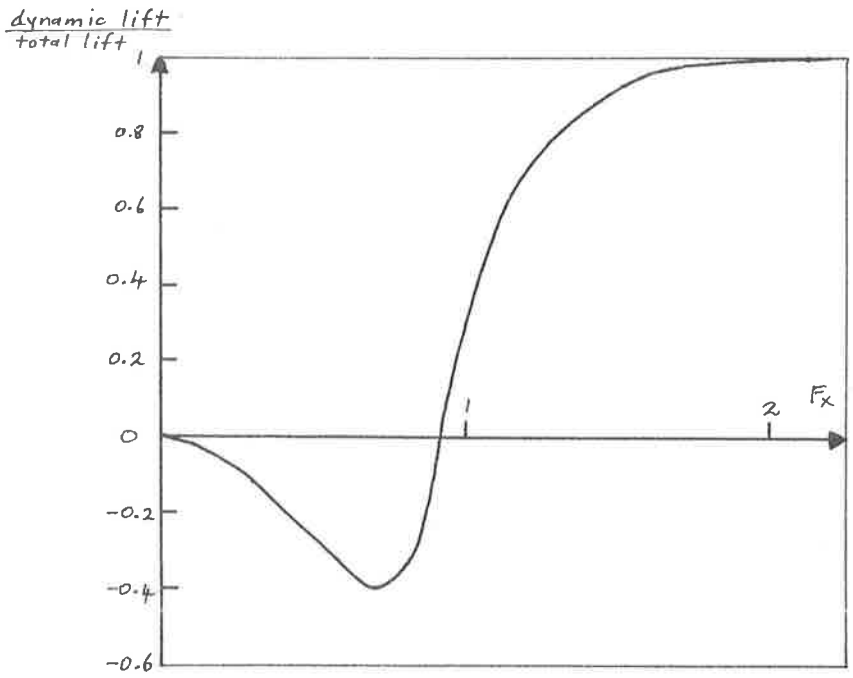

Fig. 2.3.14 - Dynamic lift/total lift against Froude number based on fixed centre of pressure for a flat plate.

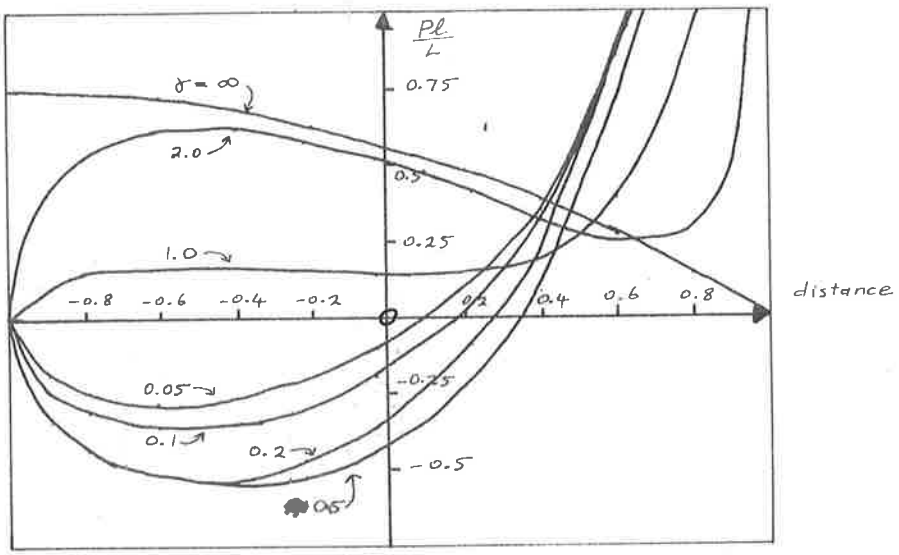

Fig. 2.4.1 - Pressure coefficient/lift coefficient for parabolic plate $\zeta = (x+1)^2$.

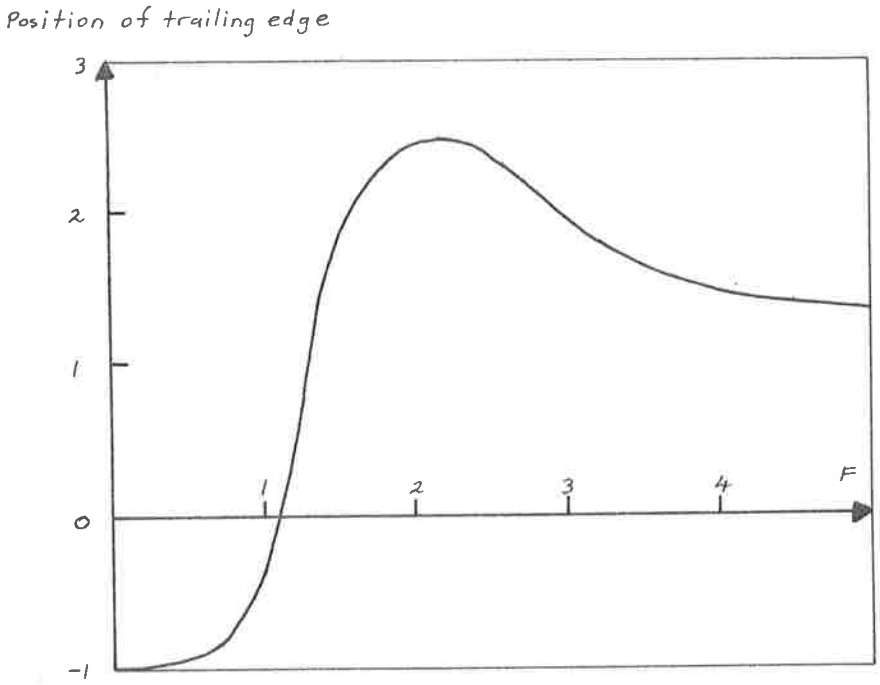

Fig. 2.4.2 - Distance trailing edge is ahead of axis of symmetry of $\zeta = \alpha x^2$ for wetted length of 2, against Froude number.

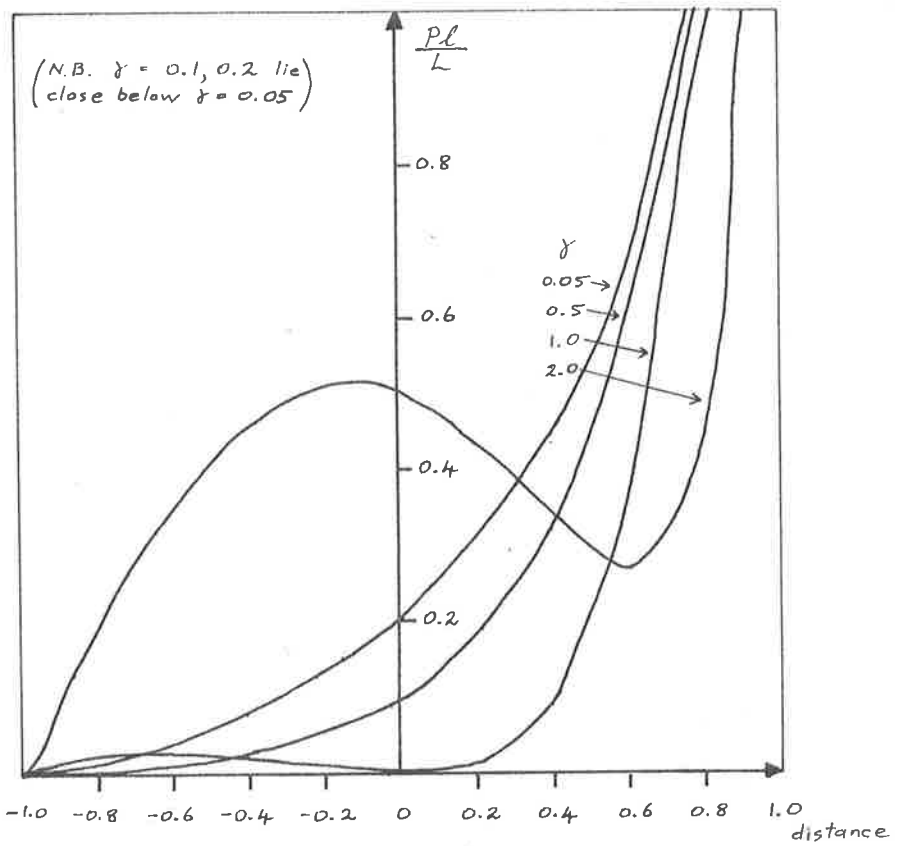

Fig. 2.4.3 - Pressure coefficient/lift coefficient for "solution" parabolic hull.

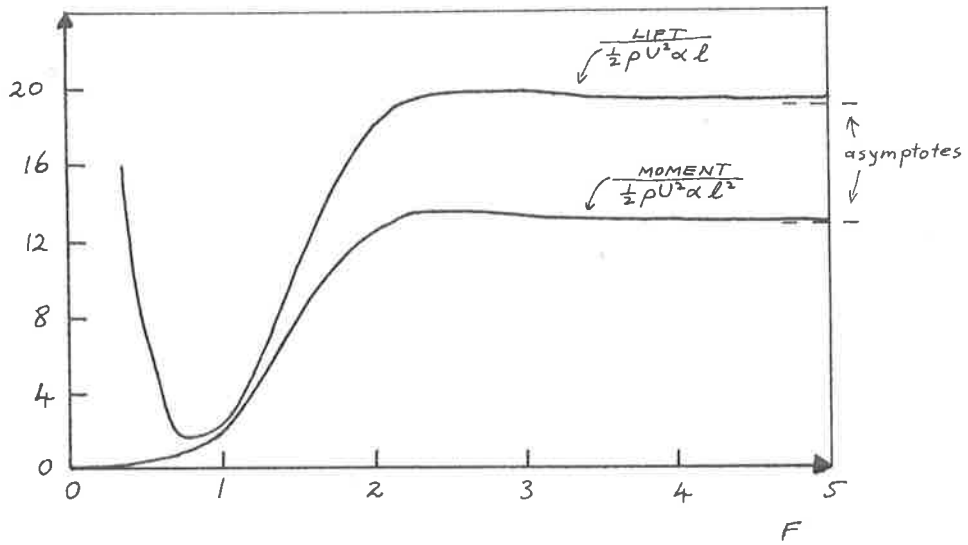

Fig. 2.4.4 - Lift coefficient and moment coefficient against Froude number for "solution" parabolic hull.

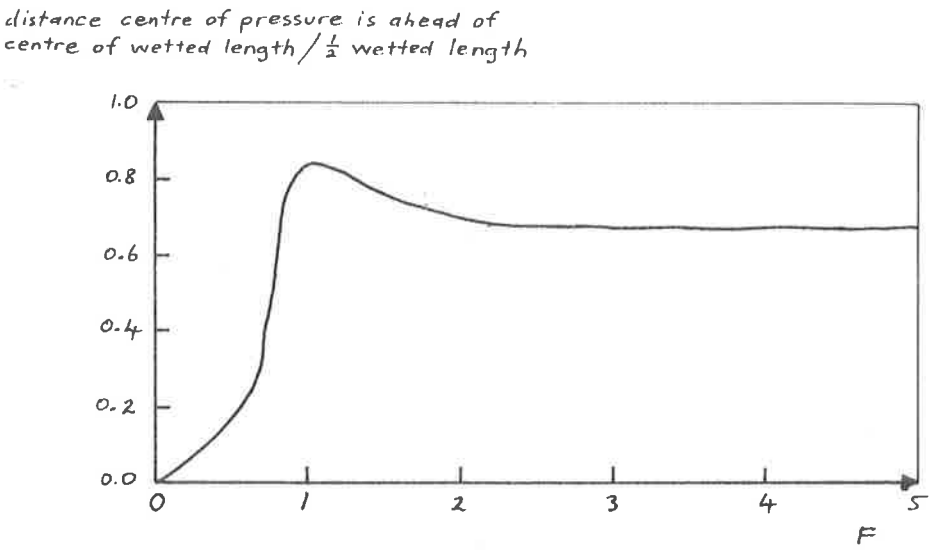

Fig. 2.4.5 - Centre of pressure coefficient against Froude number for "solution" parabolic hull.

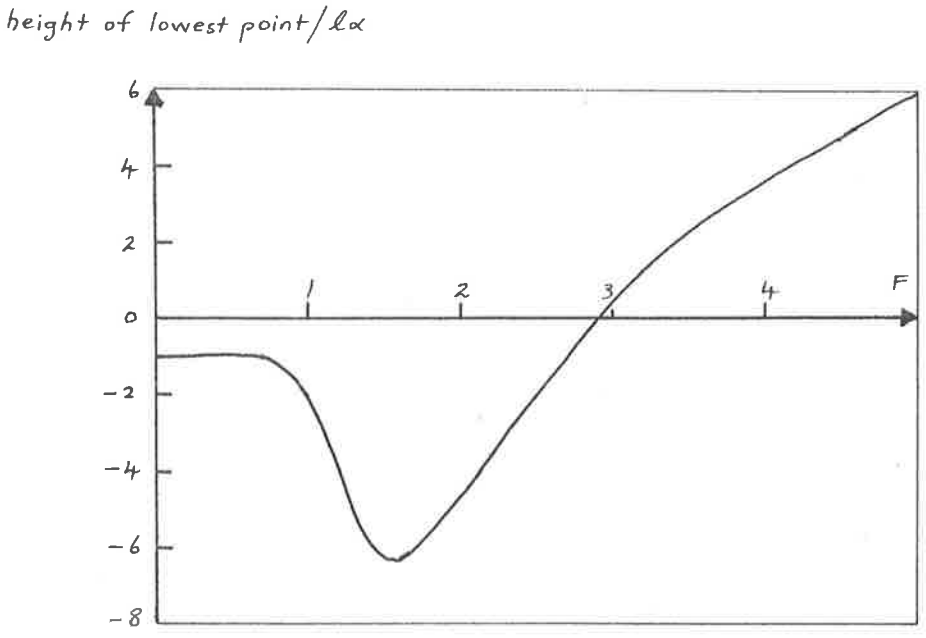

Fig. 2.4.6 - Scaled height of the lowest point of the hull against Froude number for "solution" parabolic hull.

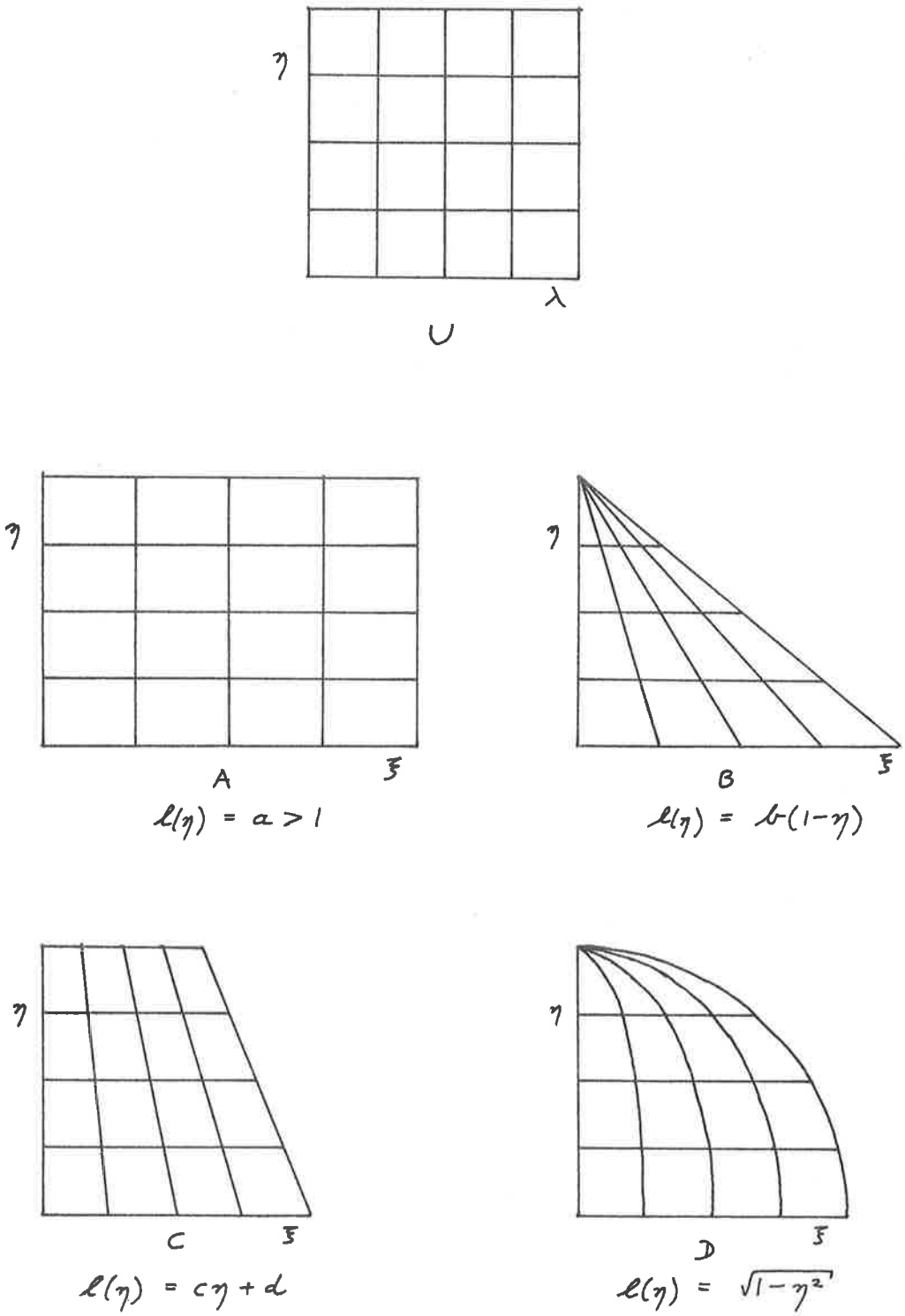

Fig. 3.3.1 - Mesh on unit square (U) and actual meshes on W' under consideration (A,B,C,D).

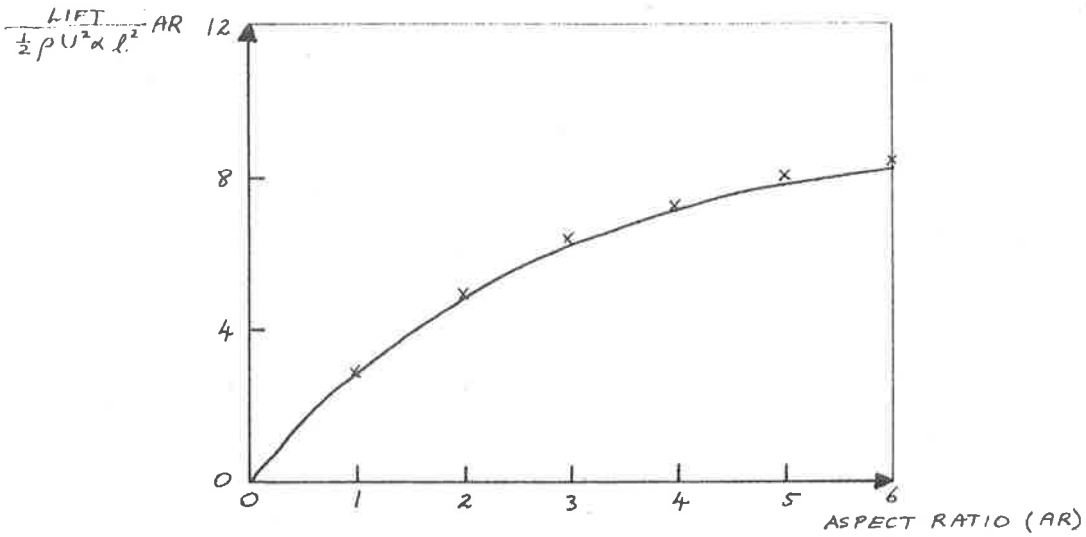

Fig. 3.4.1 - Lift slope against aspect ratio for rectangular wetted area; x Küchermann (1952) from Thwaites, p.343.

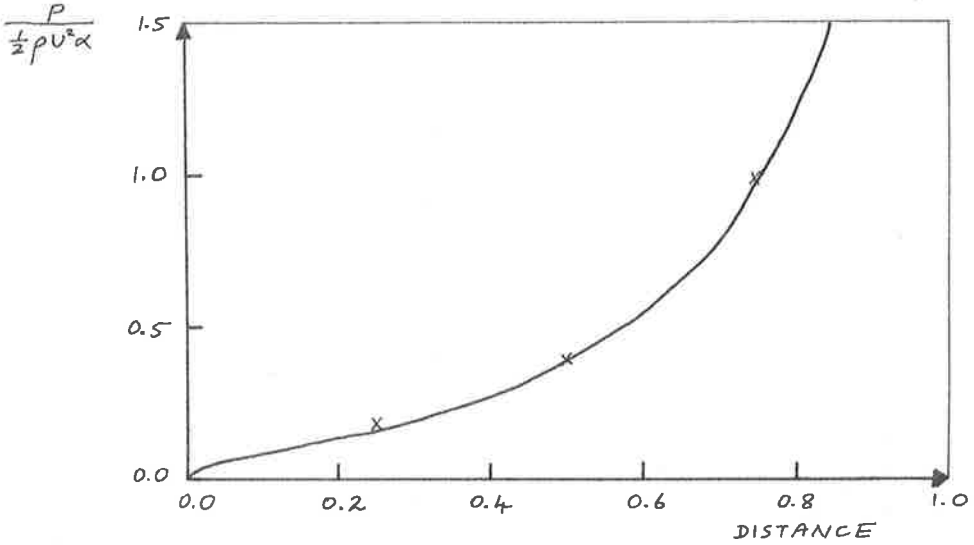

Fig. 3.4.2 - Centre-line pressure coefficient for aspect ratio one rectangle; x Wang and Rispin.

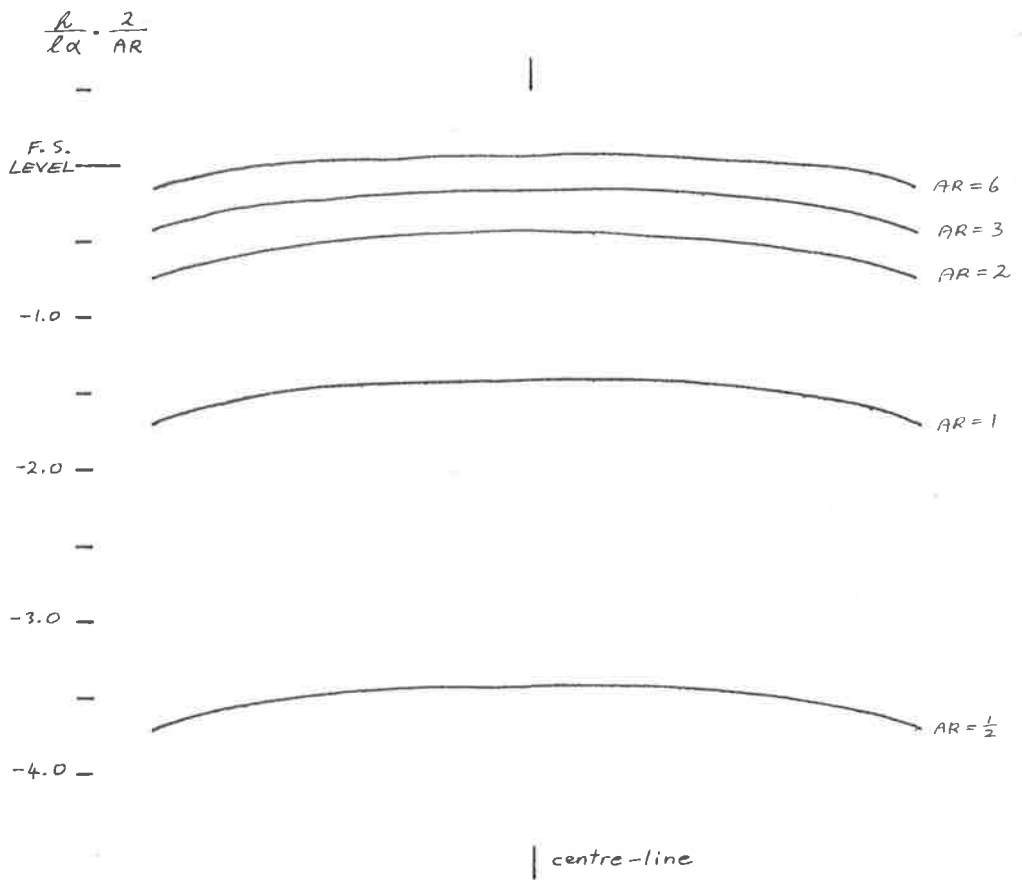

Fig. 3.4.3 - Scaled trailing edge shape and height for rectangular wetted area.

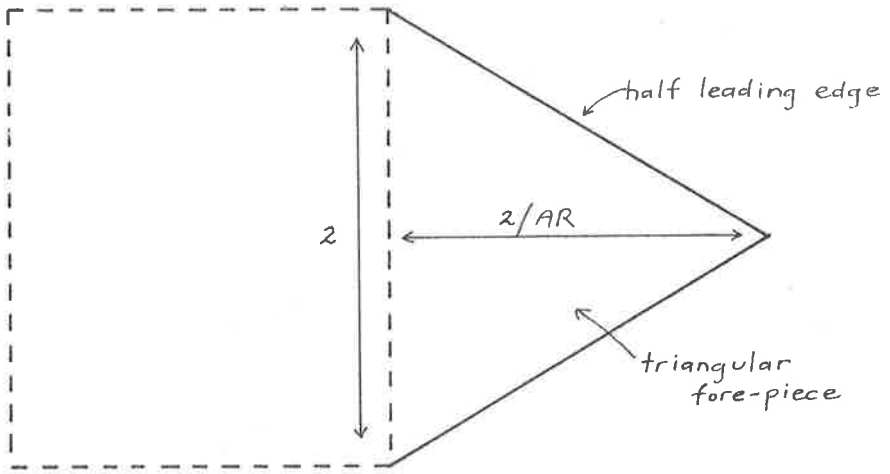

Fig. 3.5.1 - Wetted area considered in section 3.5;
AR = aspect ratio of triangular fore-piece.

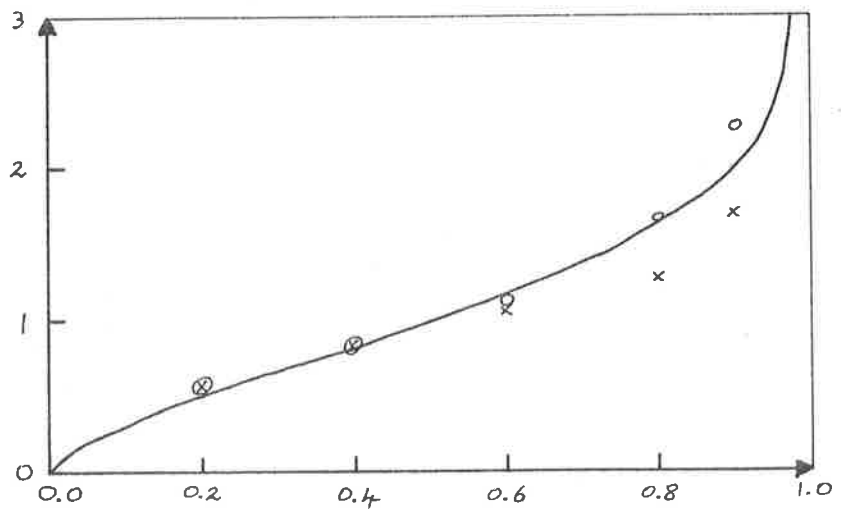

Fig. 3.5.2 - Centre-line pressure coefficient for Thwaites cropped delta; x Hancock (1953), o Küchemann (1952) from Thwaites, p.347.

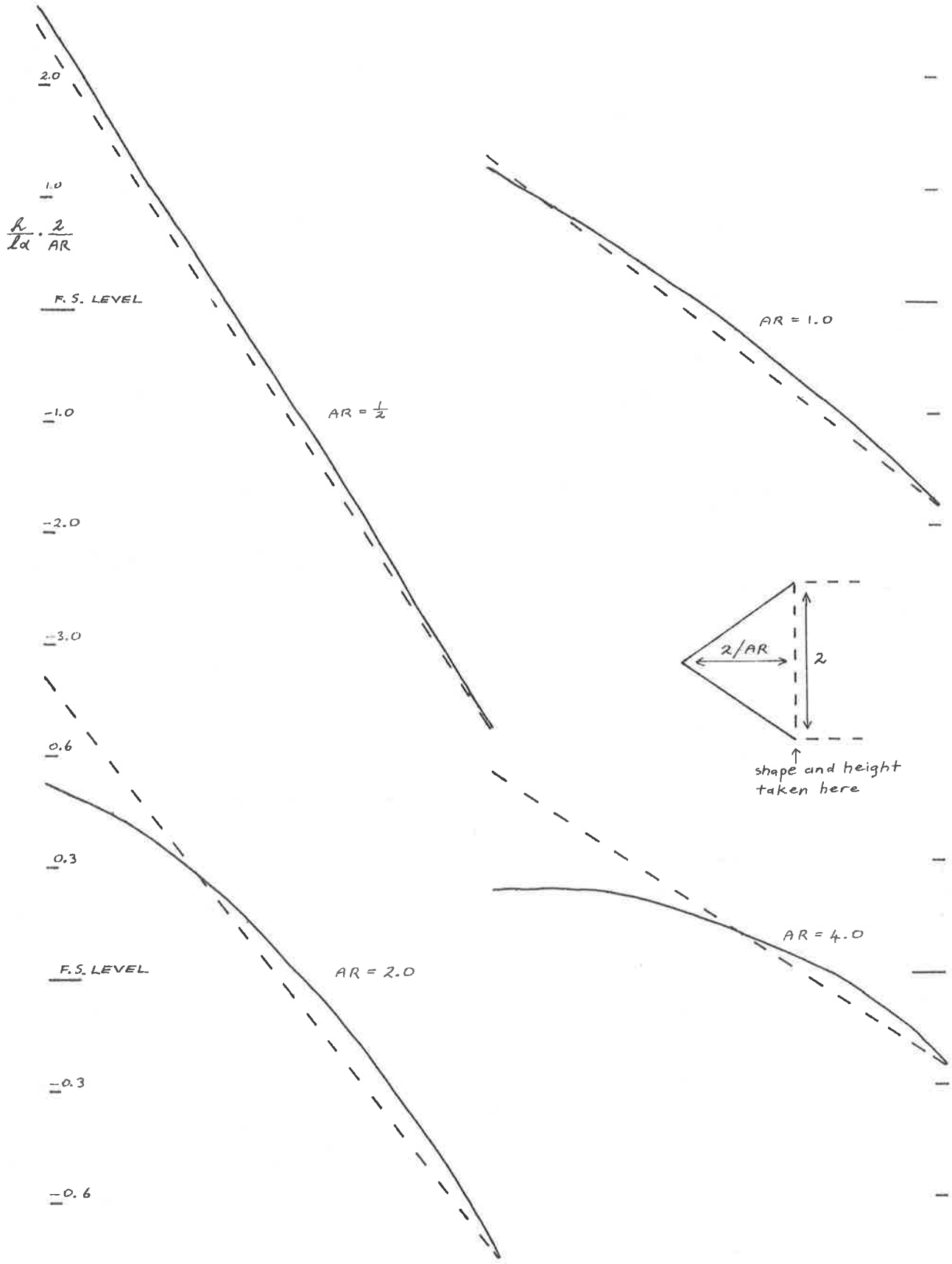

Fig. 3.5.3 - Scaled shape and height of half-body at rear of triangular fore-piece - dashed line is constant-deadrise body predicted by Savitsky's formula.

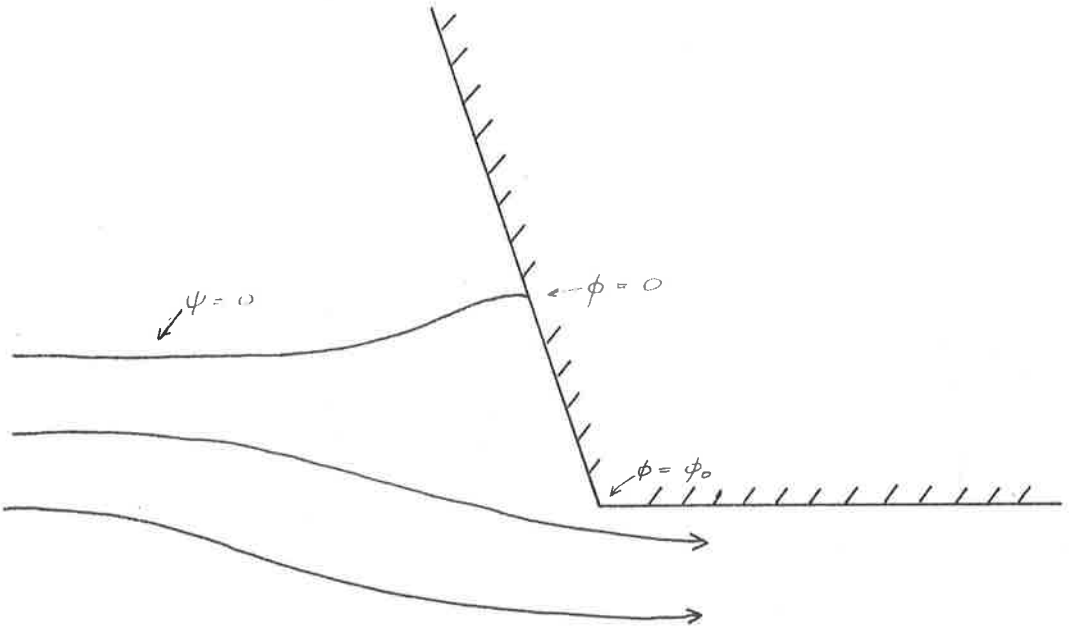

Fig. 4.2.1.

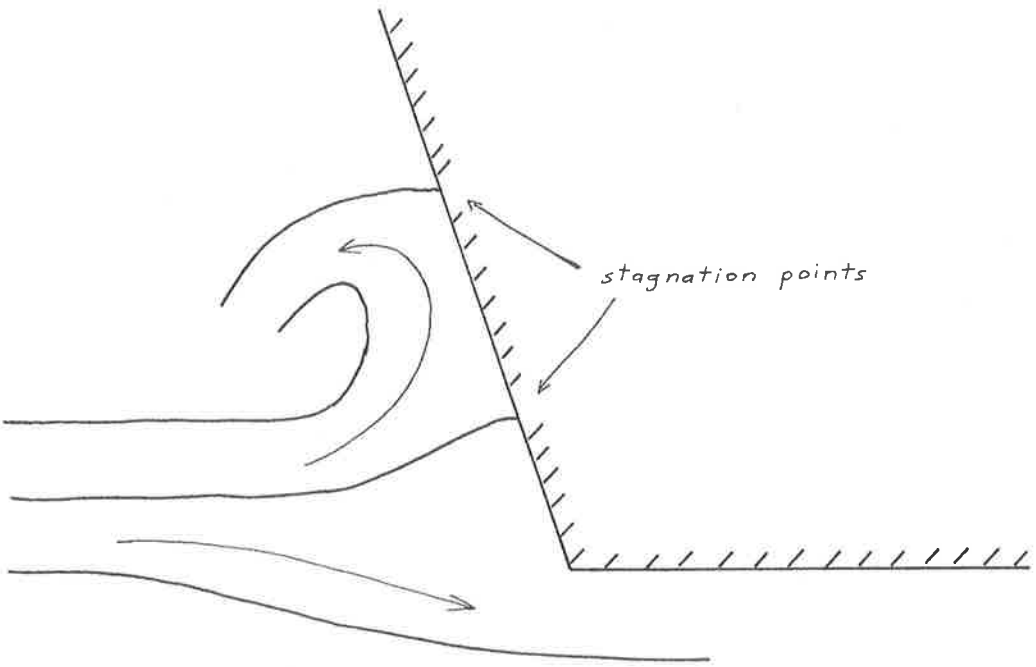

Fig. 4.2.2.

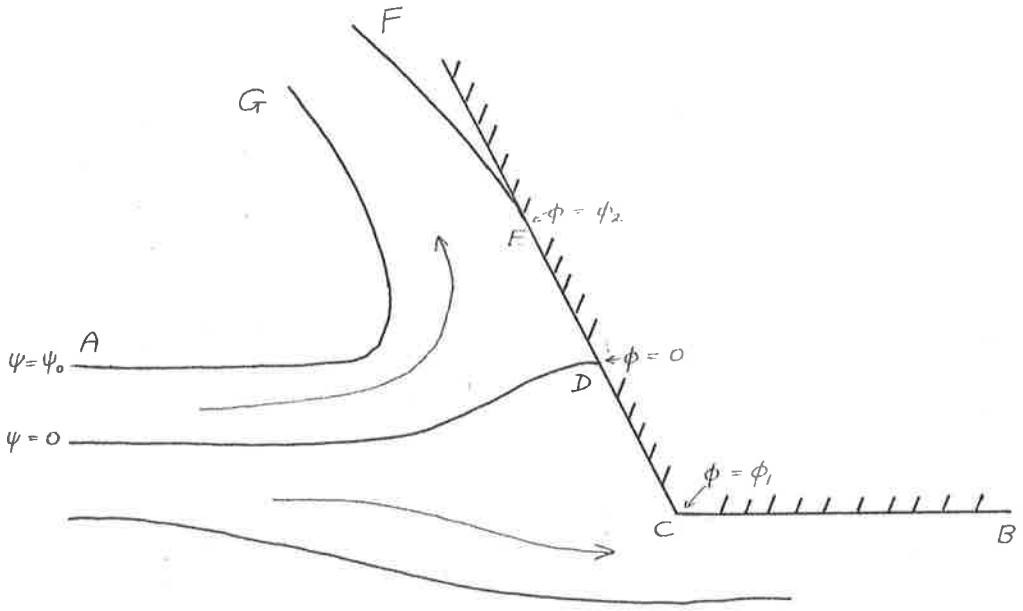

Fig. 4.3.1 - The physical plane.

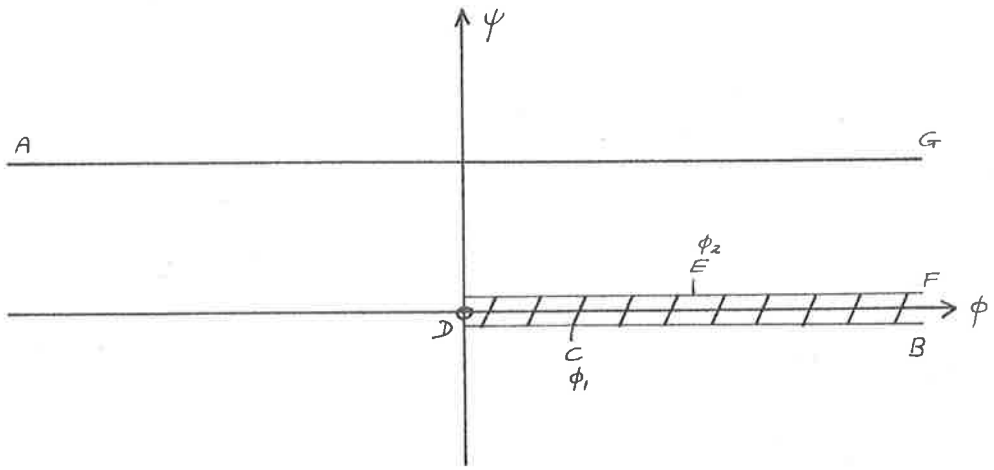

Fig. 4.3.2 - The f-plane.

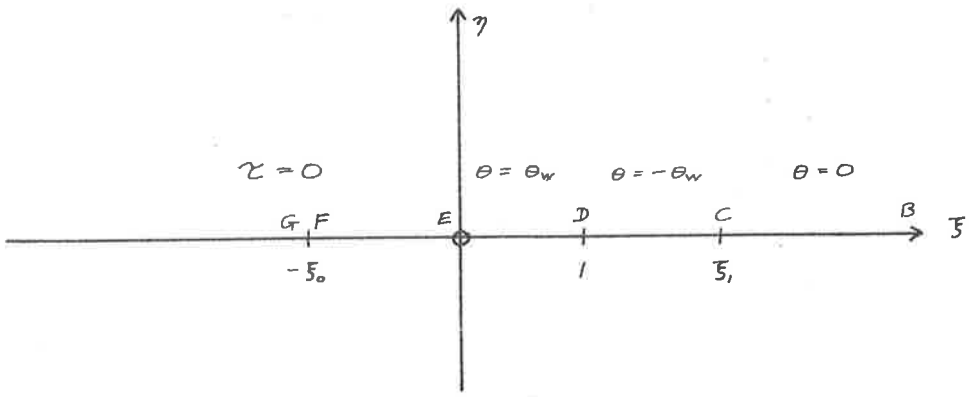

Fig. 4.3.3 - The ζ-plane.

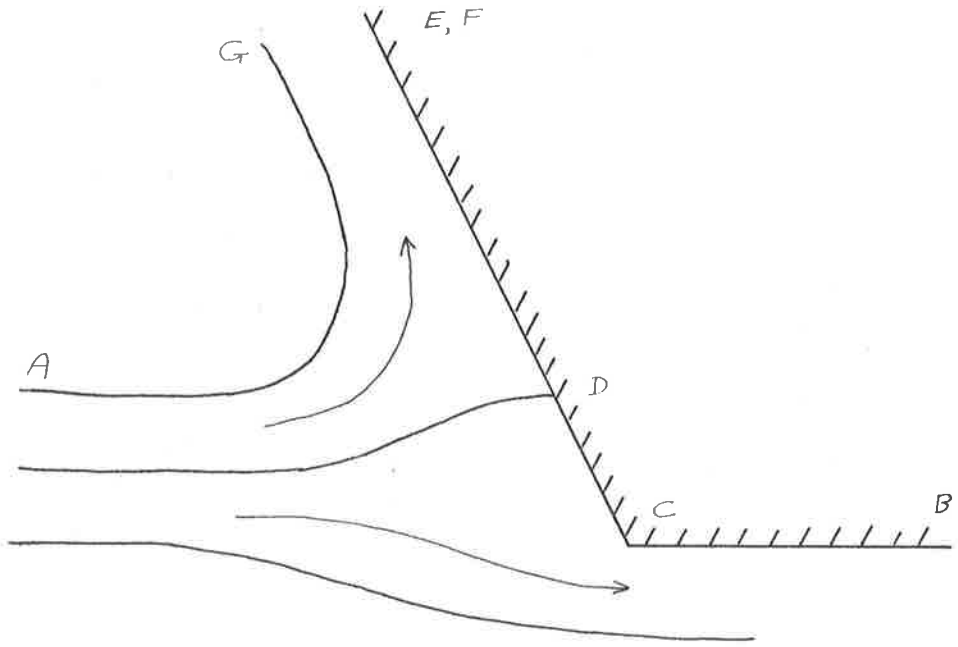

Fig. 4.3.4 - Infinite bow; E,F coincident.

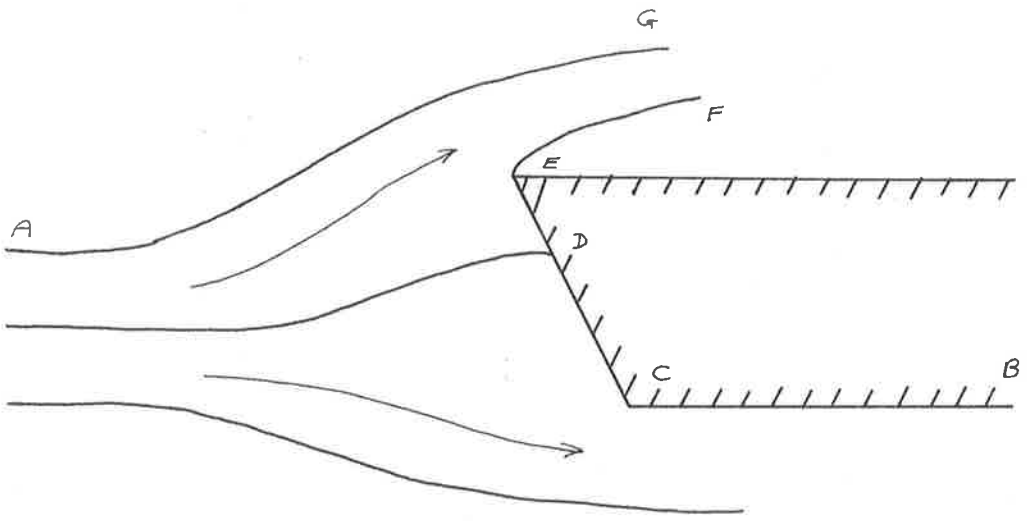

Fig. 4.3.5 - Cut-off bow; free jet over body.

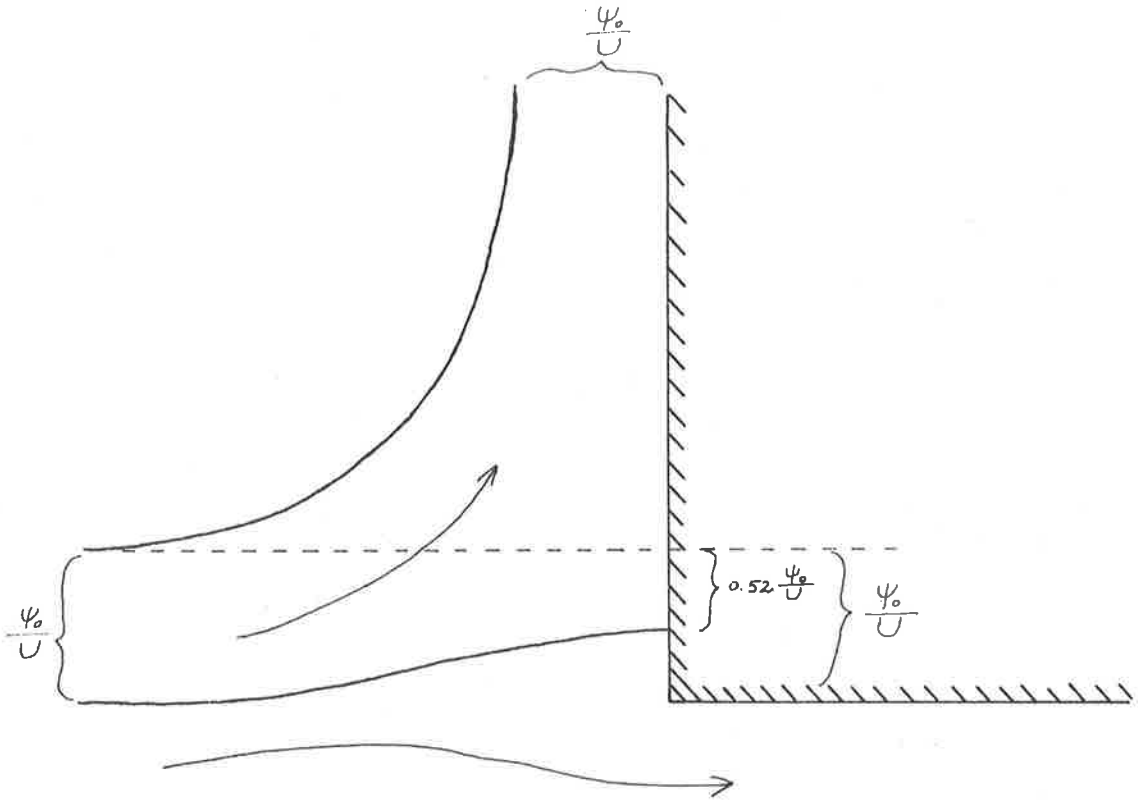

Fig. 4.3.6 - Bow flow with a jet at infinite Froude number.

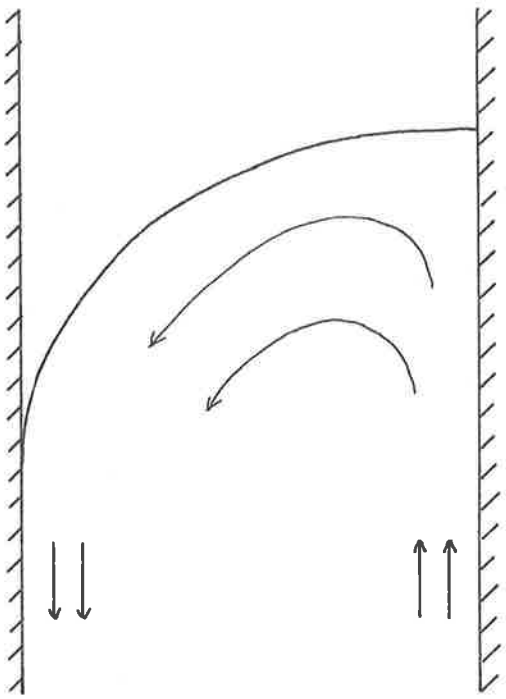

Fig. 4.3.7 - Richardson's flow.